Integrative analysis from the epigenome through translation exposes patterns of dominant nuclear regulation during transient stress

Running Head: Dynamic Nuclear Gene Regulatory Control by Hypoxia

Travis A Lee[1] and Julia Bailey-Serres[1]

[1]Center for Plant Cell Biology and Botany and Plant Sciences Department, University of California, Riverside, California 92521, USA

ORCID ID: 0000-0002-8352-8956 (T.A.L.)

ORCID ID: 0000-0002-8568-7125 (J.B.-S.)

The current address of T.L. is: Plant Biology Laboratory, The Salk Institute for Biological Studies, La Jolla, CA 92037, USA

Corresponding authors: Travis A Lee and Julia Bailey-Serres

Abstract

Gene regulation is modulated from chromatin to translation. To better understand the integration of nuclear and cytoplasmic gene regulatory dynamics, we performed a multi-omic survey of the epigenome through the translatome of the response of *Arabidopsis* seedlings to hypoxia and reoxygenation. This included eight assays of chromatin (histones, accessibility, RNAPII and transcription factor binding) and three assays of RNA (nuclear, polyadenylated, and ribosome-associated). Dynamic patterns of nuclear regulation distinguished stress-induced and growth-associated mRNAs. The rapid upregulation of hypoxia-responsive gene transcripts and their preferential translation was accompanied by increased chromatin accessibility, RNAPII engagement and reduced Histone 2A.Z association. The more progressive upregulation of heat stress gene transcripts was characterized by early engagement of RNAPII and elevation of nuclear over polyadenylated RNA. Promoters of the rapidly versus progressively upregulated gene cohorts were enriched for *cis*-elements of ethylene-responsive and heat shock factor transcription factor families, respectively. By contrast, genes associated with growth including ribosomal proteins underwent distinct histone modifications, yet retained RNAPII engagement and accumulated nuclear transcripts during the stress. Upon reaeration, many of the progressively upregulated and growth-associated gene transcripts were mobilized to ribosomes. Thus, multi-level nuclear regulation distinguishes transcript synthesis, accumulation and translation in response to a transient stress.

37 **Background**

38 The regulated expression of protein coding genes in eukaryotes involves processes within the
39 nucleus including remodeling of chromatin, recruitment of RNA polymerase II (RNAPII), co-
40 transcriptional processing, and the export of mature mRNA to the cytoplasm, where it may be
41 translated, sequestered and then degraded. These processes are modulated by conditions that
42 necessitate alterations in metabolism and growth to maintain viability. In *Arabidopsis thaliana*,
43 cellular hypoxia promotes activation of anaerobic metabolism to enable ATP production for
44 basic cellular processes. This involves the rapid activation of transcription of 49 hypoxia
45 responsive genes (*HRG*s) followed by the active translation of their mRNAs, while most other
46 transcripts are sequestered from translation complexes until re-aeration (Branco-Price et al.,
47 2005, 2008a; Juntawong et al., 2014; Sorenson and Bailey-Serres, 2014). The well translated
48 *HRG* mRNAs lack notable sequences or features that can explain their effective translation
49 (Branco-Price et al., 2005; Juntawong et al., 2014; Sorenson and Bailey-Serres, 2014), leading
50 to the hypothesis that their preferential translational may reflect aspects of their nuclear
51 regulation.

52 Transcriptional activation of many *HRG*s involves the evolutionarily conserved group VII
53 ethylene response factor (ERFVII) transcription factors (TFs) that are required for survival of
54 hypoxia (Xu et al., 2006; Hattori et al., 2009; Gibbs et al., 2011; Licausi et al., 2011; Yang et al.,
55 2011; Abbas et al., 2015; Eysholdt-Derzsó and Sauter, 2017; Paul et al., 2016; Giuntoli and
56 Perata, 2017). The five Arabidopsis ERFVIIs are stabilized under hypoxia due to attenuation of
57 their oxygen-stimulated proteolysis via the Arginine branch of the N-degron pathway (Gibbs et
58 al., 2011; Licausi et al., 2011; Paul et al., 2016; White et al., 2017; Millar et al., 2019). These
59 include three constitutively synthesized ERFVIIs (RELATED TO APETALA 2.2, 2.3, and 2.12
60 [RAP2.2, RAP2.3, RAP2.12]) shown to transactivate *HRG* promoters in protoplasts through a
61 hypoxia-responsive promoter *cis*-element (HRPE) identifiable in ~50% of the *HRGs (Gasch et*
62 *al., 2015; Giuntoli et al., 2014; Giuntoli and Perata, 2017)*. Two other ERFVIIs, HYPOXIA-
63 RESPONSIVE ERF 1/2 (HRE1/2) are upregulated by hypoxia along with *ALCOHOL*
64 *DEHYDROGENASE 1* (*ADH1*) and *PLANT CYSTEINE OXIDASE 1/2* (*PCO1/2*) that facilitate
65 anaerobic metabolism and catalyze turnover of the ERFVIIs, respectively (Giuntoli et al., 2014,
66 2017; Weits et al., 2014; White et al., 2017).

67 Transcription requires binding of TFs to specific *cis*-elements typically located near the
68 transcription start site (TSS) that facilitate assembly of an RNAPII initiation complex. The
69 depletion of nucleosomes near a TSS is controlled by ATP-dependent chromatin remodelers
70 and can be influenced by interactions with the transcriptional apparatus. TF binding and RNAPII

activity both influence and are influenced by specific modifications and variants of histones(Talbert and Henikoff, 2017; Gates et al., 2017), which thereby provide a proxy of gene activity. For example, tri-methylated Histone 3-lysine 27 (H3K27me3) and H3K4me3 are prevalent in the gene body of lowly and actively transcribed genes, respectively (Asensi-Fabado et al., 2017; Gates et al., 2017). Acetylation of Histone H3 lysine residues (H3K9ac, H3K14ac) reduce interactions between DNA and histones and are associated with ongoing transcription(Gates et al., 2017), including genes actively transcribed during environmental stress in plants (Eberharter and Becker, 2002; Kim et al., 2008, 2012). A characteristic of heat-stress activated genes of Arabidopsis is high levels of the Histone 2A variant H2A.Z at the first nucleosome within the gene body, a feature proposed to reduce the energy required to commence transcriptional elongation at elevated temperatures (Kumar and Wigge, 2010; Sura et al., 2017; Cortijo et al., 2017; Dai et al., 2017; Torres and Deal, 2018).

As transcription commences, the phosphorylation of specific residues within the heptad repeats of the carboxyl terminal domain (CTD) of RNAPII orchestrate interactions with factors that facilitate transcription-coupled histone modifications as well as the co-transcriptional 5' capping, splicing, and polyadenylation of the nascent transcript (Hajheidari et al., 2013; Milligan et al., 2016). CTD phosphorylation at Serine 2 (Ser2P) demarks active elongation (Phatnani and Greenleaf, 2006). In animals, pausing of RNAPII downstream of the TSS is common among genes activated by heat stress (Jonkers and Lis, 2015). The mapping of the 5' end of nascent transcripts by Native Elongating Transcript sequencing indicated that elongation can be rate-limiting shortly after initiation in Arabidopsis seedlings (Zhu et al., 2018), although this was not discernable when nascent transcripts were surveyed by global nuclear run-on sequencing (GRO-seq) (Hetzel et al., 2016). Yet, both studies found transcription becomes rate-limited as RNAPII pauses just beyond the site of cleavage and polyadenylation. Following initiation, co-transcriptional intron splicing, polyadenylation and export are regulated by environmental cues including hypoxia (Branco-Price et al., 2008a; Mustroph et al., 2009; Juntawong et al., 2014; Van Veen et al., 2016; de Lorenzo et al., 2017; Niedojadło et al., 2016).

To better understand the integration of nuclear and cytoplasmic regulation of gene activity in response to hypoxia and reoxygenation we carried out a multi-omic study of dynamics in histones, open regions of chromatin, HRE2 binding and RNAPII-Ser2P distribution. Eight chromatin readouts were compared with modulation of nuclear RNA (nRNA), polyadenylated RNA (polyA RNA) and polyadenylated ribosome-associated RNA. The meta-analysis of these data exposed patterns of histone modifications, dynamic regulation of chromatin accessibility, *cis*-element enrichment, and temporal regulation of nRNA that accompanied dynamics in mRNA

105 abundance and translation. This exposed underappreciated layers of gene regulation including
106 rapid and complete upregulation of *HRGs*, progressive upregulation of heat stress-response
107 genes, and incomplete downregulation of genes associated with growth, including ribosomal
108 proteins. Both transcriptional elongation and nuclear export appear to be points of regulation in
109 response to oxygen availability. The dataset provides a resource for evaluation of epigenetic
110 state and RNAPII activity through translation in a model organism.
111
112 **Results**
113 **A multiscale dataset for analysis of dynamics from chromatin to translation**
114 Here, generated 11 distinct chromatin and RNA-based genome-scale datasets to evaluate gene
115 regulatory dynamics in seedlings treated with normoxia (2h, 2NS; 9h, 9NS), non-lethal hypoxic
116 stress (2HS, 9HS), and reaeration (2HS followed by 1-2 h NS, R). All growth and treatment
117 conditions were consistent with prior analyses (Branco-Price et al., 2008a; Mustroph et al.,
118 2009; Juntawong et al., 2014) (Figure 1a; Supplemental Figure 1a). Chromatin
119 immunopurification and sequencing (ChIP-seq) was used to survey the position and abundance
120 of H3K9ac, H3K14ac, H3K4me3, H3K27me3, and H2A.Z along genes. The capture of nuclei by
121 Isolation of Nuclei Tagged in Specific Cell Types (INTACT) (Deal and Henikoff, 2010; Maher et
122 al., 2018) was coupled with Assay for Transposase-Accessible Chromatin using sequencing
123 (ATAC-seq) to map regions of chromatin depleted of nucleosomes (Buenrostro et al., 2013).
124 We also used ChIP-seq to survey regions bound by RNAPII-Ser2P and the hypoxia-induced
125 ERFVII HRE2. Finally, three transcript populations defined by methods of purification were
126 assayed: nRNA (rRNA subtracted nuclear transcriptome obtained by INTACT (Reynoso et al.,
127 2017)), polyA RNA selected by binding to oligo(dT) beads (transcriptome), and TRAP RNA
128 obtained by Translating Ribosome Affinity Purification and oligo(dT) selection (translatome)
129 (Juntawong et al., 2014; Zanetti et al., 2005). Each RNA population was reproducible and
130 distinguishable when plotted by t-SNE (Figure 1b-c; Supplemental Figure 1).
131
132 **Stress- and growth-associated genes contrast in chromatin accessibility, histone,**
133 **modifications and RNA modulation under hypoxia**
134 For the nucleosome level evaluation, the histone data were plotted along each annotated
135 protein-coding gene and global averages were compared for each condition (Figure 1d;
136 Supplemental Figure 2a). H3 modifications associated with transcription (H3K9ac, H3K14ac,
137 H3K4me3) and stress-activated transcription (H2A.Z) were enriched just 3' of the position of
138 TSS and tapered off at the primary site of polyadenylation (TES), whereas H3K27me3 was

139 distributed more evenly across gene bodies. Hypoxia had little effect on these modifications at
140 the global level, with the exception of a slight elevation of H3K14ac and reduction of H3K4me3
141 near the TSS.
142 Dynamic alteration in histone modification, abundance, and distribution was observed for
143 the induced and translated *HRG*s and stable but poorly translated cytosolic *RIBOSOMAL*
144 *PROTEIN* (*RP*) genes. *HRGs* significantly increased in H3K9ac and decreased in H2A.Z
145 association at 2HS, with limited changes in these marks on *RP*s (Figure 1e, f; Supplemental
146 Figure 1b, S3a-c). H3K4me3 levels were notably reduced on the *RP*s but not *HRG*s in response
147 to 2HS. When the stress was extended from 2 to 9 h, H3K9ac significantly increased on 863
148 and 3,646 genes and H3K14ac on 2 and 1,216 genes after 2HS and 9HS, respectively
149 (Supplemental Supplemental Table 2). A progressive increase of H3K14ac but not H3K9ac on
150 *RPs* was accompanied by little change in steady-state transcript abundance (Figure 1f;
151 Supplemental Figure 1c; Supplemental Figure 3a,c). These data indicate that these two gene
152 cohorts undergo distinct epigenetic regulation in response to hypoxia.
153 Next, we evaluated dynamics in chromatin accessibility in genic regions by ATAC-seq
154 (Figure 2a-b). Accessibility in 5' promoter regions is associated with depletion of nucleosomes
155 and binding of TFs and other transcriptional machinery (Lu et al., 2016; Sijacic et al., 2017;
156 Maher et al., 2018), whereas accessibility in 3' flanking regions is associated with formation of
157 chromatin loops and transcriptional termination (Ansari and Hampsey, 2005; Ozsolak et al.,
158 2008). The ATAC-seq reads mapped almost exclusively within 1000 bp 5' of the TSS and ~300
159 bp 3' of the major TES of genes in all four conditions (Figure 2c). The average ATAC signal
160 increased within the promoters of both *HRGs* and *RP*s (1.8- and 1.4-fold, respectively) after
161 2HS, yet ATAC reads showed expansion into more 5' and 3' flanking regions on the *HRG*s.
162 Peak-calling of Tn5 hypersensitive insertion sites (THSs) across the genome identified
163 constitutively present (8,072) and and an even larger group of stress-specific THSs (25,795)
164 (Figure 2d-f; Supplemental Table 1a).
165 To complete our survey of gene activity, we compared the distribution of the $\log_2$ fold
166 change (FC) (2HS/2NS) values of the chromatin, RNAPII-Ser2P, and the four RNA populations
167 at the genome-scale as well as for the *HRG*s and *RP*s (Figure 3a; Supplemental Table 2a). We
168 found that stress-induced RNAPII-Ser2P engagement was generally correlated with increased
169 H3K9ac (global R = 0.43; *HRGs* R = 0.17) and H2A.Z eviction (global R = -0.27), particularly for
170 the *HRGs* (R = -0.79) (Figure 3 b,c; Supplemental Figures 3b, 4). *RPs* contrasted to the *HRGs*,
171 displaying only minor changes in RNAPII-Ser2P association at 2HS but increased H3K14ac and
172 nRNA elevation at 9HS (Figure 3a; Supplemental Figure 3b, c). These results further

173 demonstrate that the epigenetic regulation of stress-induced and growth-associated genes is
174 distinct under hypoxia.
175
176 **Regulation at nuclear and cytoplasmic scales can be concordant or discordant**
177 Next we evaluated the generally presumed but untested hypothesis that *HRGs* are coordinately
178 transcribed and translated under hypoxia. To do so, we performed a global-scale systematic
179 analysis of the RNAPII-Ser2P, nRNA, polyA, and TRAP RNA datasets using co-regulation and
180 cluster analyses. When we examined whether significantly up- and downregulated genes
181 (DRGs; $|\log_2$ fold change$| > 1$; FDR < 0.05) were similarly regulated in all readouts of gene
182 activity, we found that the previously non-surveyed nRNA had the greatest (1,722) and polyA
183 RNA the fewest (602) up-DRGs (Figure 4a). The vast majority (92%) of the polyA up-DRGs
184 were also upregulated in at least one other readout, but only 213 genes were significantly
185 upregulated in all four readouts. Notably, these coordinately up-DRGs included 38 of the 49
186 *HRG*s. A parallel analysis found 72% of the polyA down-DRGs were significantly reduced in at
187 least one other dataset with only 10 coordinately down-DRGs (Figure 4b). nRNA displayed the
188 greatest number of down-DRGs (Ser2P [206], nRNA [2,608], polyA [291], TRAP [578]).
189 A lack of consensus in nRNA and polyA dynamics in response to the stress was not
190 unexpected, as the nuclear RNA purification method did not require the presence of a polyA tail
191 and therefore includes nascent transcripts. Indeed, the pairwise comparison of nRNA and polyA
192 RNA abundance in the 2NS and 2HS samples identified transcripts that were enriched in nRNA
193 or polyA RNA (Supplemental Figure 5; Supplemental Table 3). In both conditions, transcripts
194 that were overrepresented in the nucleus included many associated with the cell cycle and gene
195 silencing, whereas transcripts overrepresented in the polyA pool were associated with plastid
196 and ribosome biogenesis and function. Our data reveal a complex nuclear and cytoplasmic
197 regulatory landscape that was further explored by more integrative analyses of the chromatin
198 and RNA datasets.
199
200 **Coordinate and progressive upregulation are characterized by distinct patterns of**
201 **histone alterations**
202 To better resolve genes with similar patterns of regulation, DRGs identified in at least one of the
203 four datasets (n=3,042) were clustered into 16 groups and evaluated by Gene Ontology (GO)
204 term enrichment (Figure 4c; Supplemental Table 4a). This confirmed coordinately up-DRGs
205 (clusters 1-3) and down-DRGs (cluster 16). Genes in the remaining clusters that showed
206 discordant regulation in one or more readout.

207 To better understand the regulatory variation at the chromatin, RNAPII, and RNA scales,
208 we plotted the average signal value for each data type for each cluster along genic regions
209 (Figure 4d; Supplemental Figure 6). This revealed that the rapid and complete upregulation of
210 cluster 1-3 genes at 2HS was accompanied by enhanced chromatin accessibility, eviction of
211 H2A.Z, as well as elevation of H3K9ac and RNAPII-Ser2P across the gene body. The
212 concomitant rise in TRAP RNA indicated these transcripts were translated in proportion to their
213 increased abundance, as shown for the *HRG*s by high-resolution ribosome footprint analysis
214 (Juntawong et al., 2014). Not unexpectedly, the first two clusters were enriched for genes
215 associated with decreased oxygen (cluster 1, p-adj. $<6.73e^{-22}$) and general stress (cluster 2,
216 $<1.06e^{-21}$) (Supplemental Table 4a). Genome browser views of *ADH1* and *PCO2* illustrate the
217 coordinate upregulation of *HRGs* in all four of the assays of gene activity (Figure 5a,b).
218 Genes of clusters 4-8 were not upregulated to the same extent from RNAPII
219 engagement through translation, indicating they are regulated by multiple mechanisms that are
220 influenced by hypoxia. For cluster 4, the rise in nRNA coincided with elevation of H3K9ac and
221 RNAPII-Ser2P, indicative of increased transcription, yet this was not accompanied by a
222 concomitant rise in polyA or TRAP RNA (Figure 4c; Supplemental Figure 6). This incomplete
223 upregulation could reflect nuclear retention or cytoplasmic destabilization of these transcripts.
224 Clusters 6-8 genes showed elevated nRNA at 2HS, suggesting these transcripts are nascent or
225 remain in the nucleus. Of these, cluster 8 displayed little change in H3K9ac but a rise in
226 H3K14ac as well as nRNA at 2HS and 9HS (Supplemental Figures 6 and 7), consistent with the
227 regulation of the *RP*s that are enriched in this cluster (Figure 3; Supplemental Figure 3b,c). This
228 pattern of regulation is illustrated by *RPL37B* (Figure 5d).
229 One of the most distinct gene regulatory patterns was observed for cluster 9, which
230 showed a dramatic increase in RNAPII-Ser2P engagement that was not accompanied by a rise
231 in nRNA or polyA RNA. This could reflect an increase in RNAPII engagement (initiation) without
232 completion of transcript synthesis or elevated rates of transcription accompanied by high
233 cytoplasmic turnover. By comparison to cluster 1 genes, those of cluster 9 had lower and more
234 5' skewed H2A.Z at 2NS that was only slightly reduced at 2HS (Figure 4d; Supplemental Figure
235 9a). The association of H3K4me3, a mark typical of actively transcribed genes, was significantly
236 lower than genes of cluster 1 at 2HS (Supplemental Figure 9c,d). By 9HS the promoter
237 accessibility, H3K9ac, H3K14ac, nRNA and polyA RNA abundance of cluster 9 genes
238 increased (Supplemental Figure 7), indicating that they are progressively activated by hypoxia.
239 Cluster 9 genes were enriched for heat ($<6.20e^{-13}$) and oxidative stress ($<8.23e^{-11}$), which were
240 also prevalent in cluster 2 (heat [$7.74e^{-14}$]; oxidative stress [$<1.13e^{-12}$]). Cluster 2 was

241 distinguishable from cluster 9 by induced Ser2P engagement that produced nRNA and
242 translated RNA. *HEAT SHOCK PROTEIN 70-4* (*HSP70-4*), as an example, displayed a 3.4-fold
243 increase in RNAPII-Ser2P across the gene body region accompanied with increased nRNA and
244 TRAP RNA, but a delayed rise in polyA RNA (Figure 5c). The pronounced early engagement of
245 RNAPII-Ser2P followed by delayed elevation of polyA RNA indicates genes of cluster 9 are
246 progressively upregulated by hypoxia.
247
248 **Highly downregulated genes undergo distinct stimulus-regulated histone modifications**
249 A survey of the down-DRG genes (clusters 10-16) demonstrated stimulus-driven dynamics of
250 chromatin, RNAPII, and RNAs with two dominant patterns: coordinate downregulation (cluster
251 16) and incomplete downregulation (clusters 10-15) (Figure 4a). Cluster 10-14 were primarily
252 distinguished by a significant reduction in nRNA at 2HS that was generally accompanied by
253 increased H2A.Z and H3K14ac, and decreased H3K9ac downstream of the TSS (Supplemental
254 Figures 6 and 7). Cluster 15 and 16 genes stood out as strongly and coordinately reduced in
255 RNAPII-Ser2P engagement and at least two of the three RNA readouts at 2HS (Figure 4a;
256 Supplemental Figure 6). These clusters displayed reduced chromatin accessibility, elevation of
257 H2A.Z, and a sharp decline in H3K9ac,all of which were antithetical to the changes observed for
258 the continuously up-DRGs (Supplemental Figure 9a,c). Clusters 15 and 16 were enriched for
259 GO categories including: root development (cluster 15, $<3.7e^{-8}$) and regulation of transcription
260 and RNA biosynthesis (cluster 16, $<7.78e^{-7}$). Despite their opposing regulation, the most highly
261 up- (cluster 1-2) and down-DRGs (cluster 15-16) were characterized by H3 modifications that
262 were more broadly distributed along the gene body than in other clusters. Thus, H2A.Z
263 presence across a gene body, limited chromatin accessibility near the TSS, and reduced
264 RNAPII engagement are signatures of restricted transcription under hypoxia.
265
266 **Prolonged hypoxia promotes variations of nuclear regulation of growth-associated genes**
267 As seedling response to sub-lethal hypoxic stress changes over time (Branco-Price et al.,
268 2008b), we compared the change in H3K9ac, H3K14ac, nRNA, and polyA RNA at 2HS and
269 9HS relative to untreated seedlings (Figure 6a,b; Supplemental Figure 8; Supplemental Table
270 2a). H3K9ac and H3K14ac levels were progressively yet distinctly altered for the *HRG* and *RP*
271 cohorts (Figure 6a). Over 350 genes were progressively upregulated, displaying a rise in
272 H3K9ac, nRNA, and polyA RNA at 2HS and 9HS (clusters 1b-2b; 38 *HRG*s). The remainder
273 were incompletely up- or downregulated (clusters 4b-11b), indicating the regulatory patterns of
274 genes within these clusters changed as hypoxia was prolonged. Many genes with elevated

275 nRNA at 9HS were enriched for H3K14ac near their TSS (clusters 2b-8b) (Supplemental Figure
276 8), as exemplified by the *RPs* (enriched in clusters 5b and 8b). The increase in nRNA and
277 H3K14ac without an accompanying rise in polyA RNA suggests that these genes are
278 transcriptionally active but the nascent transcript remains in the nucleus or the mature (polyA)
279 transcript is rapidly degraded. Other genes demonstrated dynamic up- (cluster 6b) or down-
280 regulation between 2HS and 9HS (clusters 8b-11b). The downregulation at 9HS was
281 pronounced for photosynthesis (cluster 8b, $<5.8e^{-7}$ and $<1.5e^{-6}$), root development (cluster 10b,
282 $<1.7e^{-6}$), and transcription (cluster 11b, $<7.6e^{-6}$) (Supplemental Table 4b). A key finding was that
283 temporal regulation of nuclear and polyA transcript abundance during hypoxia can be distinct.
284 A number of genes associated with phasing of the circadian clock were perturbed when
285 hypoxia was prolonged (cluster 6b; circadian rhythm $<7.9e^{-10}$). Upon closer examination we
286 found this included dampened upregulation of several morning gene and prolonged elevation of
287 evening gene mRNAs, which normally peak towards the end of the light cycle when the stress
288 was initiated (Figure 6c). Examples of this perturbation include the morning-expressed clock
289 regulators *CIRCADIAN CLOCK ASSOCIATED 1* (cluster 16b) and *LATE ELONGATED*
290 *HYPOCOTYL* (cluster 15b) which had dampened mRNA accumulation, and *TIMING OF CAB*
291 *EXPRESSION* that had elevated polyA RNA after 9HS as compared to 9NS (Figure 6c,d). Thus,
292 hypoxia imposed at the end of the light cycle delays or arrests circadian phasing.
293
294 **Many coordinately hypoxia-upregulated genes are targets of ERFVII regulation**
295 We hypothesized that the coordinately up-DRGs might be transcriptionally activated by the low-
296 oxygen stabilized ERFVIIs. Motif scans for the HRPE within promoters (500 bp 5' of the TSS)
297 across the genome confirmed significant enrichment of this *cis*-motif in the cluster 1 genes
298 resolved in the 2HS analysis (Figure 7a; Supplemental Table 5), including the genes with strong
299 coordinate upregulation.
300 The ERFVII HRE2 is encoded by an *HRG*. To gain insight into the role of HRE2, ChIP-
301 seq was performed on 2HS seedlings overexpressing a stabilized version of this protein. Over
302 75% of the ~1800 peaks identified mapped within 1 kb upstream of TSSs, with clear enrichment
303 of binding within 500 bp upstream of the TSS (Supplemental Figure 10; Supplemental Table
304 2a), as evident in the promoters of *ADH1* and *PCO2* (Figure 5a,b; Supplemental Figure 10c,d).
305 The binding of HRE2 to promoter regions was highest for cluster 1, but also significantly
306 enriched for genes of clusters 2 and 3 of the 2HS analysis (Figure 7b). Overall, HRE2 peaks
307 were present in 28% of the 213 coordinately up-DRGs (Supplemental Table 2).

308 We anticipated that HRE2 might be associated with the HRPE, known to be
309 transactivated by RAP2.12, 2.2 and 2.3 (Gasch et al., 2015; Bui et al., 2015). But *de novo* motif
310 discovery using the HRE2 peak regions yielded an overrepresented multimeric 5'-GCC-3'
311 element (p-value $<1e^{-351}$) (Figure 7c; Supplemental Table 5) that resembles the GCC-rich EBP
312 box bound RAP2.12 in the *in vitro* DNA affinity purification and sequencing (DAP-seq) assay
313 (O'Malley et al., 2016)) and by RAP2.3 based on ChIP-qPCR and electrophoretic mobility shift
314 assays (Büttner and Singh, 1997; Gibbs et al., 2014). The HRE2/GCC motif was enriched in
315 cluster 1 but also was more prevalent than the HRPE in other clusters (Figure 7c). Our data
316 strongly suggest that HRE2 binds promoter regions containing a GCC-rich EBP-like box. Yet, in
317 over 50% of the 213 coordinately up-DRGs an HRPE is also present (Supplemental Table 2).
318 Collectively, these observations support the conclusion that many of the coordinately up-DRGs
319 are transcriptionally activated by one or more ERFVII.
320
321 **Hypoxic-stress progressively activates genes in heat and oxidative stress networks**
322 The regulatory variation of oxidative stress and heat response genes displayed by clusters 2-3
323 and 9 genes at 2HS (Figure 4b) was of interest. Anoxia upregulates heat-stress associated
324 genes (Banti et al., 2010; Loreti et al., 2005) and both the onset of hypoxia and reoxygenation
325 trigger a reactive oxygen species (ROS) burst associated with signal transduction (Chang et al.,
326 2012). Elevation of RNAPII-Ser2P without a commensurate increase in polyA RNA was
327 characteristic of *HSP*s, *RESPIRATORY BURST OXIDASE D* and transcriptional co/activators
328 associated with heat and oxidative stress (i.e., *MULTIPROTEIN BRIDGING FACTOR 1C*
329 (*AtMBP1C*), *DEHYDRATION-RESPONSIVE 2A* (*DREB2A*), *ZINC FINGER PROTEIN 12*
330 (*ZAT12*)). We also noted that several *HEAT SHOCK FACTOR* transcriptional activators were
331 elevated in TRAP RNA at 2HS (*HSFA2, HSFA4A, HSFA7A*). We considered that the
332 progressive upregulation of gene activity seen for cluster 9 genes may be mediated by HSFs
333 and distinguished by specific chromatin features. Indeed, motif-enrichment analysis confirmed
334 that HSF *cis*-elements (HSEs) were significantly enriched in promoters of cluster 9 (85% of
335 genes) and to a lesser extent in cluster 2 and 3 genes (Figure 7d). Moreover, progressively up-
336 DRGs with a 5' HSE motif were distinguishable from the continuously upregulated HRE2-bound
337 DRGs in four ways (Figure 7f): (1) a 5' bias in nucleosomes, (2) more 5' localized H2A.Z with
338 less dramatic eviction at 2HS, (3) reduced H3K4me3 and increased H3K14ac that preceded the
339 rise in H3K9ac, and (4) a delay in the increase in polyA RNA until 9HS. Thus, the regulatory
340 variations for progressively up-DRGs with promoter-localized HSEs are distinct from those of
341 the coordinately up-DRGs bound by HRE2 under hypoxia.

342

343 **Nuclear regulated stress responsive genes are highly translated upon reaeration**

344 The discovery of genes with RNAPII-Ser2P engagement accompanied with 5' biased nRNA but
345 little to no polyA accumulation at 2HS (cluster 6; Figure 4b) indicates that some genes may be
346 poised for upregulation upon release from oxygen deprivation. By evaluating dynamics in
347 chromatin and RNA upon reaeration, the *HRG*s, *RP*s, and heat-responsive genes again showed
348 distinct patterns of regulation (Figure 8a,b; Supplemental Figures 12-13). The co-clustering of all
349 genes differentially expressed under hypoxia (2HS/2NS) or reaeration (R/2HS) identified cluster
350 8_R as upregulated in nRNA at 2HS but not in polyA RNA until R (Figure 8a,b; Supplemental
351 Figure 12a). These genes were enriched for GO categories associated with heat ($4.55e^{-31}$), high
352 light intensity ($1.92e^{-33}$), protein folding ($8.91e^{-33}$), and reactive oxygen species ($9.03e^{-25}$).
353 Notably, over 50% of cluster 8_R genes had an HSE. The pattern of these HSE-containing
354 genes contrasted to that of rapid progression towards non-stress conditions by *HRG*s and *RP*s
355 in all three RNA readouts, as shown by the genome browser views of five representative genes
356 (Figure 8c). The expression pattern demonstrated by HSE-containing genes may be
357 physiologically relevant, as reaeration is associated with a rapid restoration of protein synthesis
358 and a ROS burst. Together, our data demonstrate functional nuclear segregation of a subset of
359 newly synthesized RNAs from cytoplasmic localized ribosomes in response to oxygen
360 availability.

361

362 **Discussion**

363 **Gene activity dynamics in response to hypoxic stress involves regulation of chromatin,**
364 **transcription, and post-transcriptional processes**

365 The dataset assembled of genome-wide measurements of chromatin state and intermediary
366 steps of gene expression in seedlings exposed to sub-lethal hypoxic stress and reaeration
367 identified time-dependent chromatin and transcript dynamics not appreciated by routine
368 transcriptomics. Hypoxic stress modulated the (1) position and degree of open chromatin near
369 the TSS, (2) modification of H3 lysines, (3) eviction of H2A.Z, (4) engagement of RNAP II-
370 Ser2P, and (5) the abundance of nuclear, polyadenylated and ribosome-associated gene
371 transcripts. The results illustrate clear distinctions between steady-state nuclear and polyA
372 transcriptomes, as shown with similar methods for rice (Reynoso et al., 2017). The data also
373 identified dynamics in chromatin accessibility and confirm translational dynamics in response to
374 hypoxia and reaeration (Branco-Price et al., 2005, 2008a; Juntawong et al., 2014; Mustroph et
375 al., 2009).

376 The monitoring of RNAPII-Ser2P engagement as a proxy for transcriptional elongation
377 revealed that global levels of transcription were not dramatically dampened by 2HS (Figure 1c),
378 although there was considerable regulation of individual genes (Figure 1c; Figure 4c).
379 Remarkably, less than 10% of all DRGs were coordinately up- or downregulated from
380 transcriptional elongation through translation at 2HS. Three patterns of discontinuous gene
381 regulation were apparent: (1) progressive upregulation, characterized by high RNAPII-Ser2P
382 engagement and delayed elevation of polyA RNA, as observed for heat and oxidative stress
383 genes, (2) incomplete downregulation, characterized by maintained RNAPII-Ser2P engagement
384 and increased nRNA abundance with limited change in polyA RNA, as observed for *RP*s; and
385 (3) enhanced or reduced translational status, measured by comparison of TRAP RNA and polyA
386 RNA abundance (Branco-Price et al., 2008a; Mustroph et al., 2009; Juntawong et al., 2014). We
387 also identified variations in nuclear regulation (chromatin accessibility, histone modification,
388 RNAPII engagement and nRNA abundance) that foreshadowed changes in polyA RNA
389 abundance and translation. Finally, the evaluation of the three transcript populations following
390 brief reaeration demonstrated a rapid rebound to homeostasis in the nRNA of the continuously
391 up-DRGs, discontinuously up-DRGs and discontinuously down-DRGs. In sum, these data
392 illuminate remarkable complexity in the transcriptional and post-transcriptional regulation of
393 genes associated with stress-responses and growth.
394
395 **Coordinate upregulation of hypoxia-responsive genes is characterized by histone**
396 **modification, histone variant eviction, and increased chromatin accessibility**
397 Hypoxia had marked effects on the position, composition, and modifications of specific histones
398 of nucleosomes. The genes that were coordinately upregulated from transcription through
399 ribosome included the *HRG*s, critical to low-oxygen stress survival (Gibbs et al., 2011; Gasch et
400 al., 2015; Mustroph et al., 2009, 2010; Giuntoli et al., 2014; Giuntoli and Perata, 2017). The
401 strong and coordinate upregulation of *HRG*s was characterized by eviction of H2A.Z, a rise in
402 gene body H3K9ac, promoter accessibility, RNAP-Ser2P engagement, nRNA, polyA and
403 ribosome-associated mRNAs (Figure 9). The co-transcriptional placement of a positive charge
404 on the N-terminus of H3K9 by histone acetyltransferases is a reliable signature of active
405 transcription (Eberharter and Becker, 2002) and is common for stress-activated genes (Kim et
406 al., 2008; Zhou et al., 2010; Kim et al., 2012). In animals, H3K9ac is promoted by H3K4me3 and
407 stimulates the release of poised RNAPII complexes (Jonkers and Lis, 2015). H3K4me3
408 generally rose on *HRG*s in response to 2HS, but was not as strongly correlated with RNAPII-
409 Ser2P engagement as H3K9ac (Figure 3b; Supplemental Figure 4d). The stress-activated

410 transcription coincided with eviction of H2A.Z from nucleosomes that were broadly distributed
411 across the bodies of *HRGs* at 2NS. This is consistent with prior reports that H2A.Z eviction from
412 nucleosomes is a prerequisite for activation of temperature responsive genes (Kumar and
413 Wigge, 2010; Sura et al., 2017; Cortijo et al., 2017; Dai et al., 2017; Torres and Deal, 2018).
414 H2A.Z deposition, eviction, and the impact on transcriptional regulation are complex and
415 not fully understood. Deposition requires ACTIN-RELATED PROTEIN 6 (ARP6), a component
416 of the SWR1 remodeling complex complex, and other factors in Arabidopsis (Asensi-Fabado et
417 al., 2017; Kumar, 2018). Yet disruption of H2A.Z deposition in an *arp6* mutant has limited effect
418 on regulation of *HRG*s under aerated growth conditions (Torres and Deal, 2018). Other
419 chromatin remodeling proteins or specific TFs could be important. In response to small
420 increases in temperature, displacement of H2A.Z was facilitated by HSF1A in the activation of
421 the heat response network (Cortijo et al., 2017). H2A.Z eviction from *HRG*s could involve
422 ERFVIIs. Indeed, the hypoxia-stabilized ERFVII RAP2.2 interacts with the SWI-SNF remodeler
423 BRAHMA and contributes to H2A.Z eviction associated with increased chromatin accessibility
424 (Efroni et al., 2013). Many of the HRGs displayed increased chromatin accessibility in their
425 proximal promoter regions and gene bodies. Moreover, 69 of the >200 coordinately up-DRGs
426 had one or more HRPE within 1 kb of their TSS and many were bound by HRE2 at 2HS (Figure
427 7e; Supplemental Table 2). RAP2.12 is stabilized and nuclear localized as external oxygen
428 levels decline below 10 kPa (Kosmacz et al., 2015). The rise in nuclear levels of ERFVIIs under
429 hypoxia may coordinate RNAPII initiation, facilitating H2A.Z eviction to promote productive
430 elongation that is coupled with H3K9 acetylation. ERFVII interaction with the ATP-dependent
431 chromatin remodeling machinery could also contribute to the expansion of regions of accessible
432 chromatin to facilitate high levels of transcriptional activation. The uniform upregulation from
433 transcription to translation of the up-DRGs with an HRPE and/or HRE2 bound promoter is
434 reminiscent of the production of translationally competent mRNAs during nutrient starvation in
435 yeast that is associated with specific transcription factors (Zid and O'Shea, 2014). We
436 hypothesize that transcriptional activation by the ERFVIIs could promote the fidelity of co-
437 transcriptional processing, export and translation of their targets under hypoxia.
438
439 **Genes associated with heat and oxidative stress are progressively upregulated by**
440 **hypoxia**
441 The stress distinctly activated genes associated with heat and oxidative stress. The progressive
442 upregulation of cluster 9 genes after 2HS (Figure 4c; Supplemental Figure 7) became more
443 evident when their activity was compared at 2HS and 9HS using two chromatin and two RNA

444 readouts (Figure 7g). A significant proportion of these genes had HSEs within their promoters
445 (Figure 4c, Figure 7d, Supplemental Figures 6 and 7). Their pattern of regulatory variation
446 included a 5' bias in histone marks and moderate to very high RNAPII-Ser2P engagement at
447 2HS accompanied by elevated nRNA and TRAP RNA, but limited full-length polyA RNA (Figure
448 8).
449 Previously, heat stress-responsive genes were recognized as highly induced in
450 Arabidopsis seedlings directly transferred to anoxia (Loreti et al., 2005; Banti et al., 2010).
451 Remarkably, a brief pre-treatment with heat stress increased the resilience to anoxia of wild-
452 type seedlings but not loss-of-function *hsfa2* or *hsf1a hsf1b* mutant seedlings (Banti et al.,
453 2008). This is enigmatic because high temperatures do not typically precede flooding in natural
454 environments, but the availability of HSPs could reduce cellular damage under extreme stress
455 conditions such as anoxia. Indeed, *HSPs* were plentiful in cluster 9 after 2HS. Limited synthesis
456 of ATP-dependent chaperones after brief hypoxia by nuclear sequestration of their transcripts
457 could minimize demands on limited energy reserves. However, as the stress is prolonged or
458 upon reaeration, the rapid synthesis of chaperones and proteins that provide protection from
459 ROS could aid survival. As an example, the upregulation of *RESPIRATORY BURST OXIDASE*
460 *D* (*RBOHD*) contributes to survival of hypoxia, submergence and post-submergence recovery
461 (Baxter-Burrell et al., 2002; Pucciariello et al., 2012; Gonzali et al., 2015; Yeung et al., 2018).
462 The nucleosome dynamics of cluster 2 and 9 genes after 2HS included similar
463 modifications with notable exceptions (Figure 4c,d; Supplemental Figures 7 and 11). Genes of
464 both clusters underwent a loss of H2A.Z near the TSS of the gene body in conjunction with
465 increased H3K9ac, but cluster 9 genes showed a loss of H3K4me3 proximal to their TSS. This
466 was not evident for cluster 2 or other coordinately up-DRGs. The decrease in H3K4me3 may be
467 an indication of non-productive RNAPII-Ser2P engagement, as this modification is associated
468 with RNAPII elongation (Kwak and Lis, 2013; Ding et al., 2012). Intriguingly, there was
469 significant enrichment of HSEs in promoters of both rapidly and progressively upregulated
470 genes (Figure 7d).
471 We predict that recruitment of specific TFs together with chromatin modifying enzymes
472 may influence histone or RNAPII CTD modifications that influence the rate of RNAPII
473 elongation, termination, or post-transcriptional processing, thereby tuning the temporal
474 production of stress-induced transcripts. The progressive upregulation of heat and oxidative
475 stress networks could be mediated by the upregulation of TF genes encoding HSFs (i.e.,
476 HSFB2B) and ZINC FINGER PROTEIN 10 (ZAT10), and others during the early hours of the
477 stress. Notably, the level of polyA mRNA accumulation and translation of these mRNA was

478 enhanced upon reaeration (Figure 8a). Our datasets provide an opportunity for further meta-
479 analyses of heat and oxidative stress gene regulatory networks.
480
481 **Genes associated with major cellular processes continue to be transcribed during**
482 **hypoxia**
483 Intriguing patterns of transcriptional and RNA regulation of genes associated with processes
484 associate with growth became evident from our multi-tier evaluation (Figure 8). Our prior
485 comparisons of the transcriptome and translatome determined that hypoxia limits the investment
486 of energy into the production of abundant cellular machinery such as ribosomes. mRNAs
487 encoding *RPs* and other abundant proteins were seen to be maintained but poorly translated
488 under hypoxic stress (Branco-Price et al., 2008a, 2005; Juntawong et al., 2014; Sorenson and
489 Bailey-Serres, 2014). The stress-limited translation of *RP*s mRNAs is associated with their
490 sequestration in UBP1C-associated macromolecular complexes (Sorenson and Bailey-Serres,
491 2014). Upon reaeration, *RP* mRNAs rapidly re-associate with polysomes (Branco-Price et al.,
492 2008a; Juntawong et al., 2014; Sorenson and Bailey-Serres, 2014). This is the first study to
493 consider at the global scale if *RP* or other translationally limited mRNAs are synthesized during
494 hypoxia, although nuclear run-on transcription assays determined that housekeeping gene
495 transcriptions continues in roots of fully submerged maize seedlings (Fennoy et al., 1998). Our
496 RNAP-Ser2P and nRNA data confirmed that genes encoding RPs, metabolic enzymes and
497 some photosynthetic apparati are synthesized and retained as partially or completely processed
498 transcripts in the nucleus during hypoxia (Figure 6), a situation readily reversed by re-aeration
499 (Figure 8a). These genes showed progressive increases in H3K14ac but not H3K9ac between
500 2HS and 9HS. The limited increase in their polyA RNAs could be due to limited cleavage and
501 polyadenylation or increased turnover. Similar uncoupling of the H3K9ac and H3K14ac marks
502 associated with active transcription but limited polyA RNA accumulation was reported for
503 promoters deemed inactive but primed for future activation in pluripotent embryonic stem cells
504 of mice (Karmodiya et al., 2012). The incomplete downregulation of housekeeping genes may
505 poise cells for the observed rapid recovery upon reaeration.
506 Our genome-scale analysis demonstrate retention of transcripts within the nucleus
507 during hypoxia, consistent with visualization studies of specific mRNAs in Arabidopsis and
508 lupine (Niedojadło et al., 2016). mRNAs associated with the cell cycle are reportedly enriched in
509 the nucleus under control conditions in Arabidopsis (Yang et al., 2017). This was confirmed in
510 our comparison of the nRNA and polyA RNA transcriptomes under control and hypoxia stress
511 (Figure 5). These data support a scenario wherein the nuclear compartmentalization of

512 abundant transcripts contributes to energy conservation by limiting translation, similar to the
513 cytoplasmic sequestration associated with the RNA binding protein UBP1C. Nuclear retention
514 and cytoplasmic sequestration could provide two reservoirs of transcripts that can be deployed
515 upon reaeration, enabling rapid restoration of cellular processes. Indeed, our data provide
516 evidence that nuclear retained transcripts increase in translation status upon reaeration (Figure
517 8a).
518 Thus, the comparative monitoring of nRNA, polyA and TRAP RNA populations strongly
519 support the conclusion that nuclear export and subsequent accumulation and translation of
520 mRNAs is dynamically regulated by stress in plants. Factors such as chromatin accessibility,
521 RNAPII elongation and termination and histone modification (i.e., H3K14ac) could contribute to
522 dynamic in nuclear transcript abundance. Circumstantial evidence of altered co-transcriptional
523 processing includes hypoxia-promoted intron retention (Juntawong et al., 2014) and alternative
524 polyadenylation site selection (de Lorenzo et al., 2017). Although there is no clear evidence of a
525 general disruption of splicing or polyadenylation during hypoxia (Koroleva et al., 2009;
526 Juntawong et al., 2014; de Lorenzo et al., 2017), these processes could be altered by changes
527 in chromatin, RNAPII elongation or association with certain proteins The RNA helicase eIF4AIII
528 (Koroleva et al., 2009) and several RNA binding proteins (UBP1A/B/C and CML38) form
529 macromolecular complexes present in the nucleus but primarily cytoplasmic under hypoxia
530 (Sorenson and Bailey-Serres, 2014; Lokdarshi et al., 2016). Further experimentation is required
531 to better understand the controlled dynamics in transcript synthesis, processing and export
532 during hypoxia stress.
533
534 **An ERFVII hierarchy drives transcriptional activation in response to hypoxia**
535 This study included the first genome-wide analysis of the *cis*-element targets of an ERFVII.
536 ChIP-seq of the hypoxia-induced ERFVII HRE2 identified a multimeric 5'-GCC-3' *cis*-element
537 that is distinct from the HRPE that is enriched in *HRG* promoters and activated by ERFVIIs
538 (Gasch et al., 2015). This is consistent with the observation that neither HRE1 nor HRE2
539 interacted with a 33 bp promoter fragment containing the HRPE in a Yeast-1 hybrid assay or
540 provided significant transactivation via the HRPE in protoplasts (Gasch et al., 2015). The HRE2
541 binding motif strongly resembled the double GCC motif of the EBP box that was first defined for
542 an ERF of *Nicotiana tabacum* (Sato et al., 1996). Previously, RAP2.3 was shown to bind the
543 *ACID INSENSITIVE 5* (*ABI5*) promoter in a region with two EBP boxes; transactivation of the
544 *ABI5* promoter in protoplasts by all three constitutively expressed ERFVIIs (RAP2.2/2.3/2.12)
545 was dependent on the EBP box (Gibbs et al., 2014).

546 Collectively, our observations support earlier conclusions that members of the two
547 ERFVII subgroups are not functionally redundant (Gasch et al., 2015; Gibbs et al., 2014). Yet,
548 the situation remains somewhat enigmatic. The HRPE contains a sequence resembling a
549 double 5'-GCC-3'. Moreover, promoter regions with high scores for the HRPE and HRE2 motif
550 coincided in 40 of the 213 coordinately up-DRGs, of which 13 were bound by HRE2
551 (Supplemental Table 1) and the Arabidopsis *ADH1* promoter region that is sufficient for hypoxic
552 upregulation contains both of these motifs (Gasch et al., 2015). The current model is that the
553 low-oxygen-mediated stabilization of the constitutively-expressed RAP-type ERFVIIs is
554 responsible for rapid transactivation of *HRG*s that include *HRE2* (van Dongen and Licausi,
555 2015; Voesenek and Bailey-Serres, 2013), which is synthesized and stabilized under hypoxia
556 (Gibbs et al., 2011). We propose that HRE2 production and binding to promoters via the
557 multimeric GCC element (HRE2 motif) is important for continued upregulation of *HRG*s, as an
558 *hre1 hre2* double mutant fails to maintain the upregulation of these genes after 4 h of anoxia
559 (Licausi et al., 2010). It may also enable cells to circumvent the inhibition of RAP2.12 activity by
560 its interaction with the HYPOXIA RESPONSE ATTENUATOR (HRA1) (Giuntoli et al., 2014).
561 Further analyses are required to comprehend the independent or overlapping roles of the RAP-
562 type and HRE ERFVIIs in the temporal activation of transcription during hypoxia.
563 Mammals regulate transcriptional activity in response to hypoxia in a manner that is
564 remarkably analogous to Arabidopsis (Watson et al., 2010). Hypoxia-responsive genes are
565 activated by the two-subunit Hypoxia Inducible Factor (HIF) TF complex, that includes the
566 oxygen-destabilized HIF1A subunit (LaGory and Giaccia, 2016). Similar to the three RAP-
567 ERFVIIs of Arabidopsis, HIF1A is a constitutively synthesized protein that is destabilized in the
568 presence of oxygen. A group of prolylhydroxlases catalyze the oxygen-dependent hydroxylation
569 of specific residues of HIF1A that triggers its ubiquitylation and protoeasome-mediated turnover.
570 In animals, the chromatin landscape is additionally regulated through chromatin accessibility
571 (Buck et al., 2014) and the post-translational modification of histones (Chervona and Costa,
572 2012) in an oxygen-sensitive manner. HIF signaling itself directly facilitates histone modification
573 of target genes through interactions with chromatin modifying enzymes (Watson et al., 2010),
574 several histone modifying enzymes are directly targeted by HIF transcriptional activation, and
575 HIF1A expression itself is regulated by histone acetylation (Kim et al., 2007). Moreover, specific
576 histone modifying enzymes function as direct oxygen sensors through the mediation of their
577 activity based on cellular oxygen levels (Batie et al., 2019; Chakraborty et al., 2019), confirming
578 the integration of oxygen sensing with epigenetic regulation. The low-oxygen stabilized
579 transcriptional regulators and the coordination of their function with chromatin modifications in

580 Arabidopsis is evidence of convergence in gene activity regulation in response to hypoxia in
581 plants and animals. This may extend beyond transcriptional regulation as cytoplasmic
582 sequestration and selective translation of mRNAs is also observed in plants and metazoa (Blais
583 et al., 2004; Young et al., 2008; Branco-Price et al., 2008a; Juntawong et al., 2014). It remains
584 to be explored if hypoxia influences the synthesis and accumulation of nascent transcripts
585 associated with growth in animals, as demonstrated in this multi-omic analysis of Arabidopsis.
586
587 **Conclusions**
588 This multi-level investigation into gene regulatory processes revealed unexpectedly complex
589 regulation of gene activity within the nucleus and cytoplasm that fine tune cellular and
590 physiological acclimation to transient hypoxia, providing a model for response to an acute
591 stress. A key finding is that there are rapid changes in the epigenome in response to short-term
592 hypoxic stress that continue as the stress becomes more severe. Coordinate up-regulation from
593 chromatin accessibility to translation was observed for over 200 hypoxia-responsive genes.
594 Extreme stress-responsive and growth-associated genes showed more discontinuous
595 upregulation of nascent transcript production, export to the cytoplasm, and recruitment to
596 ribosomes. Each of these broadly defined gene cohorts showed a distinct pattern of epigenetic,
597 nuclear and cytoplasmic transcript regulation upon re-aeration. Future investigations can
598 consider roles of specific TF and their interactions with RNAPII, transcriptional coactivators, the
599 chromatin landscape, and the post-transcriptional apparatus in directing the nuanced nuclear
600 regulation uncovered in this study.
601
602 **Materials and Methods**
603
604 **Genetic Material**
605 The following genotypes were used for genome wide experiments: Col-0, Histone modification
606 ChIP-seq, RNAP II ChIP-seq; *pHTA11:HTA11-3xFLAG (Cortijo et al., 2017)*, H2A.Z ChIP-seq;
607 *pUBQ10:NTF/pACT2:BirA (Sullivan et al., 2014)*, ATAC-seq, nRNA-seq, polyA mRNA-seq;
608 *p35S:HF-RPL18* (Zanetti et al., 2005), TRAP-seq, mRNA-seq; and HRE ChIP-seq *p35S:C2A-*
609 *HRE2-HA* (Gibbs et al., 2011).
610
611 **Plant Growth and Treatment**
612 Arabidopsis seeds were sterilized by incubation in 70% EtOH for 5 min, followed by incubation
613 in 20% (v/v) bleach, 0.01% (v/v) TWEEN-20, followed by three washes in ddH_2O for 5 min, in

614 triplicate. Sterilized seeds were placed onto 1x MS media (1.0x Murishige Skoog (MS) salts,
615 0.4% (w/v) Phytagel (Sigma-Aldrich), and 1% (w/v) Suc, pH 5.7) in 9 cm^2 Petri dishes and
616 stratified by incubation at 4°C for 3 d in complete darkness. Following stratification, plates were
617 placed vertically into a growth chamber (Percival) with 16 h light / 8 h dark cycle at ~120 µmol
618 photons$\cdot s^{-1} \cdot m^{-2}$, at 23 °C for 7 d. For hypoxic stress, seedlings were removed from the growth
619 chamber at Zeitgeber time (ZT) 16 and were subjected to hypoxic stress by bubbling argon gas
620 into sealed chambers in complete darkness for 2 or 9 h at 24 °C. The chamber set-up was as
621 described by (Branco-Price et al., 2008a). Oxygen partial pressure in the chamber was
622 measured with the NeoFox Sport O_2 sensor and probe (Ocean Optics). Hypoxia ($[O_2] < 2\%$) was
623 attained within 15 min of initiation of the stress. Control samples were placed in an identical
624 chamber that was open to ambient air under the same light and temperature conditions. For
625 reaeration, seedlings were identically subjected to hypoxic stress for 2 h and subsequently
626 placed into the control chamber for 1 h (nRNA and polyA) or 2 h (TRAP) following the stress.
627 Tissue was rapidly harvested into liquid N_2 and stored at -80 °C.
628
629 **Chromatin and Nuclei Preparation**
630 **Detailed methods are provided in the supplement.** ChIP was performed according to (Deal
631 and Henikoff, 2010) with minor modifications provided in the supplemental methods. INTACT
632 was performed according to (Deal and Henikoff, 2010) with modifications provided in the
633 supplemental methods. ATAC-seq was performed on fifty-thousand INTACT-purified nuclei from
634 root tissue according to (Buenrostro et al., 2013). Nuclear RNA extraction of INTACT-purified
635 nuclei was performed according to (Reynoso et al., 2017). Additional details are provided in
636 Supplemental File 1.
637
638 **Nuclear, PolyA and TRAP-RNA Isolation and Library Construction**
639 Total RNA was extracted from 50 mg frozen pulverized tissue using Trizol (Life Sciences),
640 treated with DNaseI, purified using AMPure XP beads, and eluted in 50 µL H_2O and polyA
641 selected. PolyA RNA selection was performed using Oligo $(dT)_{25}$ Dynabeads by two rounds of
642 magnetic capture (Townsley et al., 2015). TRAP (Translating Ribosome Affinity Purification) of
643 mRNA-ribosome complexes was performed following the procedure of (Mustroph et al., 2009).
644 TRAP RNA extraction (Townsley et al., 2015) was performed with minor modifications and then
645 polyA RNA was selected as described by (Townsley et al., 2015). RNA-seq library preparation
646 for nRNA, polyA, and TRAP RNA was performed according to (Kumar et al., 2012). Additional
647 details are provided in Supplemental File 1.

648

649 **Bioinformatic Analyses**

650 For all high throughput outputs, short reads were trimmed using FASTX-toolkit to remove
651 barcodes and filter short and low quality reads prior to alignment to the TAIR10 genome with
652 Bowtie2/Tophat2. Read quality reports were generated using fastqc. For all datasets excluding
653 ATAC-seq and HRE2 ChIP-seq, counting of aligned reads was performed on entire transcripts
654 (Lawrence et al., 2013) using the latest Araport 11 annotation (201606) and reads per kilobase
655 of transcript per million mapped reads (RPKM) values were calculated. Differentially expressed
656 genes were determined by edgeR, |FC| > 1, FDR < 0.01. *Data visualization and file generation*:
657 Bigwig files for Integrated Genome Viewer (IGV) visualization were generated from aligned bam
658 files and normalized by RPKM values using the deepTools command bamCoverage with the -
659 normalizeUsingRPKM specification. Within IGV, all chromatin based outputs were normalized to
660 the same scale and all RNA outputs were normalized to a separate scale. *Peak calling:* For
661 ChIP-seq and ATAC-seq datasets, peak calling was performed using independent replicates in
662 combination as input for HOMER using the findPeaks command (Heinz et al., 2010). For
663 downstream analyses, peaks identified from each time point comparison were combined and
664 counting was performed on individual replicates. Peaks were annotated using the HOMER
665 command annotatePeaks.pl. Differential regulation of peaks was performed using edgeR. *Motif*
666 *discovery:* HRE2 peaks identified by HOMER command findPeaks were used as an input for the
667 HOMER command findMotifsGenome.pl. The matrix for the top HRE2 motif (p: 1e-69) was used
668 as input the MEME command ceqlogo to generate the motif logo. *DAP-seq motif analysis:*
669 Sequences of promoter regions spanning 1 kb upstream to 500 bp downstream of the TSS were
670 extracted for genes within each cluster. The promoter sequences were compared against each
671 TF, per TF family, using motif matrices identified by (O'Malley et al., 2016). The number of
672 significant motifs identified within the promoters of each cluster were quantitated and normalized
673 to the number of genes within each cluster. *t-distributed stochastic neighbor embedding (t-*
674 *SNE)*: t-SNE analysis was performed according to (Cao et al., 2017). Briefly, a principal
675 component analysis was performed using RPKM values for each replicated dataset and
676 timepoint. t-SNE was then performed on PCs 1-10 and the results were plotted using ggplot2.
677 *Wilcoxon signed rank sum test:* Wilcoxon signed rank sum test was performed by comparing the
678 RPKM values of one genomic output for each gene within a cluster to the genes of another
679 cluster. Each cluster was compared individually to all other clusters to determine significance, p
680 < 0.05. *Fisher's exact test:* Fisher's exact test was performed by comparing the number of

681 motifs / peaks associated with genes within a cluster to the total number of motifs / peaks
682 identified for all DRGs.
683
684 **Bioinformatic Tools**
685 Analyses were performed with Bioconductor R packages particularly the Next Generation
686 Sequencing analysis software of systemPipeR (Girke, 2014). Programs used within
687 Bioconductor included: BiocParallel (Morgan et al., 2014), BatchJobs (Bernd Bischl et al., 2015),
688 GenomicFeatures (Lawrence et al., 2013), GenomicRanges (Lawrence et al., 2013), edgeR
689 (McCarthy et al., 2012), gplots (Warnes et al., 2009), ggplot2 (Wickham, 2009), RColorBrewer
690 (Neuwirth, 2011), Dplyr (Wickham and Francois, 2015), biomaRt (Durinck and Huber),
691 ChIPseeker (Yu et al., 2015), rtracklayer (Lawrence et al., 2009), Rtsne (Krijthe, 2015),
692 Pheatmap (Kolde, 2012), e1071 (Meyer et al., 2015), cluster (Maechler, 2018), ShortRead
693 (Morgan et al., 2009), clusterProfiler (Yu et al., 2012), and Rsamtools (Morgan et al., 2016). The
694 Publically available UNIX/Python/Perl packages used included Tophat (Kim et al., 2013),
695 fastx_toolkit (Gordon and Hannon, 2010), Fastqc (Andrews and Others, 2010), MEME (Bailey et
696 al., 2009), HOMER (Heinz et al., 2010), deepTools (Ramírez et al., 2016), circos (Krzywinski et
697 al., 2009), Bedtools (Quinlan and Hall, 2010), samtools (Li, 2011).
698
699 **Statistical analysis**
700 Statistical analysis of cluster motif enrichment was performed by two-tailed Fisher's exact test
701 comparing motif frequency for individual genes of each cluster; $p < 0.05$. Statistical significance
702 of cluster values was performed for each genomic output using Wilcoxon signed rank test for
703 values of all genes within each cluster. $p < 0.05$.
704
705 **Accession Numbers**
706 The Arabidopsis genes examined in this study include: ADH1, AT1G77120; PCO2, AT5G39890;
707 HSP70-4, AT3G12580; RPL37B, AT1G52300; LHY1, AT1G01060; CCA1, AT2G46830; PRR9,
708 AT2G46790; PRR7, AT5G02810; PRR5, AT5G24470; RV8, AT3G09600; LUX, AT3G46640;
709 CIR1, AT5G37260; ELF3, AT2G25930; ELF4, AT2G40080; LWD1, AT1G12910; ZTL,
710 AT5G57350; GI, AT1G22770; LNK1, AT5G64170; LNK2, AT3G54500; TOC1, AT5G61380;
711 CML38, AT1G76650; LBD41, AT3G02550; ALAAT1, AT1G17290; HSP20 like AT1G53540;
712
713 **Funding**

714 This work was supported by U.S. National Science Foundation (Grant Nos. IOS−1121626, IOS-
715 1238243, MCB-1716913) and the U.S. Department of Agriculture, National Institute of Food and
716 Agriculture - Agriculture and Food Research Initiative (Grant No. 2011−04015) to J.B.-S..
717
718
719
720 **Supplemental Data**
721 Supplemental Figure 1. Expanded overview of the multiscale chromatin and RNA gene
722 regulatory analyses.
723 Supplemental Figure 2. Average signal plots and heat maps for the global distribution of reads
724 of chromatin and RNA data.
725 Supplemental Figure 3. Multi-level evaluation of histone and gene regulation activity of the
726 *HRG*s and *RP*s.
727 Supplemental Figure 4. Evidence of cooperative association between H2A.Z eviction and
728 H3K9ac and the relation between Histone H3 modification and RNAPII engagement.
729 Supplemental Figure 5. Genome-wide comparison of nRNA to polyA RNA demonstrates nuclear
730 and cytoplasmic enrichment of transcripts under two conditions.
731 Supplemental Figure 6. Distinctions in histones, RNAPII-Ser2P and RNA levels on genes that
732 are co-regulated in response to hypoxic stress.
733 Supplemental Figure 7. Progressive regulation of variations in gene activity in response to
734 hypoxia.
735 Supplemental Figure 8. Histone and gene activity comparisons of genes co-regulated after 9 h
736 of hypoxic stress.
737 Supplemental Figure 9. Quantitative analysis of dynamics in histone modifications of co-
738 regulated gene clusters after 2 h of hypoxic stress.
739 Supplemental Figure 10. Genome-wide binding dynamics of HRE2 determined by ChIP-seq.
740 Supplemental Figure 11. Genome browser view of normalized read coverage of histone, ATAC-
741 seq, RNAPII-Ser2P, HRE2-chromatin immunopurification and RNA outputs for representative
742 genes of cluster 9.
743 Supplemental Figure 12. Reoxygenation following hypoxia promotes global dynamics in
744 chromatin accessibility and RNA populations.

745 Supplemental Figure 13. Regulation of variations in gene activity in response to hypoxia and
746 reoxygenation.
747 Supplemental Table 1. Tabulation of ATAC and HRE2-ChIP peaks on chromatin
748 Supplemental Table 2. Survey of histones, RNAPII, HRE2 and three RNA sub-populations in
749 response to two durations of hypoxic stress
750 Supplemental Table 3. nRNA Enrichment and Gene Ontology Analysis
751 Supplemental Table 4. Gene Ontology Analysis for two durations of hypoxic stress in
752 Supplemental Table 5. List of Arabidopsis Blacklisted Chromatin (ABC)
753 Supplemental File 1. Supplementary Methods
754 Supplemental File 2. BED file of Arabidopsis Blacklisted Chromatin (ABC)
755
756 **Supplemental Note**
757 ***Arabidopsis* blacklisted chromatin**
758 The variety of genome-wide outputs in this study recording dynamics at the level of chromatin
759 and RNA has permitted the identification of Tn5 bias/genomic regions with high nonspecific
760 background and/or high signal/read counts in Arabidopsis irrespective of experiment, similar to
761 regions identified by the ENCODE project for other organisms (ENCODE Project Consortium,
762 2012). The identification and filtering of genomic blacklisted regions is especially important for
763 calculation of genome wide Pearson correlations and the generation of signal tracks used for
764 accurate browser views. The *Arabidopsis* Blacklisted Chromatin (ABC) regions (Supplemental
765 Table 5, Supplemental File 2) can be used to remove these defined regions that create
766 statistical artefacts of the nuclear genome prior to performing analyses of chromatin-based data.
767
768 **Figure Legends**
769
770 **Figure 1. Multiscale chromatin and RNA gene regulatory analyses of control (normoxic)**
771 **and hypoxic seedlings of *Arabidopsis*. a** Schematic of experiments performed. Seven-day-
772 old seedlings were subjected to control (normoxic) (2NS, 9NS), hypoxic stress (2HS, 9HS), or
773 re-oxygenation following 2HS (R) conditions. Vertical arrows indicate time of harvest. Chromatin
774 immunopurification (ChIP) was performed to evaluate genomic regions bound by the Ser2
775 phospho-isoform of RNA Polymerase II (Ser2P), the Histone 2 variant H2A.Z, modified Histone
776 3 (H3K4me3, H3K27me3, H3K9ac, H3K14ac), and the group VII Ethylene Responsive Factor
777 (ERF) transcription factor HYPOXIA RESPONSIVE ERF 2 (HRE2). Isolation of Nuclei TAgged
778 in specific Cell Types (INTACT) purified nuclei were used for Assay for Transposase Accessible

779 Chromatin (ATAC) and purification of nuclear RNA. Ribosome-associated mRNA was obtained
780 by Translating Ribosome Affinity Purification (TRAP). **b** Individual replicate samples of nuclear
781 [nRNA], polyadenylated mRNA [polyA] and ribosome-associated polyA mRNA [TRAP]) were
782 compared by t-Distributed stochastic neighbor embedding (t-SNE). **c-e** Distributions of histone
783 modifications/variants across genic regions **c**, for the core hypoxia responsive genes (*HRG*s,
784 *n*=49) **d,** and cytosolic ribosomal proteins (*RP*s, *n*=246) **e**. Read distributions are plotted from 1
785 kb upstream to 1 kb downstream of gene units defined by the transcription start site (TSS) and
786 transcription end site (TES).
787
788 **Figure 2. Regions of chromatin accessibility determined by Assay of Transposase-**
789 **Accessible Chromatin using sequencing (ATAC-seq) are dynamically regulated by**
790 **hypoxic stress. a-b** Average ATAC-seq read distribution of chromatin accessibility for protein-
791 coding genes (**a**), HRGs and RPs (**b**). **c** Distribution of transposase hypersensitive sites (THSs)
792 on genomic features for each condition. **d-e** Volcano plot of the $\log_2$ fold change in THSs
793 identifiable under two conditions and the significance value of their difference. Genes indicated
794 in pink meet the criteria of $\log_2$ fold change value > |1|, 0.05 < p. value. **f** Overlap in THSs
795 identified for each of four conditions.
796
797 **Figure 3. Short term hypoxic stress promotes pronounced changes in chromatin,**
798 **transcription and nascent transcripts that are not uniformly reflected in transcript steady-**
799 **state abundance or translation.** Comparison of genome-wide data for chromatin and RNA for
800 2 h hypoxic stress (2HS) relative to the normoxic control (2NS). **a** Combined violin and boxplot
801 of $\log_2$ fold change (2HS/2NS) of histone, RNAPII-Ser2P and RNA outputs. Violin, all genes;
802 boxplot for the *HRG*s plotted in orange with *ALCOHOL DEHYDROGENASE 1* (*ADH1*) depicted
803 as a red dot and the cytosolic *RP*s plotted in blue, with *RIBOSOMAL PROTEIN 37B* depicted as
804 a dark blue dot. **b** Comparison of $\log_2$ fold change (2HS/2NS) between H2A.Z on the gene body
805 and Ser2P on the gene body. **c** Comparison of $\log_2$ fold change (FC) (2HS/2NS) between
806 H3K9ac and Ser2P on the gene body. For b and c, *HRG*s are plotted in pink and *RP*s in blue;
807 Pearson's coefficient of determination is shown for all genes.
808
809 **Figure 4. Multi-scale analysis of hypoxia-regulated genes reveals concordant and**
810 **discordant patterns of gene regulation.** Number of **a** up- and **b** down-differentially regulated
811 genes (DRGs) in response to 2 h of hypoxic stress (|$\log_2$ fold change (FC)| > 1; False Discovery
812 Rate (FDR) < 0.05) identified in each of the four readouts related to RNA: Ser2P ChIP, nRNA,

813 polyA RNA, and TRAP RNA. Arc of circle circumference indicated by the grey line represents
814 the DRGs in each of the four readouts. Genes differentially regulated in 2 to 4 readouts were
815 tabulated (number in parentheses) and depicted by links within the circle. Genes differentially
816 regulated in only one readout are represented by unlinked grey lines. **c** Heatmap showing
817 similarly regulated genes based on four assays of gene activity. Partitioning around medoids
818 clustering of 3,042 DRGs; 16 clusters. Selected enriched Gene Ontology terms are shown at
819 right (p adj. < 1.47e-09), |FC| > 1, FDR < 0.05. Clusters displaying increased or decreased
820 translational status (ribosome-associated [TRAP] relative to total abundance [polyA]) are shown.
821 **d** Average signal of various chromatin and RNA outputs for genes of three clusters plotted from
822 1 kb upstream of the transcription start site (TSS) to 1 kb downstream of the transcript end site
823 (TES) for the 2 h (2NS, 2HS) timepoints. Signal scale of graphs differ. Dashed lines used to plot
824 hypoxic stress data. Upper panel, ATAC-seq data shaded. Lower panel 2HS polyA data
825 shaded.
826
827 **Figure 5. Genome browser view of normalized read coverage of histone, ATAC-seq,**
828 **RNAPII-Ser2P, HRE2-chromatin immunopurification and RNA outputs for representative**
829 **genes. a-d** Normoxia (2NS) and 2 h hypoxic stress (2HS). **e-h** Normoxia (9NS) and 9 h hypoxia
830 stress (9HS) samples. **a,e** *ALCOHOL DEHYDROGENASE 1* (*ADH1*), **b,f** *PLANT CYSTEINE*
831 *OXIDASE 2* (*PCO2*), **c,g** *HEAT SHOCK PROTEIN 70-4* (*HSP70-4*) and **d,h** *RIBOSOMAL*
832 *PROTEIN L37B* (*RPL37B*). The maximum read scale value used for chromatin based and RNA
833 based outputs is equivalent for all genes depicted. At bottom, the transcription unit is shown in
834 grey with the transcription start site marked with an arrow. *PCO2* shows a stronger decline in
835 H2A.Z than *ADH1* in response to hypoxia at 2HS (*PCO2*, -1.15 $\log_2$ FC; *ADH1*, -0.33 $\log_2$ FC)
836 and provides an example of elevated H3K4me3 under hypoxic stress.
837
838 **Figure 6. Prolonged hypoxia leads to further variation in epigenetic, transcriptional and**
839 **posttranscriptional regulation. a** Combined violin and boxplot of H3K9ac and H3K14ac,
840 nRNA, and polyA RNA data. Violin plots of $\log_2$ fold change (9HS/9NS) data for all genes.
841 Boxplots are data for the 49 *HRGs* plotted in orange with *ALCOHOL DEHYDROGENASE 1*
842 (*ADH1*) depicted as a red dot and data for the cytosolic ribosomal proteins (RPs) plotted in blue
843 with *RIBOSOMAL PROTEIN 37B* depicted as a dark blue dot. **b** Heatmap showing similarly
844 regulated genes based on two dynamics in nRNA and polyA RNA. Partitioning around medoids
845 clustering of 3,897 differentially regulated genes; 16 clusters. Selected enriched Gene Ontology
846 terms are shown at right (p adj. < 1.37E-06), |FC| > 1, FDR < 0.05. **c** Heatmap of chromatin and

847 RNA readouts of select circadian regulated genes under short and prolonged hypoxic stress.
848 Heatmap scales between chromatin and RNA based readouts differ. **d** Brower views of a
849 morning (*CIRCADIAN CLOCK ASSOCIATED 1*, CCA1), evening (*CIRCADIAN 1*, CIR1), and
850 night (*TIMING OF CAB EXPRESSION 1*, TOC1) expressed genes. RNA scale of *TOC1* is
851 three-fold lower than the scale used for *CCA1* and *CIR1*.
852
853 **Figure 7. Regulation of hypoxic responses by two ERFVII and HSF TF families. a-d** Motif
854 and peak enrichment in the promoter regions (1 kb upstream to 500 bp downstream of the TSS)
855 of genes in clusters identified in Figure 4c for **a**. Hypoxia Responsive Promoter Element
856 (HRPE), **b**. HRE2-ChIP peaks, **c** HRE2-motif, and **d.** Heat Shock sequence Elements (HSE).
857 Frequency of motif and peak occurrence was calculated as number of motifs per number genes
858 in cluster. Clusters with significant enrichment were identified by two-tailed Fisher's exact test p
859 < 0.05. **e**. Genome browser view of select *HRGs* (*PLANT CYSTEINE OXIDASE 2, PCO2*;
860 *CALMODULIN-LIKE 38, CML38*; *LOB-DOMAIN CONTAINING PROTEIN 41, LBD41*; *ALANINE*
861 *AMINO TRANSFERASE 1, AAT1*). The locations of HRE2-ChIP peaks and HRPEs are depicted
862 as a horizontal blue box and vertical red line, respectively. **f**. Average signal of chromatin and
863 RNA readouts for **h,** HRE2 bound genes with coordinate upregulation and **i,** genes with
864 progressive upregulation (cluster 9) containing promoter HSEs. Average signal is plotted from 1
865 kb upstream of the transcription start site (TSS) to 1 kb downstream of the transcript end site
866 (TES).
867
868 **Figure 8. Reaeration promotes accumulation and translation of polyadenylated heat-**
869 **responsive transcripts that are nucleus-enriched under hypoxia. a** Combined violin and
870 boxplot of stress-recovery dynamics of hypoxia-induced nuclear-enriched transcripts (2HS
871 nRNA / 2NS nRNA, $\log_2$ FC > 3, n = 105). All genes shown as a violin; HRGs shown in orange,
872 with *ADH1* as a red dot; RPs shown in blue with *RPL37B* as a blue dot; Heat Shock Element-
873 containing cluster 8_R genes (C8_R, from Supplemental Figure 12) shown in purple. **b**
874 Genome browser view of stress recovery dynamics of *HRGs* (*PCO2*, *ADH1*), heat responsive
875 genes (*HSP70-4*, *HSP20 like*), and a representative *RP* (*RPL37B*). **c** Hierarchical clustering of
876 Heat Shock Element (HSE)-containing cluster 8_R genes in response to hypoxia (2HS/2NS)
877 and reoxygenation (R/2HS).
878
879 **Figure 9. Three patterns of dominant nuclear regulation in response to hypoxic stress of**
880 **two durations and reaeration. (1)** Coordinate upregulation from chromatin to translation of

881 hypoxia responsive genes characterized by hypoxia-triggered H2A.Z eviction, H3K4me3, and
882 H3K9ac elevation. Over half of the genes with this pattern of regulation showed HRE2 binding
883 by chromatin immunopurification. Transcript abundance and translation declines upon
884 reoxygenation. (2) Progressive upregulation of genes associated with heat and oxidative stress
885 responses characterized by a strong 5' bias in histone marks, hypoxia-triggered H2A.Z eviction,
886 H3K9ac elevation, and H3K4me3 reduction. Many are known targets of HSFs. These genes are
887 lowly transcribed under normoxia (nonstress conditions), with evidence of transcriptional
888 activation in response to brief hypoxia (2 h hypoxia) as shown by elevated RNAPII-Ser2P
889 binding, nuclear (nRNA), and ribosome-associated transcripts (TRAP RNA), yet elevation in
890 polyadenylated transcripts (polyA RNA) was limited until the stress was prolonged (9 h
891 hypoxia). Transcript abundance increases upon reoxygenation. (3) Compartmentalized
892 downregulation of many genes associated with growth and photosynthesis, including ribosomal
893 protein genes characterized by maintained RNAPII-Ser2P and nRNA levels under the stress,
894 reduced H3K9ac, and progressive acquisition of H3K14ac. Transcript abundance and
895 translation is restored upon reoxygenation. Cartoons illustrate histone modifications as defined
896 by the key. HRE2, Hypoxia-Responsive ERF 2; HSF, Heat Shock Factor transcriptional
897 activator; Ser2P, RNAPII with the Ser2P modification.
898
899 **Supplemental Figure 1. Expanded overview of the multiscale chromatin and RNA gene**
900 **regulatory analyses. a** Schematic of library types and data analysis performed on 7-day-old
901 seedlings subjected to control (normoxic) (2NS, 9NS) or hypoxic stress (2HS, 9HS) as shown in
902 Figure 1a. Control seedlings were compared to hypoxia stress seedlings independently within
903 each chromatin- and RNA-based dataset. Low abundance reads were filtered (< 2 CPM).
904 Differentially regulated genes were identified and utilized for downstream analyses. The
905 chromatin and RNA datasets were also analyzed in combination. **b-c** Violin plots comparing
906 distribution of genome-wide abundance (reads per kilobase per million reads [RPKM]) of histone
907 and mRNA-related outputs for control (2NS, 9NS) and hypoxic (2HS, 9HS) treatments for all
908 readouts assayed at 2HS **b**, and 9HS **c.** RPKM values for the 49 core hypoxia responsive
909 upregulated genes (HRGs) (Mustroph et al., 2009) are plotted as orange dots. The HRG,
910 *ALCOHOL DEHYDROGENASE 1* (*ADH1*) is tracked as a red line. RPKM values for cytosolic
911 ribosomal proteins (RPs) are plotted in blue, with *RIBOSOMAL PROTEIN 37B* tracked between
912 datasets (blue dashed line). Mean ± SD are depicted within violins as a dark gray dashed line.
913

914 **Supplemental Figure 2. Average signal plots and heat maps for the global distribution of**
915 **reads of chromatin and RNA data. a-h** The genomic region from 1 kb upstream of the
916 transcription start site (TSS) to 1 kb downstream of the transcription end site (TES) is depicted
917 for each histone modification and variant, RNAPII-Ser2P (Ser2P), nuclear RNA (nRNA),
918 polyadenylated RNA (polyA RNA) and ribosome- associated RNA (TRAP RNA) for nonstress
919 (2NS, 9NS) and hypoxia (2HS, 9HS) stressed seedlings. Each heat map ranks genes from the
920 highest signal (top) to the lowest (bottom). Heatmap intensity scale values differ between plots
921 of different readouts and are shown. Blacklisted regions of the genome with disproportionately
922 high reads are tabulated in Supplemental Table 5 and depicted as a black line.
923
924 **Supplemental Figure 3. Multi-level evaluation of histone and gene regulation activity of**
925 **the *HRG*s and *RP*s. a** The average signal profile and read distribution heatmap for *HRG*s (blue)
926 and *RPs* (green) is depicted for each histone dataset and condition. Analysis of the hypoxia
927 responsive genes (*HRG*s) (n=49) and cytosolic ribosomal protein genes (n=223). Each row in
928 the heat map represents an individual gene; gene order is the same in all plots. **b,c** Box plots of
929 $\log_2$ fold change assayed for (**b**) short (2 h) and (**c**) prolonged (9 h) hypoxic stress compared to
930 control (2HS/2NS, 9HS/9NS). Data for *ADH1* is indicated as a red dot and that of *RPL37B* is
931 indicated as a blue dot. Range of dataset and upper and lower quantiles are depicted within
932 each boxplot.
933
934 **Supplemental Figure 4. Evidence of cooperative association between H2A.Z eviction and**
935 **H3K9ac and the relation between Histone H3 modification and RNAPII engagement.** Plots
936 comparing genome-wide changes in histone modifications and RNAP-Ser2P on individual gene
937 bodies in response to hypoxia. **a** Comparison of $\log_2$ fold change (2HS/2NS) values of H3K9ac
938 and H2A.Z association on gene bodies. **b-d** Comparison of $\log_2$ fold change (2HS/2NS) values
939 of (**b**) H3K14ac, (**c**) H3K27me3, and (**d**) H3K4me3 and Ser2P on gene bodies. In all panels,
940 *HRG*s are plotted in pink and *RP*s in green; the Pearson correlation coefficient for all genes is
941 shown and the slope depicted with a blue line.
942
943 **Supplemental Figure 5. Genome-wide comparison of nRNA to polyA RNA demonstrates**
944 **nuclear and cytoplasmic enrichment of transcripts under two conditions. a, b** Scatterplot
945 of normalized read values (per kilobase per million reads; RPKM) on genes in nRNA and polyA
946 RNA populations at (**a**) 2NS and (**b**) 2HS. Transcripts enriched in nRNA (yellow; 2NS: 2,855,
947 2HS: 2,377) or polyA RNA (blue; 2NS: 3,139, 2HS: 4,029) are depicted ($|\log_2 FC > 1|$, $p < 0.05$).

948 *HRG*s and *RP*s are also indicated in pink and green dots, respectively. The genome-wide
949 Pearson correlation coefficient is shown and the slope depicted with a blue line. The red line is a
950 slope of 1. Inserted tables describe representative Gene Ontology categories that are over-
951 represented in nuclear RNA and polyA under the two conditions (data from Supplemental Table
952 2). Many of the same groups of cell component (CC) and molecular (MF) were over-represented
953 in the nRNA and polyA RNA populations obtained in the same manner in rice (Reynoso et al.,
954 2017).
955
956 **Supplemental Figure 6. Distinctions in histones, RNAPII-Ser2P and RNA levels on genes**
957 **that are co-regulated in response to hypoxic stress.** Average signal of chromatin and RNA
958 outputs for clustered genes identified from the 2HS comparison in Figure 4c. Hypoxic sample
959 data are dashed lines. Signal values are plotted from 1 kb upstream of the TSS to 1 kb
960 downstream of the TES. Signal scale of graphs may differ.
961
962 **Supplemental Figure 7. Progressive regulation of variations in gene activity in response**
963 **to hypoxia.** Average signal of chromatin and RNA outputs for clustered genes identified from
964 the 9HS (9HS/9NS) comparison in Figure 4c. Plotting is as described for Supplemental Figure
965 6.
966
967 **Supplemental Figure 8. Histone and gene activity comparisons of genes co-regulated**
968 **after 9 h of hypoxic stress.** Average signal of chromatin and RNA data for co-regulated gene
969 clusters identified from the 9 h hypoxic stress comparison (9HS/9NS) in Figure 6b. Plotting is as
970 described for Supplemental Figure 6.
971
972 **Supplemental Figure 9. Quantitative analysis of dynamics in histone modifications of co-**
973 **regulated gene clusters after 2 h of hypoxic stress. a, c, e** Box plots of $\log_2$ fold change in
974 response to 2 h hypoxic stress of H2A.Z, H3K4me3 and H3K9ac for the 16 clusters shown in
975 Panels **b**, **d**, **f** provide Wilcoxon signed rank test values of gene clusters in an all by all matrix.
976 Grey boxes denote no significant difference between clusters. Heatmap scale depicts
977 significance values of $p < 0.05$.
978
979 **Supplemental Figure 10. Genome-wide binding dynamics of HRE2 determined by ChIP-**
980 **seq. a** Distribution of 1,764 mapped HRE2 peaks on genomic features. **b, c** Average HRE2-
981 ChIP read distribution in regions spanning 1 kb upstream to 1 kb downstream of gene features:

982 **b** genome wide and **c** for the *HRG*s, Coordinately upregulated genes (Co-Up), and Down
983 regulated genes (RGs). **d** Heat map of the HRE2- ChIP reads for genes in each group (*HRG*s)
984 (n=49) and co-UP (n=213, and down-RGs (n=297). Each row in the heat map represents an
985 individual gene; gene order is the same in all plots.
986
987 **Supplemental Figure 11. Genome browser view of normalized read coverage of histone,**
988 **ATAC-seq, RNAPII-Ser2P, HRE2-chromatin immunopurification and RNA outputs for**
989 **representative genes of cluster 9. a-d** Normoxia (2NS) and 2 h hypoxic stress (2HS). **e-h** 9NS
990 and 9HS samples. **a,e** *HEAT SHOCK PROTEIN (HSP) 98-7* **b,f** *HSP70-3,* **c,g** *HEAT SHOCK*
991 *TRANSCRIPTION FACTOR B2B* and **d,h** *ZAT10.* The maximum read scale value used for
992 chromatin based and RNA based outputs is provided. At bottom, the transcription unit is shown
993 in grey with the transcription start site marked with an arrow.
994
995 **Supplemental Figure 12. Reoxygenation following hypoxia promotes global dynamics in**
996 **chromatin accessibility and RNA populations. a** Heatmap showing similarly regulated genes
997 based on dynamics in nRNA, polyA RNA, and TRAP in response to hypoxia (2HS/2NS) and
998 reoxygenation (R/2HS). Partitioning around medoids (PAM) clustering of 4,784 differentially
999 regulated genes; 16 clusters. Selected enriched Gene Ontology terms are shown at right (p adj.
1000 < 1.37E-06), |FC| > 1, FDR < 0.05. **a** number of clusters showed high nRNA at 2 HS that was
1001 not accompanied by high polyA or TRAP mRNA at 2HS clusters 5_R, 8_R, 10_R-13_R). Of
1002 these, cluster 8_R was the only with elevated polyA mRNA at R, suggesting these mRNAs
1003 accumulate to higher levels during reaeration. *HSP70-4* is a member of cluster 5_R. Both
1004 cluster 5_R and cluster 8_R genes are enriched for HSE elements within their promoters
1005 (cluster 5_R 85 of 123 genes have an HSE; cluster 8_R 81 of 153 genes have an HSE). Cluster
1006 14_R is enriched for GOs associated with osmotic and salt stress. These stress-related mRNAs
1007 show preferential TRAP RNA accumulation at R, indicating a preferential translation at at this
1008 time point. **b** Average ATAC-seq read distribution of chromatin accessibility for all protein-
1009 coding genes at three timepoints and distribution of transposase hypersensitive sites on
1010 genomic features for each condition. **c** Dynamic chromatin accessibility in response to
1011 reaeration. 457 up- and 974 downregulated THSs. An increase in accessibility near the TSS
1012 was observed for the *RP*s but neither the *HRG*s nor the HSE-containing genes of cluster 8_R
1013 showed reduced accessibility within this time period. **d** Average signal of chromatin and RNA
1014 readouts for HRGs, RPs, and HSE containing cluster 8_R genes. Average signal is plotted from
1015 1 kb upstream of the transcription start site (TSS) to 1 kb downstream of the transcript end site

1016 (TES). **d** Volcano plot of log_2 fold change in THSs identifiable under 2HS and R conditions and
1017 the significance value of their difference. Genes indicated in pink meet the criteria of log_2 fold
1018 change value > |1|, 0.05 < p. value.
1019
1020
1021 **Supplemental Figure 13. Regulation of variations in gene activity in response to hypoxia**
1022 **and reoxygenation.** Average signal of chromatin and RNA outputs for clustered genes
1023 identified from the reoxygenation (2HS/2NS, R/2HS) comparison in Supplemental Figure 12.
1024 Plotting is as described for Supplemental Figure 6.
1025
1026
1027 **Acknowledgements**

1028 We thank Mauricio Reynoso, Roger Deal, Marko Bajic, Seung-Cho Lee, Maureen Hummel,
1029 Lauren Dedow, Sonja Winte, Jérémie Bazin, Thomas Girke, and Thomas Eulgem for helpful
1030 discussions. This work was supported by U.S. National Science Foundation (Grant Nos.
1031 IOS−1121626, IOS-1238243, MCB-1716913) and the U.S. Department of Agriculture, National
1032 Institute of Food and Agriculture - Agriculture and Food Research Initiative (Grant No.
1033 2011−04015) to J.B.-S.
1034
1035 **Author contributions**
1036 T.L. and J.B.-S. designed research; T.L. performed research; T.L. and J.B.-S. analyzed data;
1037 and T.L. and J.B.-S. wrote the paper.
1038
1039 **References**

1040 **Abbas, M., Berckhan, S., Rooney, D.J., Gibbs, D.J., Vicente Conde, J., Sousa Correia, C.,**
1041 **Bassel, G.W., Marín-de la Rosa, N., León, J., Alabadí, D., Blázquez, M.A., and**
1042 **Holdsworth, M.J.** (2015). Oxygen sensing coordinates photomorphogenesis to facilitate
1043 seedling survival. Curr. Biol. **25**: 1483–1488.

1044 **Andrews, S. and Others** (2010). FastQC: a quality control tool for high throughput sequence
1045 data.

1046 **Ansari, A. and Hampsey, M.** (2005). A role for the CPF 3'-end processing machinery in RNAP
1047 II-dependent gene looping. Genes Dev. **19**: 2969–2978.

1048 **Asensi-Fabado, M.-A., Amtmann, A., and Perrella, G.** (2017). Plant responses to abiotic
1049 stress: The chromatin context of transcriptional regulation. Biochim. Biophys. Acta **1860**:
1050 106–122.

1051 **Bailey, T.L., Boden, M., Buske, F.A., Frith, M., Grant, C.E., Clementi, L., Ren, J., Li, W.W.,**
1052 **and Noble, W.S.** (2009). MEME SUITE: tools for motif discovery and searching. Nucleic
1053 Acids Res. **37**: W202–8.

1054 **Banti, V., Loreti, E., Novi, G., Santaniello, A., Alpi, A., and Perata, P.** (2008). Heat
1055 acclimation and cross-tolerance against anoxia in Arabidopsis. Plant Cell Environ. **31**:
1056 1029–1037.

1057 **Banti, V., Mafessoni, F., Loreti, E., Alpi, A., and Perata, P.** (2010). The heat-inducible
1058 transcription factor HsfA2 enhances anoxia tolerance in Arabidopsis. Plant Physiol. **152**:
1059 1471–1483.

1060 **Batie, M., Frost, J., Frost, M., Wilson, J.W., Schofield, P., and Rocha, S.** (2019). Hypoxia
1061 induces rapid changes to histone methylation and reprograms chromatin. Science **363**:
1062 1222–1226.

1063 **Baxter-Burrell, A., Yang, Z., Springer, P.S., and Bailey-Serres, J.** (2002). RopGAP4-
1064 dependent Rop GTPase rheostat control of Arabidopsis oxygen deprivation tolerance.
1065 Science **296**: 2026–2028.

1066 **Bernd Bischl, Michel Lang, Olaf Mersmann, Jörg Rahnenführer, and Claus Weihs** (2015).
1067 BatchJobs and BatchExperiments&58; Abstraction Mechanisms for Using R in Batch
1068 Environments. J. Stat. Softw. **64**: 1–25.

1069 **Blais, J.D., Filipenko, V., Bi, M., Harding, H.P., Ron, D., Koumenis, C., Wouters, B.G., and**
1070 **Bell, J.C.** (2004). Activating transcription factor 4 is translationally regulated by hypoxic
1071 stress. Mol. Cell. Biol. **24**: 7469–7482.

1072 **Branco-Price, C., Kaiser, K.A., Jang, C.J.H., Larive, C.K., and Bailey-Serres, J.** (2008a).
1073 Selective mRNA translation coordinates energetic and metabolic adjustments to cellular
1074 oxygen deprivation and reoxygenation in Arabidopsis thaliana. Plant J. **56**: 743–755.

1075 **Branco-Price, C., Kaiser, K.A., Jang, C.J.H., Larive, C.K., and Bailey-Serres, J.** (2008b).
1076 Selective mRNA translation coordinates energetic and metabolic adjustments to cellular
1077 oxygen deprivation and reoxygenation in Arabidopsis thaliana. Plant J. **56**: 743–755.

1078 **Branco-Price, C., Kawaguchi, R., Ferreira, R.B., and Bailey-Serres, J.** (2005). Genome-wide
1079 analysis of transcript abundance and translation in Arabidopsis seedlings subjected to
1080 oxygen deprivation. Ann. Bot. **96**: 647–660.

1081 **Buck, M.J., Raaijmakers, L.M., Ramakrishnan, S., Wang, D., Valiyaparambil, S., Liu, S.,**
1082 **Nowak, N.J., and Pili, R.** (2014). Alterations in chromatin accessibility and DNA
1083 methylation in clear cell renal cell carcinoma. Oncogene **33**: 4961–4965.

1084 **Buenrostro, J.D., Giresi, P.G., Zaba, L.C., Chang, H.Y., and Greenleaf, W.J.** (2013).
1085 Transposition of native chromatin for fast and sensitive epigenomic profiling of open
1086 chromatin, DNA-binding proteins and nucleosome position. Nat. Methods **10**: 1213–1218.

1087 **Bui, L.T., Giuntoli, B., Kosmacz, M., Parlanti, S., and Licausi, F.** (2015). Constitutively
1088 expressed ERF-VII transcription factors redundantly activate the core anaerobic response
1089 in Arabidopsis thaliana. Plant Sci. **236**: 37–43.

1090 **Büttner, M. and Singh, K.B.** (1997). Arabidopsis thaliana ethylene-responsive element binding
1091 protein (AtEBP), an ethylene-inducible, GCC box DNA-binding protein interacts with an ocs
1092 element binding protein. Proc. Natl. Acad. Sci. U. S. A. **94**: 5961–5966.

1093 **Cao, J. et al.** (2017). Comprehensive single-cell transcriptional profiling of a multicellular
1094 organism. Science **357**: 661–667.

1095 **Chakraborty, A.A. et al.** (2019). Histone demethylase KDM6A directly senses oxygen to
1096 control chromatin and cell fate. Science **363**: 1217–1222.

1097 **Chang, R., Jang, C.J.H., Branco-Price, C., Nghiem, P., and Bailey-Serres, J.** (2012).
1098 Transient MPK6 activation in response to oxygen deprivation and reoxygenation is
1099 mediated by mitochondria and aids seedling survival in Arabidopsis. Plant Mol. Biol. **78**:
1100 109–122.

1101 **Chervona, Y. and Costa, M.** (2012). The control of histone methylation and gene expression by
1102 oxidative stress, hypoxia, and metals. Free Radic. Biol. Med. **53**: 1041–1047.

1103 **Cortijo, S., Charoensawan, V., Brestovitsky, A., Buning, R., Ravarani, C., Rhodes, D., van**
1104 **Noort, J., Jaeger, K.E., and Wigge, P.A.** (2017). Transcriptional Regulation of the Ambient
1105 Temperature Response by H2A.Z Nucleosomes and HSF1 Transcription Factors in
1106 Arabidopsis. Mol. Plant **10**: 1258–1273.

1107 **Dai, X., Bai, Y., Zhao, L., Dou, X., Liu, Y., Wang, L., Li, Y., Li, W., Hui, Y., Huang, X., Wang,**
1108 **Z., and Qin, Y.** (2017). H2A.Z Represses Gene Expression by Modulating Promoter
1109 Nucleosome Structure and Enhancer Histone Modifications in Arabidopsis. Mol. Plant **10**:
1110 1274–1292.

1111 **Deal, R.B. and Henikoff, S.** (2010). A simple method for gene expression and chromatin
1112 profiling of individual cell types within a tissue. Dev. Cell **18**: 1030–1040.

1113 **Ding, Y., Ndamukong, I., Xu, Z., Lapko, H., Fromm, M., and Avramova, Z.** (2012). ATX1-
1114 generated H3K4me3 is required for efficient elongation of transcription, not initiation, at
1115 ATX1-regulated genes. PLoS Genet. **8**: e1003111.

1116 **van Dongen, J.T. and Licausi, F.** (2015). Oxygen sensing and signaling. Annu. Rev. Plant
1117 Biol. **66**: 345–367.

1118 **Durinck, S. and Huber, W.** biomaRt: Interface to BioMart databases (eg Ensembl, COSMIC,
1119 Wormbase and Gramene). R package version **2**.

1120 **Eberharter, A. and Becker, P.B.** (2002). Histone acetylation: a switch between repressive and
1121 permissive chromatin. Second in review series on chromatin dynamics. EMBO Rep. **3**:
1122 224–229.

1123 **Efroni, I., Han, S.-K., Kim, H.J., Wu, M.-F., Steiner, E., Birnbaum, K.D., Hong, J.C., Eshed,**
1124 **Y., and Wagner, D.** (2013). Regulation of leaf maturation by chromatin-mediated
1125 modulation of cytokinin responses. Dev. Cell **24**: 438–445.

1126 **ENCODE Project Consortium** (2012). An integrated encyclopedia of DNA elements in the
1127 human genome. Nature **489**: 57–74.

1128 **Eysholdt-Derzsó, E. and Sauter, M.** (2017). Root Bending Is Antagonistically Affected by
1129 Hypoxia and ERF-Mediated Transcription via Auxin Signaling. Plant Physiol. **175**: 412–423.

1130 **Fennoy, S.L., Nong, T., and Bailey-Serres, J.** (1998). Transcriptional and post-transcriptional

1131 processes regulate gene expression in oxygen-deprived roots of maize. Plant J. **15**: 727–
1132 735.

1133 **Gasch, P., Fundinger, M., Müller, J.T., Lee, T., Bailey-Serres, J., and Mustroph, A.** (2015).
1134 Redundant ERF-VII transcription factors bind an evolutionarily-conserved cis-motif to
1135 regulate hypoxia-responsive gene expression in Arabidopsis. Plant Cell.

1136 **Gates, L.A., Foulds, C.E., and O'Malley, B.W.** (2017). Histone Marks in the "Driver"s Seat':
1137 Functional Roles in Steering the Transcription Cycle. Trends Biochem. Sci. **42**: 977–989.

1138 **Gibbs, D.J. et al.** (2014). Nitric oxide sensing in plants is mediated by proteolytic control of
1139 group VII ERF transcription factors. Mol. Cell **53**: 369–379.

1140 **Gibbs, D.J., Lee, S.C., Isa, N.M., Gramuglia, S., Fukao, T., Bassel, G.W., Correia, C.S.,**
1141 **Corbineau, F., Theodoulou, F.L., Bailey-Serres, J., and Holdsworth, M.J.** (2011).
1142 Homeostatic response to hypoxia is regulated by the N-end rule pathway in plants. Nature
1143 **479**: 415–418.

1144 **Girke, T.** (2014). systemPipeR: NGS workflow and report generation environment. UC
1145 Riverside. https://github. com/tgirke/systemPipeR.

1146 **Giuntoli, B., Lee, S.C., Licausi, F., Kosmacz, M., Oosumi, T., van Dongen, J.T., Bailey-**
1147 **Serres, J., and Perata, P.** (2014). A trihelix DNA binding protein counterbalances hypoxia-
1148 responsive transcriptional activation in Arabidopsis. PLoS Biol. **12**: e1001950.

1149 **Giuntoli, B., Licausi, F., van Veen, H., and Perata, P.** (2017). Functional Balancing of the
1150 Hypoxia Regulators RAP2.12 and HRA1 Takes Place in vivo in Arabidopsis thaliana Plants.
1151 Front. Plant Sci. **8**: 591.

1152 **Giuntoli, B. and Perata, P.** (2017). Group VII Ethylene Response Factors in Arabidopsis:
1153 regulation and physiological roles. Plant Physiol.

1154 **Gonzali, S., Loreti, E., Cardarelli, F., Novi, G., Parlanti, S., Pucciariello, C., Bassolino, L.,**
1155 **Banti, V., Licausi, F., and Perata, P.** (2015). Universal stress protein HRU1 mediates
1156 ROS homeostasis under anoxia. Nat Plants **1**: 15151.

1157 **Gordon, A. and Hannon, G.J.** (2010). Fastx-toolkit. FASTQ/A short-reads preprocessing tools
1158 (unpublished) http://hannonlab. cshl. edu/fastx_toolkit **5**.

1159 **Hajheidari, M., Koncz, C., and Eick, D.** (2013). Emerging roles for RNA polymerase II CTD in
1160 Arabidopsis. Trends Plant Sci. **18**: 633–643.

1161 **Hattori, Y. et al.** (2009). The ethylene response factors SNORKEL1 and SNORKEL2 allow rice
1162 to adapt to deep water. Nature **460**: 1026–1030.

1163 **Heinz, S., Benner, C., Spann, N., Bertolino, E., Lin, Y.C., Laslo, P., Cheng, J.X., Murre, C.,**
1164 **Singh, H., and Glass, C.K.** (2010). Simple combinations of lineage-determining
1165 transcription factors prime cis-regulatory elements required for macrophage and B cell
1166 identities. Mol. Cell **38**: 576–589.

1167 **Hetzel, J., Duttke, S.H., Benner, C., and Chory, J.** (2016). Nascent RNA sequencing reveals
1168 distinct features in plant transcription. Proc. Natl. Acad. Sci. U. S. A. **113**: 12316–12321.

1169 **Jonkers, I. and Lis, J.T.** (2015). Getting up to speed with transcription elongation by RNA
1170 polymerase II. Nat. Rev. Mol. Cell Biol. **16**: 167–177.

1171 **Juntawong, P., Girke, T., Bazin, J., and Bailey-Serres, J.** (2014). Translational dynamics
1172 revealed by genome-wide profiling of ribosome footprints in Arabidopsis. Proc. Natl. Acad.
1173 Sci. U. S. A. **111**: E203–12.

1174 **Karmodiya, K., Krebs, A.R., Oulad-Abdelghani, M., Kimura, H., and Tora, L.** (2012). H3K9
1175 and H3K14 acetylation co-occur at many gene regulatory elements, while H3K14ac marks
1176 a subset of inactive inducible promoters in mouse embryonic stem cells. BMC Genomics
1177 **13**: 424.

1178 **Kim, D., Pertea, G., Trapnell, C., Pimentel, H., Kelley, R., and Salzberg, S.L.** (2013).
1179 TopHat2: accurate alignment of transcriptomes in the presence of insertions, deletions and
1180 gene fusions. Genome Biol. **14**: R36.

1181 **Kim, J.-M., To, T.K., Ishida, J., Matsui, A., Kimura, H., and Seki, M.** (2012). Transition of
1182 chromatin status during the process of recovery from drought stress in Arabidopsis
1183 thaliana. Plant Cell Physiol. **53**: 847–856.

1184 **Kim, J.-M., To, T.K., Ishida, J., Morosawa, T., Kawashima, M., Matsui, A., Toyoda, T.,**
1185 **Kimura, H., Shinozaki, K., and Seki, M.** (2008). Alterations of lysine modifications on the
1186 histone H3 N-tail under drought stress conditions in Arabidopsis thaliana. Plant Cell
1187 Physiol. **49**: 1580–1588.

1188 **Kim, S.-H., Jeong, J.-W., Park, J.A., Lee, J.-W., Seo, J.H., Jung, B.-K., Bae, M.-K., and Kim,**
1189 **K.-W.** (2007). Regulation of the HIF-1α stability by histone deacetylases. Oncol. Rep. **17**:
1190 647–651.

1191 **Kolde, R.** (2012). Pheatmap: pretty heatmaps. R package version **61**.

1192 **Koroleva, O.A., Calder, G., Pendle, A.F., Kim, S.H., Lewandowska, D., Simpson, C.G.,**
1193 **Jones, I.M., Brown, J.W.S., and Shaw, P.J.** (2009). Dynamic behavior of Arabidopsis
1194 eIF4A-III, putative core protein of exon junction complex: fast relocation to nucleolus and
1195 splicing speckles under hypoxia. Plant Cell **21**: 1592–1606.

1196 **Kosmacz, M., Parlanti, S., Schwarzländer, M., Kragler, F., Licausi, F., and Van Dongen,**
1197 **J.T.** (2015). The stability and nuclear localization of the transcription factor RAP2.12 are
1198 dynamically regulated by oxygen concentration. Plant Cell Environ. **38**: 1094–1103.

1199 **Krijthe, J.H.** (2015). Rtsne: T-distributed stochastic neighbor embedding using Barnes-Hut
1200 implementation. R package version 0. 13, URL https://github. com/jkrijthe/Rtsne.

1201 **Krzywinski, M., Schein, J., Birol, I., Connors, J., Gascoyne, R., Horsman, D., Jones, S.J.,**
1202 **and Marra, M.A.** (2009). Circos: an information aesthetic for comparative genomics.
1203 Genome Res. **19**: 1639–1645.

1204 **Kumar, R., Ichihashi, Y., Kimura, S., Chitwood, D.H., Headland, L.R., Peng, J., Maloof,**
1205 **J.N., and Sinha, N.R.** (2012). A High-Throughput Method for Illumina RNA-Seq Library
1206 Preparation. Front. Plant Sci. **3**: 202.

1207 **Kumar, S.V.** (2018). H2A.Z at the Core of Transcriptional Regulation in Plants. Mol. Plant **11**:
1208 1112–1114.

1209 **Kumar, S.V. and Wigge, P.A.** (2010). H2A.Z-containing nucleosomes mediate the
1210 thermosensory response in Arabidopsis. Cell **140**: 136–147.

1211 **Kwak, H. and Lis, J.T.** (2013). Control of transcriptional elongation. Annu. Rev. Genet. **47**:
1212 483–508.

1213 **LaGory, E.L. and Giaccia, A.J.** (2016). The ever-expanding role of HIF in tumour and stromal
1214 biology. Nat. Cell Biol. **18**: 356–365.

1215 **Lawrence, M., Gentleman, R., and Carey, V.** (2009). rtracklayer: an R package for interfacing

1216 with genome browsers. Bioinformatics **25**: 1841–1842.

1217 **Lawrence, M., Huber, W., Pagès, H., Aboyoun, P., Carlson, M., Gentleman, R., Morgan,**
1218 **M.T., and Carey, V.J.** (2013). Software for computing and annotating genomic ranges.
1219 PLoS Comput. Biol. **9**: e1003118.

1220 **Licausi, F., Kosmacz, M., Weits, D.A., Giuntoli, B., Giorgi, F.M., Voesenek, L.A.C.J.,**
1221 **Perata, P., and van Dongen, J.T.** (2011). Oxygen sensing in plants is mediated by an N-
1222 end rule pathway for protein destabilization. Nature **479**: 419–422.

1223 **Licausi, F., Van Dongen, J.T., Giuntoli, B., Novi, G., Santaniello, A., Geigenberger, P., and**
1224 **Perata, P.** (2010). HRE1 and HRE2, two hypoxia-inducible ethylene response factors,
1225 affect anaerobic responses in Arabidopsis thaliana. Plant J. **62**: 302–315.

1226 **Li, H.** (2011). A statistical framework for SNP calling, mutation discovery, association mapping
1227 and population genetical parameter estimation from sequencing data. Bioinformatics **27**:
1228 2987–2993.

1229 **Lokdarshi, A., Conner, W.C., McClintock, C., Li, T., and Roberts, D.M.** (2016). Arabidopsis
1230 CML38, a Calcium Sensor That Localizes to Ribonucleoprotein Complexes under Hypoxia
1231 Stress. Plant Physiol. **170**: 1046–1059.

1232 **de Lorenzo, L., Sorenson, R., Bailey-Serres, J., and Hunt, A.G.** (2017). Noncanonical
1233 Alternative Polyadenylation Contributes to Gene Regulation in Response to Hypoxia. Plant
1234 Cell **29**: 1262–1277.

1235 **Loreti, E., Poggi, A., Novi, G., Alpi, A., and Perata, P.** (2005). A genome-wide analysis of the
1236 effects of sucrose on gene expression in Arabidopsis seedlings under anoxia. Plant
1237 Physiol. **137**: 1130–1138.

1238 **Lu, Z., Hofmeister, B.T., Vollmers, C., DuBois, R.M., and Schmitz, R.J.** (2016). Combining
1239 ATAC-seq with nuclei sorting for discovery of cis-regulatory regions in plant genomes.
1240 Nucleic Acids Res.

1241 **Maechler, M.** (2018). Finding Groups in Data'': Cluster Analysis Extended Rousseeuw et.
1242 Documentation for software package. The Comprehensive R Archive Network (CRAN):
1243 Wien.

1244 **Maher, K.A. et al.** (2018). Profiling of Accessible Chromatin Regions across Multiple Plant
1245 Species and Cell Types Reveals Common Gene Regulatory Principles and New Control
1246 Modules. Plant Cell **30**: 15–36.

1247 **McCarthy, D.J., Chen, Y., and Smyth, G.K.** (2012). Differential expression analysis of
1248 multifactor RNA-Seq experiments with respect to biological variation. Nucleic Acids Res.
1249 **40**: 4288–4297.

1250 **Meyer, D., Dimitriadou, E., Hornik, K., Weingessel, A., and Leisch, F.** (2015). e1071: Misc
1251 Functions of the Department of Statistics (e1071), TU Wien, 2014. R package version: 1–6.

1252 **Millar, A.H., Heazlewood, J.L., Giglione, C., Holdsworth, M.J., Bachmair, A., and Schulze,**
1253 **W.X.** (2019). The Scope, Functions, and Dynamics of Posttranslational Protein
1254 Modifications. Annu. Rev. Plant Biol. **70**: 119–151.

1255 **Milligan, L., Huynh-Thu, V.A., Delan-Forino, C., Tuck, A., Petfalski, E., Lombraña, R.,**
1256 **Sanguinetti, G., Kudla, G., and Tollervey, D.** (2016). Strand-specific, high-resolution
1257 mapping of modified RNA polymerase II. Mol. Syst. Biol. **12**: 874.

1258 **Morgan, M., Anders, S., Lawrence, M., Aboyoun, P., Pagès, H., and Gentleman, R.** (2009).
1259 ShortRead: a bioconductor package for input, quality assessment and exploration of high-
1260 throughput sequence data. Bioinformatics **25**: 2607–2608.

1261 **Morgan, M., Carey, V., and Lawrence, M.** (2014). BiocParallel: Bioconductor facilities for
1262 parallel evaluation. R package version 0. 4 **1**.

1263 **Morgan, M., Pages, H., Obenchain, V., and Hayden, N.** (2016). Rsamtools: Binary alignment
1264 (BAM), FASTA, variant call (BCF), and tabix file import. R package version **1**.

1265 **Mustroph, A., Lee, S.C., Oosumi, T., Zanetti, M.E., Yang, H., Ma, K., Yaghoubi-Masihi, A.,**
1266 **Fukao, T., and Bailey-Serres, J.** (2010). Cross-kingdom comparison of transcriptomic
1267 adjustments to low-oxygen stress highlights conserved and plant-specific responses. Plant
1268 Physiol. **152**: 1484–1500.

1269 **Mustroph, A., Zanetti, M.E., Jang, C.J.H., Holtan, H.E., Repetti, P.P., Galbraith, D.W., Girke,**
1270 **T., and Bailey-Serres, J.** (2009). Profiling translatomes of discrete cell populations
1271 resolves altered cellular priorities during hypoxia in Arabidopsis. Proc. Natl. Acad. Sci. U. S.
1272 A. **106**: 18843–18848.

1273 **Neuwirth, E.** (2011). RColorBrewer: colorbrewer palettes. R package version **1**.

1274 **Niedojadło, J., Dełeńko, K., and Niedojadło, K.** (2016). Regulation of poly(A) RNA retention in
1275 the nucleus as a survival strategy of plants during hypoxia. RNA Biol. **13**: 531–543.

1276 **O'Malley, R.C., Huang, S.-S.C., Song, L., Lewsey, M.G., Bartlett, A., Nery, J.R., Galli, M.,**
1277 **Gallavotti, A., and Ecker, J.R.** (2016). Cistrome and Epicistrome Features Shape the
1278 Regulatory DNA Landscape. Cell **166**: 1598.

1279 **Ozsolak, F., Poling, L.L., Wang, Z., Liu, H., Liu, X.S., Roeder, R.G., Zhang, X., Song, J.S.,**
1280 **and Fisher, D.E.** (2008). Chromatin structure analyses identify miRNA promoters. Genes
1281 Dev. **22**: 3172–3183.

1282 **Paul, M.V., Iyer, S., Amerhauser, C., Lehmann, M., van Dongen, J.T., and Geigenberger, P.**
1283 (2016). Oxygen Sensing via the Ethylene Response Transcription Factor RAP2.12 Affects
1284 Plant Metabolism and Performance under Both Normoxia and Hypoxia. Plant Physiol. **172**:
1285 141–153.

1286 **Phatnani, H.P. and Greenleaf, A.L.** (2006). Phosphorylation and functions of the RNA
1287 polymerase II CTD. Genes Dev. **20**: 2922–2936.

1288 **Pucciariello, C., Parlanti, S., Banti, V., Novi, G., and Perata, P.** (2012). Reactive oxygen
1289 species-driven transcription in Arabidopsis under oxygen deprivation. Plant Physiol. **159**:
1290 184–196.

1291 **Quinlan, A.R. and Hall, I.M.** (2010). BEDTools: a flexible suite of utilities for comparing
1292 genomic features. Bioinformatics **26**: 841–842.

1293 **Ramírez, F., Ryan, D.P., Grüning, B., Bhardwaj, V., Kilpert, F., Richter, A.S., Heyne, S.,**
1294 **Dündar, F., and Manke, T.** (2016). deepTools2: a next generation web server for deep-
1295 sequencing data analysis. Nucleic Acids Res. **44**: W160–5.

1296 **Reynoso, M., Pauluzzi, G., Kajala, K., Cabanlit, S., Velasco, J., Bazin, J., Deal, R., Sinha,**
1297 **N., Brady, S.M., and Bailey-Serres, J.** (2017). Nuclear transcriptomes at high resolution
1298 using retooled INTACT. Plant Physiol.

1299 **Sato, F., Kitajima, S., and Koyama, T.** (1996). Ethylene-induced gene expression of osmotin-
1300 like protein, a neutral isoform of tobacco PR-5, is mediated by the AGCCGCC eft-

1301 sequence. Plant Cell Physiol. **37**: 249–255.

1302 **Sijacic, P., Bajic, M., McKinney, E.C., Meagher, R.B., and Deal, R.B.** (2017). Chromatin
1303 accessibility changes between Arabidopsis stem cells and mesophyll cells illuminate cell
1304 type-specific transcription factor networks. bioRxiv: 213900.

1305 **Sorenson, R. and Bailey-Serres, J.** (2014). Selective mRNA sequestration by
1306 OLIGOURIDYLATE-BINDING PROTEIN 1 contributes to translational control during
1307 hypoxia in Arabidopsis. Proc. Natl. Acad. Sci. U. S. A. **111**: 2373–2378.

1308 **Sullivan, A.M. et al.** (2014). Mapping and dynamics of regulatory DNA and transcription factor
1309 networks in A. thaliana. Cell Rep. **8**: 2015–2030.

1310 **Sura, W., Kabza, M., Karlowski, W.M., Bieluszewski, T., Kus-Slowinska, M., Pawełoszek,**
1311 **Ł., Sadowski, J., and Ziolkowski, P.A.** (2017). Dual Role of the Histone Variant H2A.Z in
1312 Transcriptional Regulation of Stress-Response Genes. Plant Cell **29**: 791–807.

1313 **Talbert, P.B. and Henikoff, S.** (2017). Histone variants on the move: substrates for chromatin
1314 dynamics. Nat. Rev. Mol. Cell Biol. **18**: 115–126.

1315 **Torres, E.S. and Deal, R.B.** (2018). The histone variant H2A. Z and chromatin remodeler
1316 BRAHMA act coordinately and antagonistically to regulate transcription and nucleosome
1317 dynamics in Arabidopsis. bioRxiv: 243790.

1318 **Townsley, B.T., Covington, M.F., Ichihashi, Y., Zumstein, K., and Sinha, N.R.** (2015). BrAD-
1319 seq: Breath Adapter Directional sequencing: a streamlined, ultra-simple and fast library
1320 preparation protocol for strand specific mRNA library construction. Front. Plant Sci. **6**: 366.

1321 **Van Veen, H., Vashisht, D., Akman, M., and Girke, T.** (2016). Transcriptomes of eight
1322 Arabidopsis thaliana accessions reveal core conserved, genotype-and organ-specific
1323 responses to flooding stress. Plant.

1324 **Voesenek, L.A.C.J. and Bailey-Serres, J.** (2013). Flooding tolerance: O2 sensing and survival
1325 strategies. Curr. Opin. Plant Biol. **16**: 647–653.

1326 **Warnes, G.R., Bolker, B., Bonebakker, L., Gentleman, R., Huber, W., Liaw, A., Lumley, T.,**
1327 **Maechler, M., Magnusson, A., Moeller, S., and Others** (2009). gplots: Various R
1328 programming tools for plotting data. R package version **2**: 1.

1329 **Watson, J.A., Watson, C.J., McCann, A., and Baugh, J.** (2010). Epigenetics, the epicenter of
1330 the hypoxic response. Epigenetics **5**: 293–296.

1331 **Weits, D.A., Giuntoli, B., Kosmacz, M., Parlanti, S., Hubberten, H.-M., Riegler, H., Hoefgen,**
1332 **R., Perata, P., van Dongen, J.T., and Licausi, F.** (2014). Plant cysteine oxidases control
1333 the oxygen-dependent branch of the N-end-rule pathway. Nat. Commun. **5**: 3425.

1334 **White, M.D. et al.** (2017). Plant cysteine oxidases are dioxygenases that directly enable arginyl
1335 transferase-catalysed arginylation of N-end rule targets. Nat. Commun. **8**: 14690.

1336 **Wickham, H.** (2009). ggplot2: Elegant Graphics for Data Analysis (Springer Science & Business
1337 Media).

1338 **Wickham, H. and Francois, R.** (2015). dplyr: A grammar of data manipulation. R package
1339 version 0. 4 **3**.

1340 **Xu, K., Xu, X., Fukao, T., Canlas, P., Maghirang-Rodriguez, R., Heuer, S., Ismail, A.M.,**
1341 **Bailey-Serres, J., Ronald, P.C., and Mackill, D.J.** (2006). Sub1A is an ethylene-response-
1342 factor-like gene that confers submergence tolerance to rice. Nature **442**: 705–708.

1343 **Yang, C.-Y., Hsu, F.-C., Li, J.-P., Wang, N.-N., and Shih, M.-C.** (2011). The AP2/ERF
1344 transcription factor AtERF73/HRE1 modulates ethylene responses during hypoxia in
1345 Arabidopsis. Plant Physiol. **156**: 202–212.

1346 **Yang, W., Wightman, R., and Meyerowitz, E.M.** (2017). Cell Cycle Control by Nuclear
1347 Sequestration of CDC20 and CDH1 mRNA in Plant Stem Cells. Mol. Cell **68**: 1108–
1348 1119.e3.

1349 **Yeung, E. et al.** (2018). A stress recovery signaling network for enhanced flooding tolerance in
1350 Arabidopsis thaliana. Proc. Natl. Acad. Sci. U. S. A. **115**: E6085–E6094.

1351 **Young, R.M., Wang, S.-J., Gordan, J.D., Ji, X., Liebhaber, S.A., and Simon, M.C.** (2008).
1352 Hypoxia-mediated selective mRNA translation by an internal ribosome entry site-
1353 independent mechanism. J. Biol. Chem. **283**: 16309–16319.

1354 **Yu, G., Wang, L.-G., Han, Y., and He, Q.-Y.** (2012). clusterProfiler: an R package for
1355 comparing biological themes among gene clusters. OMICS **16**: 284–287.

1356 **Yu, G., Wang, L.-G., and He, Q.-Y.** (2015). ChIPseeker: an R/Bioconductor package for ChIP

1357 peak annotation, comparison and visualization. Bioinformatics **31**: 2382–2383.

1358 **Zanetti, M.E., Chang, I.-F., Gong, F., Galbraith, D.W., and Bailey-Serres, J.** (2005).
1359 Immunopurification of polyribosomal complexes of Arabidopsis for global analysis of gene
1360 expression. Plant Physiol. **138**: 624–635.

1361 **Zhou, J., Wang, X., He, K., Charron, J.-B.F., Elling, A.A., and Deng, X.W.** (2010). Genome-
1362 wide profiling of histone H3 lysine 9 acetylation and dimethylation in Arabidopsis reveals
1363 correlation between multiple histone marks and gene expression. Plant Mol. Biol. **72**: 585–
1364 595.

1365 **Zhu, J., Liu, M., Liu, X., and Dong, Z.** (2018). RNA polymerase II activity revealed by GRO-seq
1366 and pNET-seq in Arabidopsis. Nat Plants.

1367 **Zid, B.M. and O'Shea, E.K.** (2014). Promoter sequences direct cytoplasmic localization and
1368 translation of mRNAs during starvation in yeast. Nature **514**: 117–121.

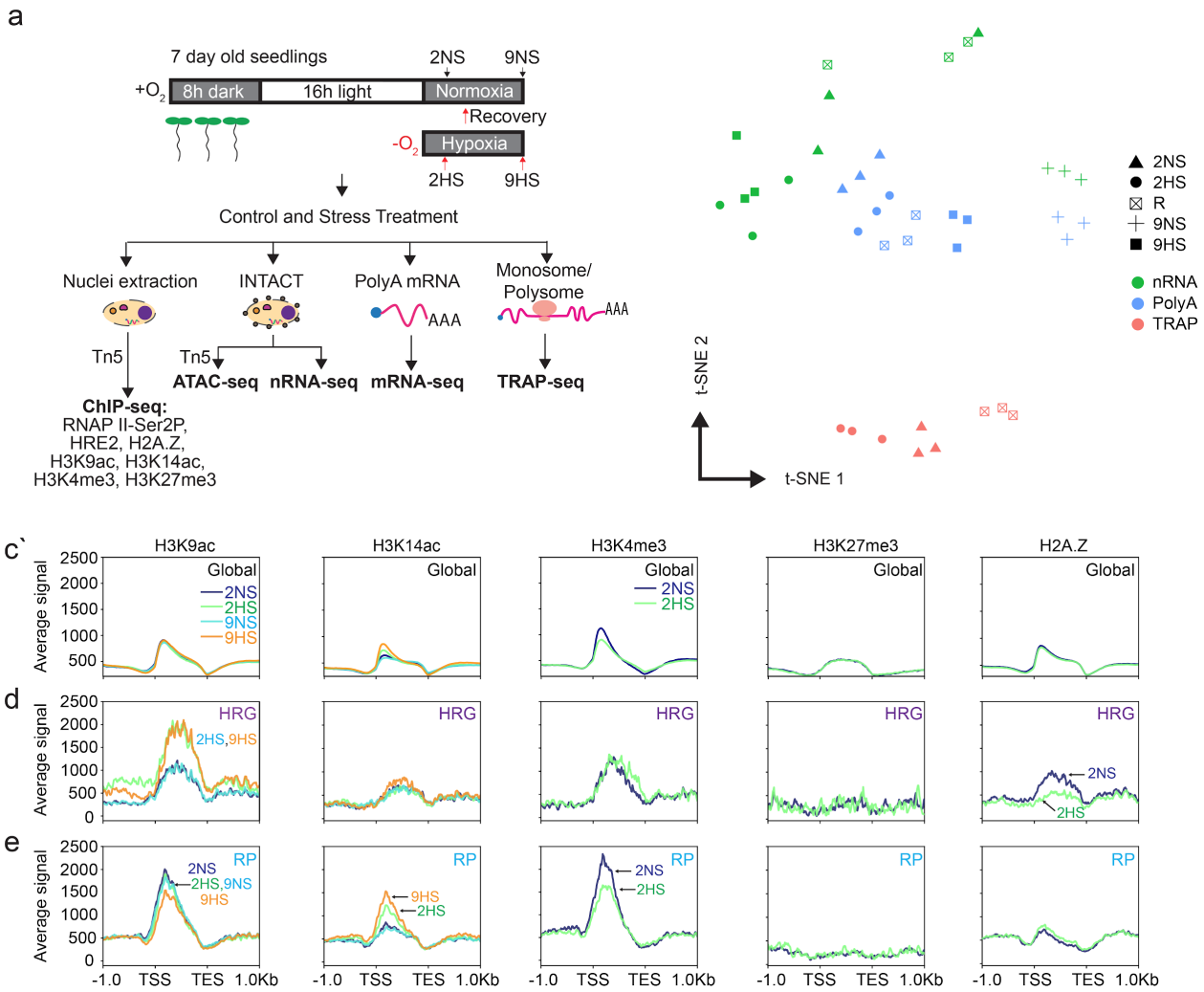

Figure 1. Multiscale chromatin and RNA gene regulatory analyses of control (normoxic) and hypoxic seedlings of *Arabidopsis*. a Schematic of experiments performed. Seven-day-old seedlings were subjected to control (normoxic) (2NS, 9NS), hypoxic stress (2HS, 9HS), or re-oxygenation following 2HS (R) conditions. Vertical arrows indicate time of harvest. Chromatin immunopurification (ChIP) was performed to evaluate genomic regions bound by the Ser2 phospho-isoform of RNA Polymerase II (Ser2P), the Histone 2 variant H2A.Z, modified Histone 3 (H3K4me3, H3K27me3, H3K9ac, H3K14ac), and the group VII Ethylene Responsive Factor (ERF) transcription factor HYPOXIA RESPONSIVE ERF 2 (HRE2). Isolation of Nuclei TAgged in specific Cell Types (INTACT) purified nuclei were used for Assay for Transposase Accessible Chromatin (ATAC) and purification of nuclear RNA. Ribosome-associated mRNA was obtained by Translating Ribosome Affinity Purification (TRAP). **b** Individual replicate samples of nuclear [nRNA], polyadenylated mRNA [polyA] and ribosome-associated polyA mRNA [TRAP]) were compared by t-Distributed stochastic neighbor embedding (t-SNE). **c-e** Distributions of histone modifications/variants across genic regions **c**, for the core hypoxia responsive genes (*HRG*s, *n*=49) **d,** and cytosolic ribosomal proteins (*RP*s, *n*=246) **e**. Read distributions are plotted from 1 kb upstream to 1 kb downstream of gene units defined by the transcription start site (TSS) and transcription end site (TES).

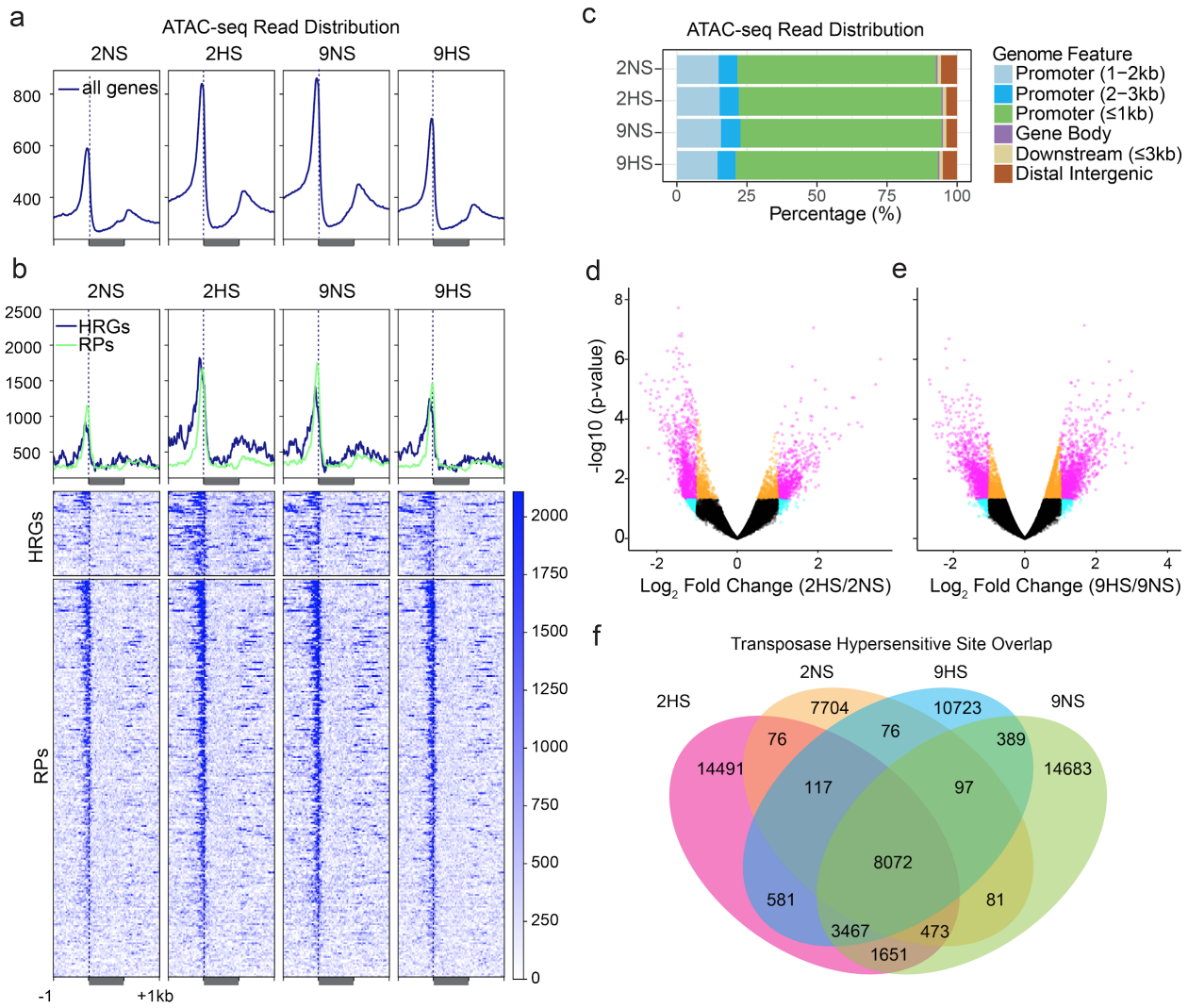

Figure 2. Regions of chromatin accessibility determined by Assay of Transposase-Accessible Chromatin using sequencing (ATAC-seq) are dynamically regulated by hypoxic stress. a-b Average ATAC-seq read distribution of chromatin accessibility for protein-coding genes (**a**), HRGs and RPs (**b**). **c** Distribution of transposase hypersensitive sites (THSs) on genomic features for each condition. **d-e** Volcano plot of the $\log_2$ fold change in THSs identifiable under two conditions and the significance value of their difference. Genes indicated in pink meet the criteria of $\log_2$ fold change value > |1|, 0.05 < p. value. **f** Overlap in THSs identified for each of four conditions.

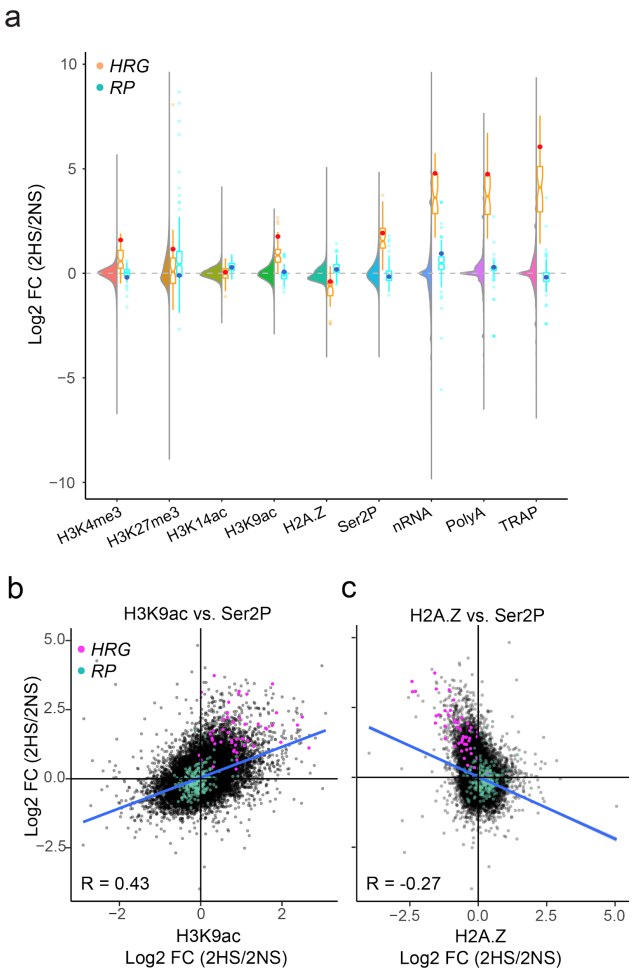

Figure 3. Short term hypoxic stress promotes pronounced changes in chromatin, transcription and nascent transcripts that are not uniformly reflected in transcript steady-state abundance or translation. Comparison of genome-wide data for chromatin and RNA for 2 h hypoxic stress (2HS) relative to the normoxic control (2NS). **a** Combined violin and boxplot of $\log_2$ fold change (2HS/2NS) of histone, RNAPII-Ser2P and RNA outputs. Violin, all genes; boxplot for the *HRG*s plotted in orange with *ALCOHOL DEHYDROGENASE 1* (*ADH1*) depicted as a red dot and the cytosolic *RP*s plotted in blue, with *RIBOSOMAL PROTEIN 37B* depicted as a dark blue dot. **b** Comparison of $\log_2$ fold change (2HS/2NS) between H2A.Z on the gene body and Ser2P on the gene body. **c** Comparison of $\log_2$ fold change (FC) (2HS/2NS) between H3K9ac and Ser2P on the gene body. For b and c, *HRG*s are plotted in pink and *RP*s in blue; Pearson's coefficient of determination is shown for all genes.

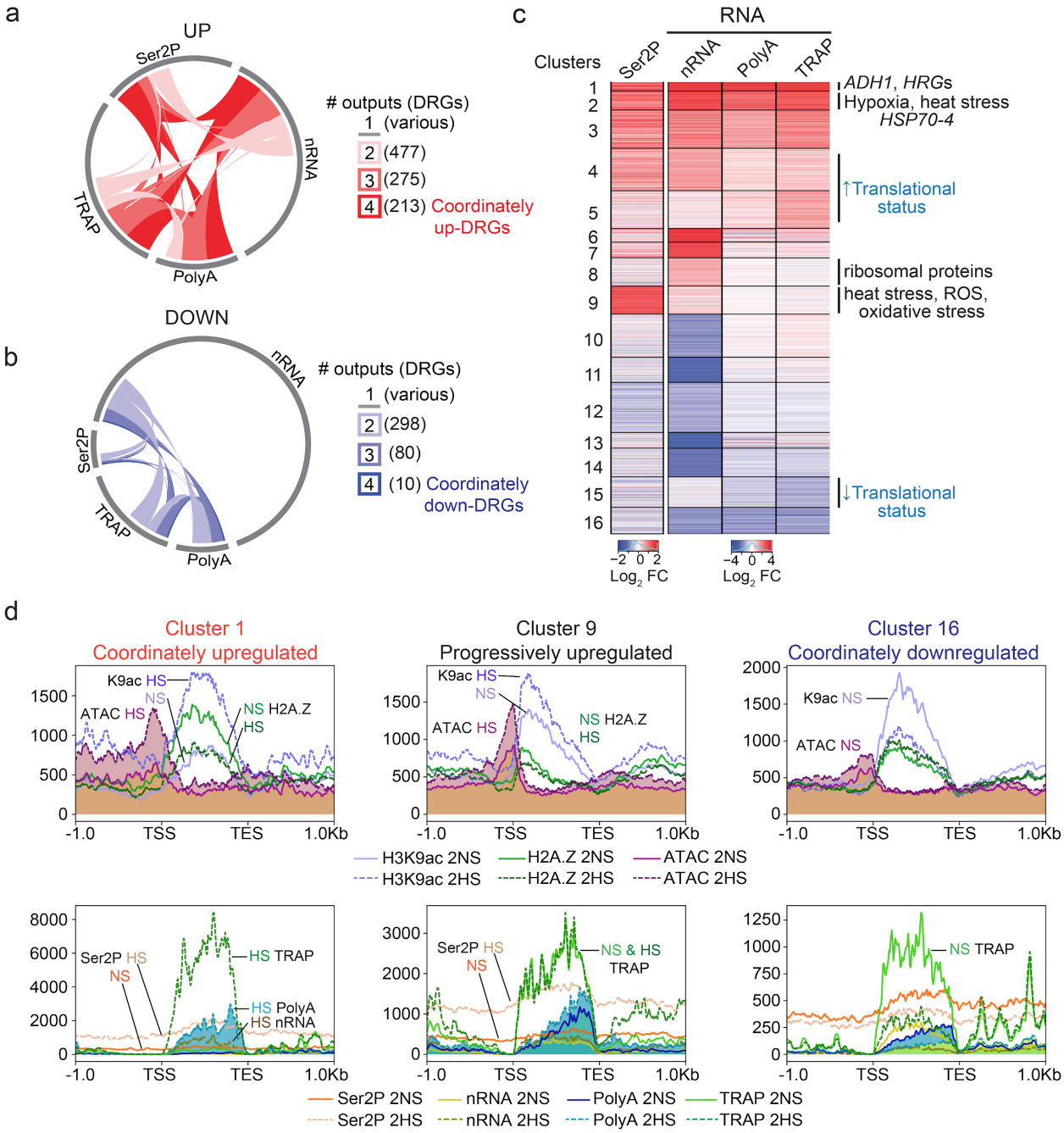

Figure 4. Multi-scale analysis of hypoxia-regulated genes reveals concordant and discordant patterns of gene regulation. Number of **a** up- and **b** down-differentially regulated genes (DRGs) in response to 2 h of hypoxic stress (|$\log_2$ fold change (FC)| > 1; False Discovery Rate (FDR) < 0.05) identified in each of the four readouts related to RNA: Ser2P ChIP, nRNA, polyA RNA, and TRAP RNA. Arc of circle circumference indicated by the grey line represents the DRGs in each of the four readouts. Genes differentially regulated in 2 to 4 readouts were tabulated (number in parentheses) and depicted by links within the circle. Genes differentially regulated in only one readout are represented by unlinked grey lines. **c** Heatmap showing similarly regulated genes based on four assays of gene activity. Partitioning

1413 around medoids clustering of 3,042 DRGs; 16 clusters. Selected enriched Gene Ontology terms are
1414 shown at right (p adj. < 1.47e-09), |FC| > 1, FDR < 0.05. Clusters displaying increased or decreased
1415 translational status (ribosome-associated [TRAP] relative to total abundance [polyA]) are shown. **d**
1416 Average signal of various chromatin and RNA outputs for genes of three clusters plotted from 1 kb
1417 upstream of the transcription start site (TSS) to 1 kb downstream of the transcript end site (TES) for the 2
1418 h (2NS, 2HS) timepoints. Signal scale of graphs differ. Dashed lines used to plot hypoxic stress data.
1419 Upper panel, ATAC-seq data shaded. Lower panel 2HS polyA data shaded.

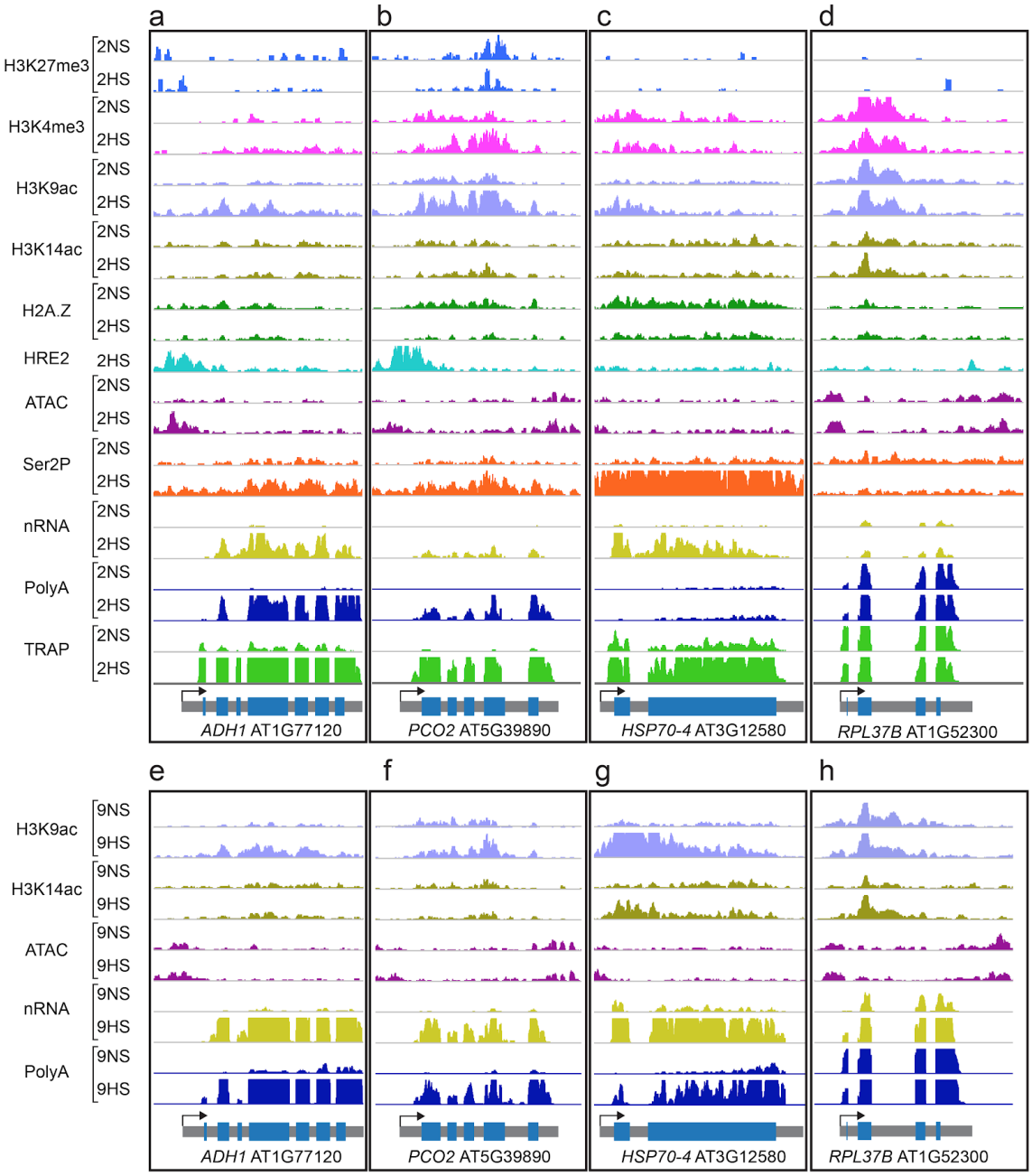

Figure 5. Genome browser view of normalized read coverage of histone, ATAC-seq, RNAPII-Ser2P, HRE2-chromatin immunopurification and RNA outputs for representative genes. a-d Normoxia (2NS) and 2 h hypoxic stress (2HS). **e-h** Normoxia (9NS) and 9 h hypoxia stress (9HS) samples. **a,e** *ALCOHOL DEHYDROGENASE 1* (*ADH1*), **b,f** *PLANT CYSTEINE OXIDASE 2* (*PCO2*), **c,g** *HEAT SHOCK PROTEIN 70-4* (*HSP70-4*) and **d,h** *RIBOSOMAL PROTEIN L37B* (*RPL37B*). The maximum read scale value used for chromatin based and RNA based outputs is equivalent for all genes depicted. At bottom, the transcription unit is shown in grey with the transcription start site marked with an arrow. *PCO2* shows a stronger decline in H2A.Z than *ADH1* in response to hypoxia at 2HS (*PCO2*, -1.15 $\log_2$ FC; *ADH1*, -0.33 $\log_2$ FC) and provides an example of elevated H3K4me3 under hypoxic stress.

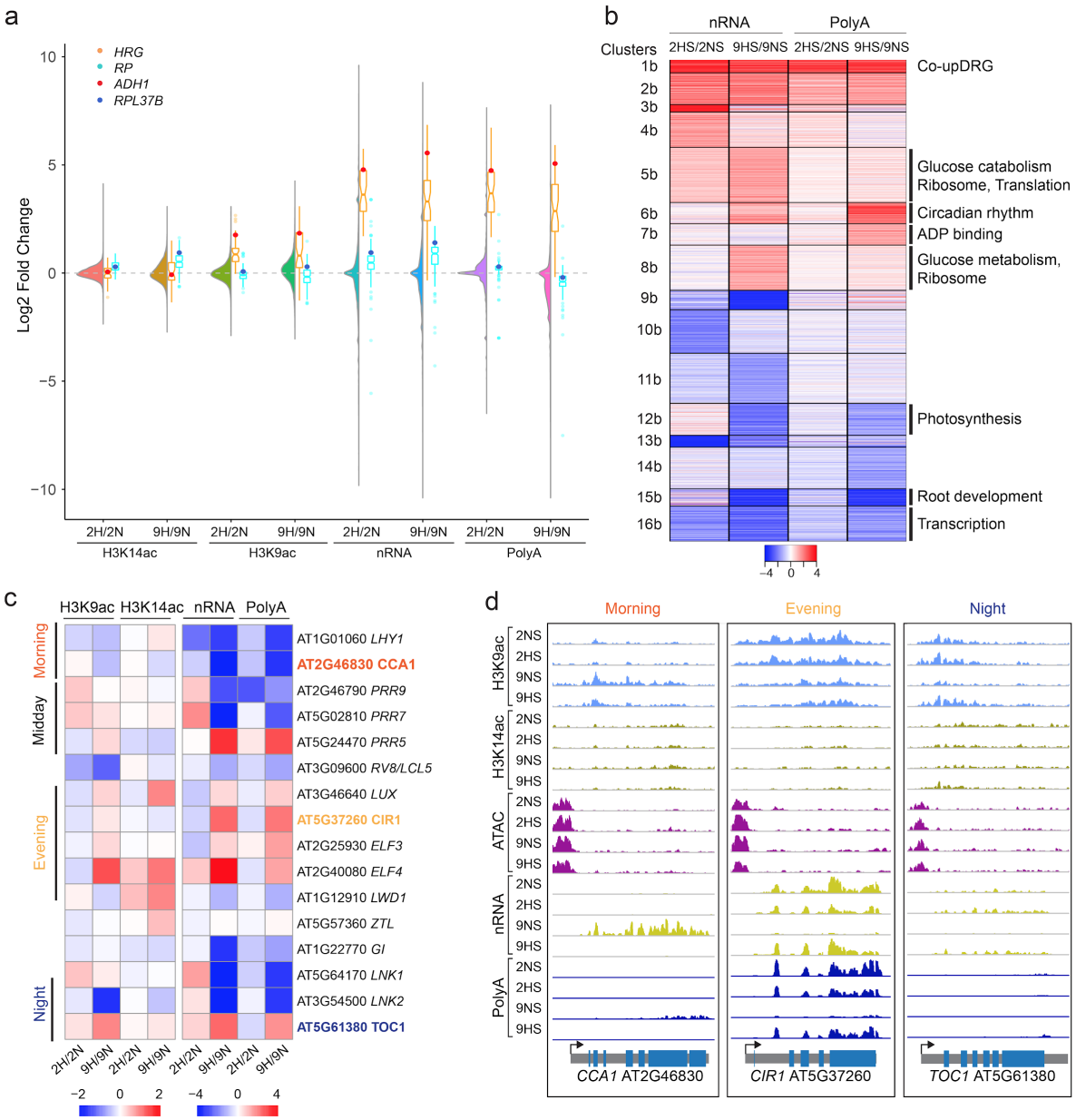

Figure 6. Prolonged hypoxia leads to further variation in epigenetic, transcriptional and posttranscriptional regulation. a Combined violin and boxplot of H3K9ac and H3K14ac, nRNA, and polyA RNA data. Violin plots of $\log_2$ fold change (9HS/9NS) data for all genes. Boxplots are data for the 49 *HRGs* plotted in orange with *ALCOHOL DEHYDROGENASE 1* (*ADH1*) depicted as a red dot and data for the cytosolic ribosomal proteins (RPs) plotted in blue with *RIBOSOMAL PROTEIN 37B* depicted as a dark blue dot. **b** Heatmap showing similarly regulated genes based on two dynamics in nRNA and polyA RNA. Partitioning around medoids clustering of 3,897 differentially regulated genes; 16 clusters. Selected enriched Gene Ontology terms are shown at right (p adj. < 1.37E-06), |FC| > 1, FDR < 0.05. **c** Heatmap of chromatin and RNA readouts of select circadian regulated genes under short and prolonged hypoxic stress. Heatmap scales between chromatin and RNA based readouts differ. **d** Brower views of a

1441 morning (*CIRCADIAN CLOCK ASSOCIATED 1*, CCA1), evening (*CIRCADIAN 1*, CIR1), and night
1442 (*TIMING OF CAB EXPRESSION 1*, TOC1) expressed genes. RNA scale of *TOC1* is three-fold lower than
1443 the scale used for *CCA1* and *CIR1*.

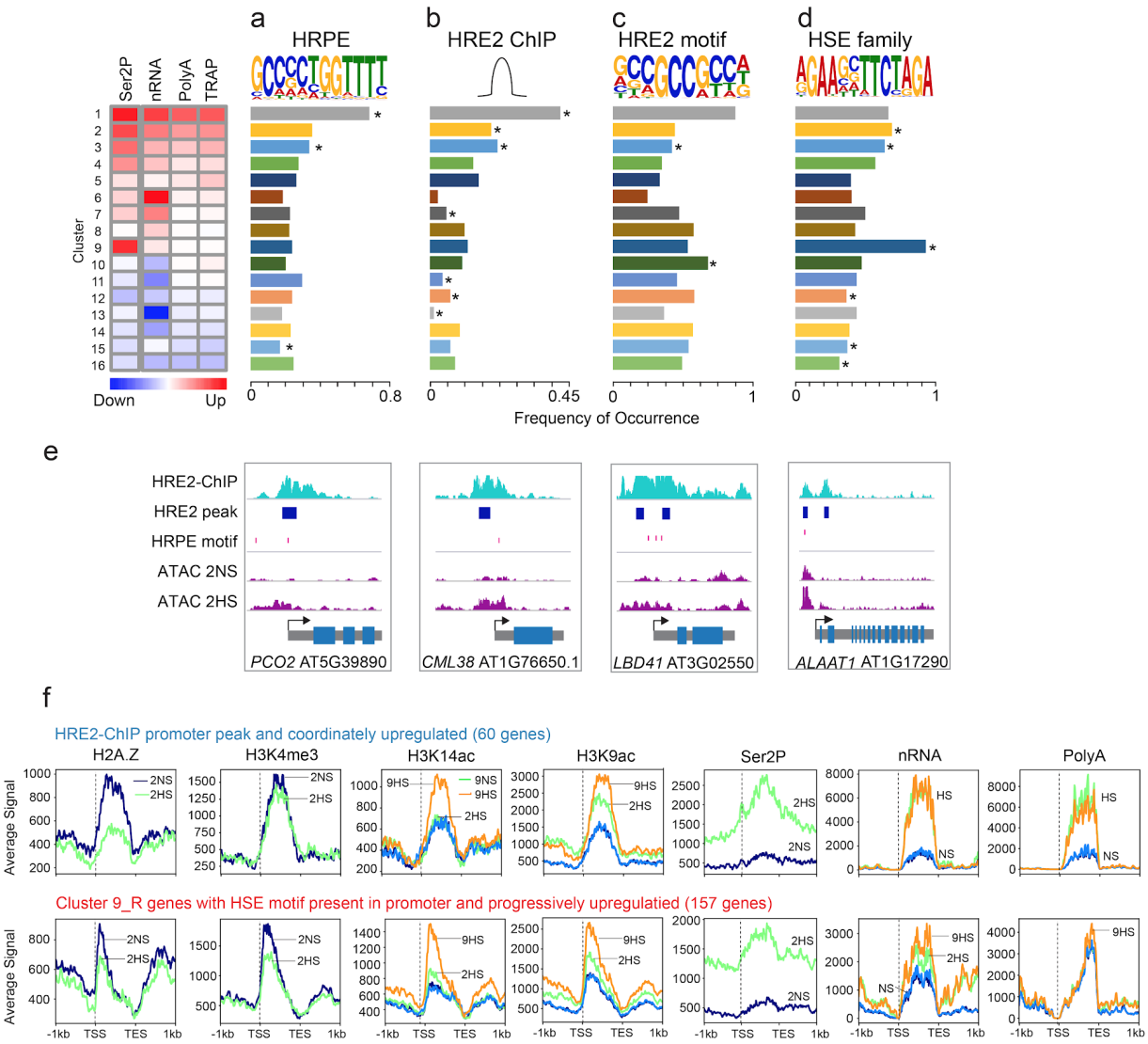

Figure 7. Regulation of hypoxic responses by two ERFVII and HSF TF families. a-d Motif and peak enrichment in the promoter regions (1 kb upstream to 500 bp downstream of the TSS) of genes in clusters identified in Figure 4c for **a**. Hypoxia Responsive Promoter Element (HRPE), **b**. HRE2-ChIP peaks, **c** HRE2-motif, and **d.** Heat Shock sequence Elements (HSE). Frequency of motif and peak occurrence was calculated as number of motifs per number genes in cluster. Clusters with significant enrichment were identified by two-tailed Fisher's exact test $p < 0.05$. **e**. Genome browser view of select *HRGs* (*PLANT CYSTEINE OXIDASE 2, PCO2*; *CALMODULIN-LIKE 38, CML38*; *LOB-DOMAIN CONTAINING PROTEIN 41, LBD41*; *ALANINE AMINO TRANSFERASE 1, AAT1*). The locations of HRE2-ChIP peaks and HRPEs are depicted as a horizontal blue box and vertical red line, respectively. **f**. Average signal of chromatin and RNA readouts for **h,** HRE2 bound genes with coordinate upregulation and **i,** genes with progressive upregulation (cluster 9) containing promoter HSEs. Average signal is plotted from 1 kb upstream of the transcription start site (TSS) to 1 kb downstream of the transcript end site (TES).

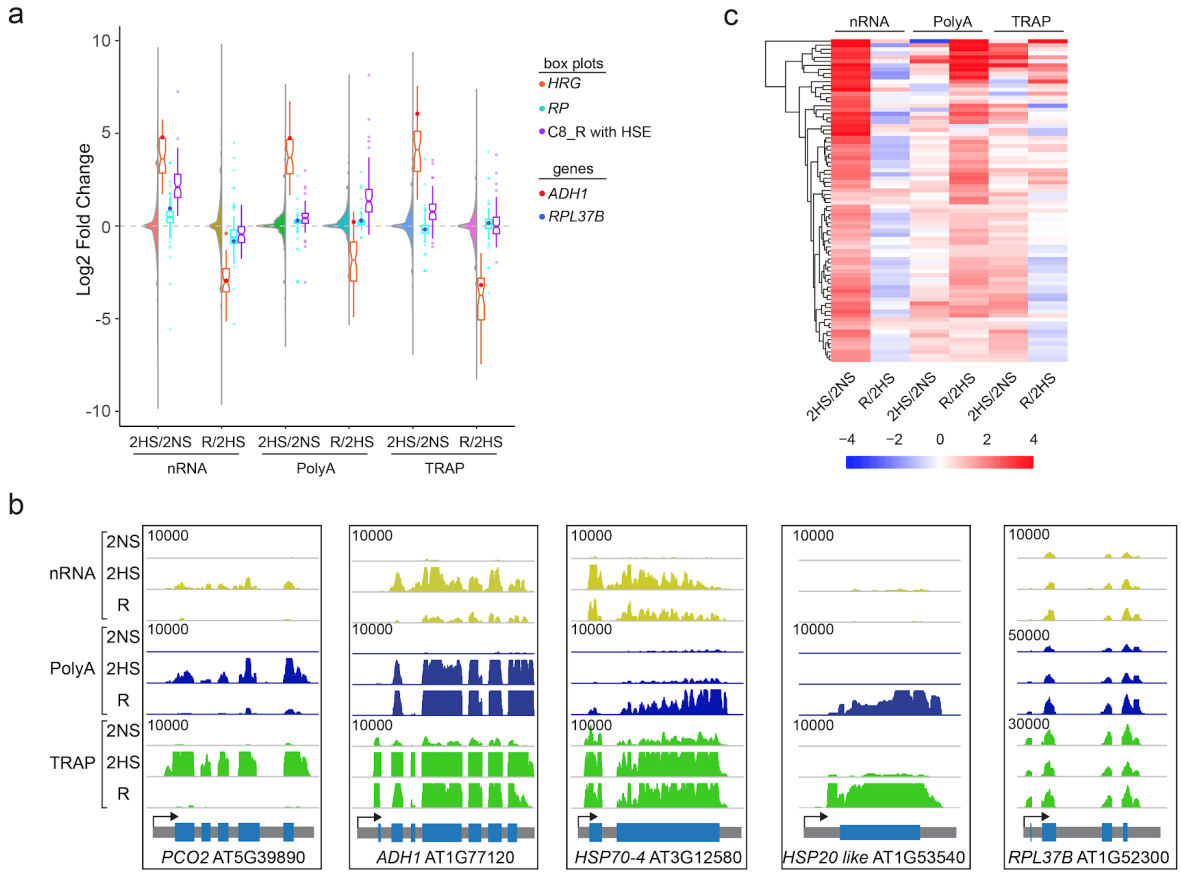

Figure 8. Reaeration promotes accumulation and translation of polyadenylated heat-responsive transcripts that are nucleus-enriched under hypoxia. a Combined violin and boxplot of stress-recovery dynamics of hypoxia-induced nuclear-enriched transcripts (2HS nRNA / 2NS nRNA, $\log_2$ FC > 3, n = 105). All genes shown as a violin; HRGs shown in orange, with *ADH1* as a red dot; RPs shown in blue with *RPL37B* as a blue dot; Heat Shock Element-containing cluster 8_R genes (C8_R, from Supplemental Figure 12) shown in purple. **b** Genome browser view of stress recovery dynamics of *HRGs* (*PCO2*, *ADH1*), heat responsive genes (*HSP70-4*, *HSP20 like*), and a representative *RP* (*RPL37B*). **c** Hierarchical clustering of Heat Shock Element (HSE)-containing cluster 8_R genes in response to hypoxia (2HS/2NS) and reoxygenation (R/2HS).

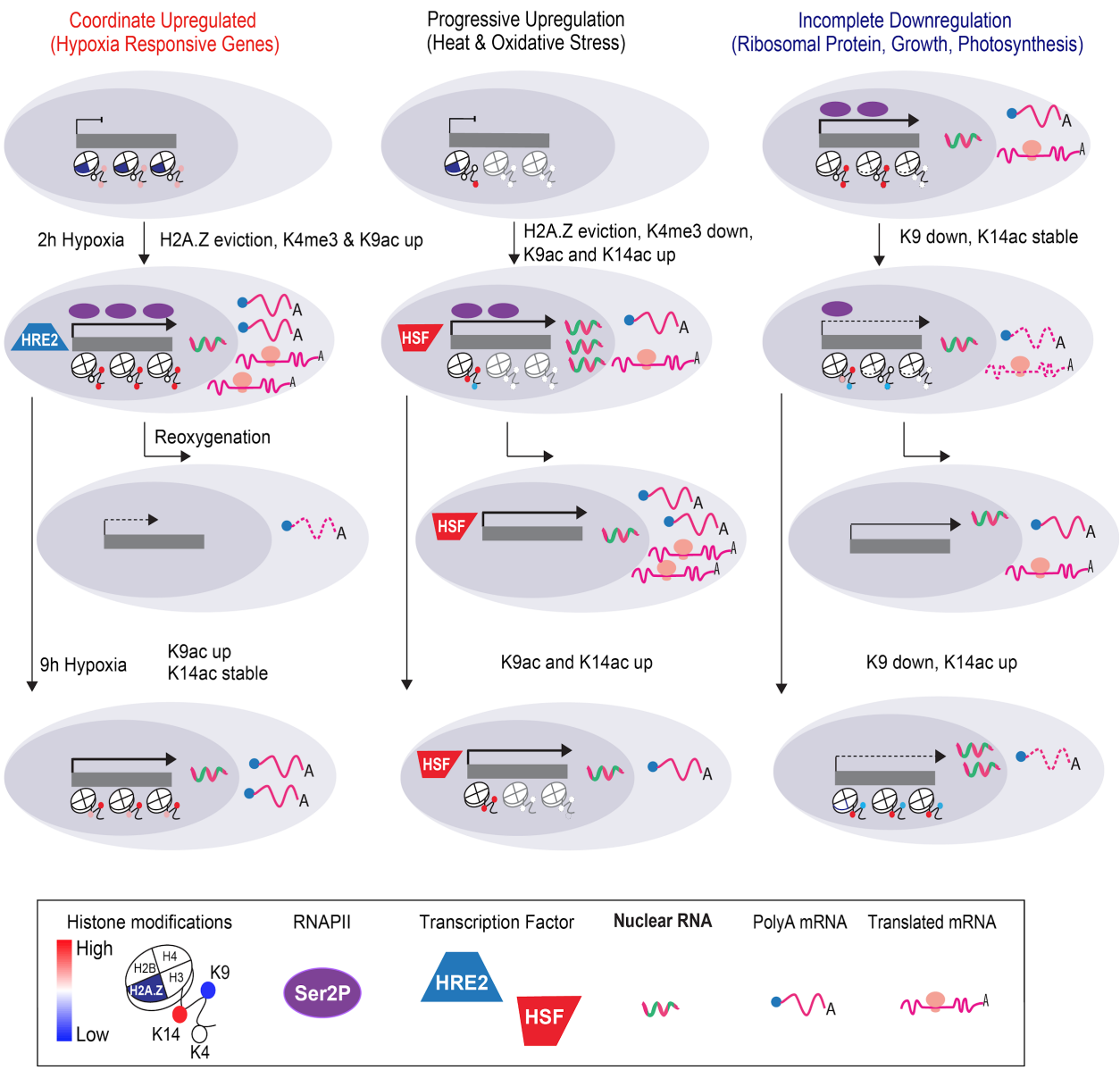

Figure 9. Three patterns of dominant nuclear regulation in response to hypoxic stress of two durations and reaeration. (1) Coordinate upregulation from chromatin to translation of hypoxia responsive genes characterized by hypoxia-triggered H2A.Z eviction, H3K4me3, and H3K9ac elevation. Over half of the genes with this pattern of regulation showed HRE2 binding by chromatin immunopurification. Transcript abundance and translation declines upon reoxygenation. (2) Progressive upregulation of genes associated with heat and oxidative stress responses characterized by a strong 5' bias in histone marks, hypoxia-triggered H2A.Z eviction, H3K9ac elevation, and H3K4me3 reduction. Many are known targets of HSFs. These genes are lowly transcribed under normoxia (nonstress conditions), with evidence of transcriptional activation in response to brief hypoxia (2 h hypoxia) as shown by elevated RNAPII-Ser2P binding, nuclear (nRNA), and ribosome-associated transcripts (TRAP RNA), yet elevation in polyadenylated transcripts (polyA RNA) was limited until the stress was prolonged (9 h

1481 hypoxia). Transcript abundance increases upon reoxygenation. (3) Compartmentalized downregulation of
1482 many genes associated with growth and photosynthesis, including ribosomal protein genes characterized
1483 by maintained RNAPII-Ser2P and nRNA levels under the stress, reduced H3K9ac, and progressive
1484 acquisition of H3K14ac. Transcript abundance and translation is restored upon reoxygenation. Cartoons
1485 illustrate histone modifications as defined by the key. HRE2, Hypoxia-Responsive ERF 2; HSF, Heat
1486 Shock Factor transcriptional activator; Ser2P, RNAPII with the Ser2P modification.

1487

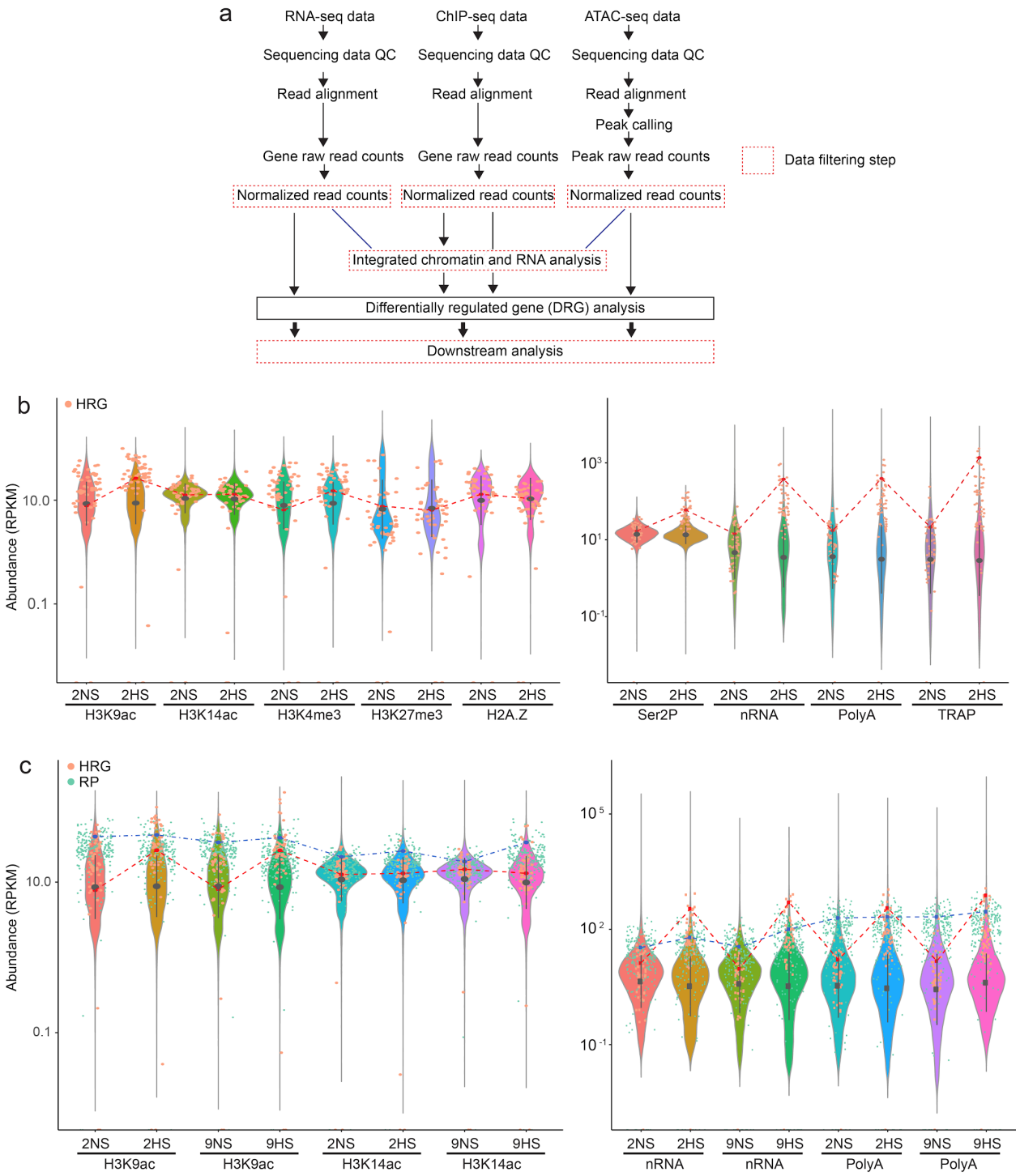

1488

1489 **Supplemental Figure 1. Expanded overview of the multiscale chromatin and RNA gene regulatory**
1490 **analyses. a** Schematic of library types and data analysis performed on 7-day-old seedlings subjected to
1491 control (normoxic) (2NS, 9NS) or hypoxic stress (2HS, 9HS) as shown in Figure 1a. Control seedlings
1492 were compared to hypoxia stress seedlings independently within each chromatin- and RNA-based
1493 dataset. Low abundance reads were filtered (< 2 CPM). Differentially regulated genes were identified and

1494 utilized for downstream analyses. The chromatin and RNA datasets were also analyzed in combination.
1495 **b-c** Violin plots comparing distribution of genome-wide abundance (reads per kilobase per million reads
1496 [RPKM]) of histone and mRNA-related outputs for control (2NS, 9NS) and hypoxic (2HS, 9HS) treatments
1497 for all readouts assayed at 2HS **b**, and 9HS **c.** RPKM values for the 49 core hypoxia responsive
1498 upregulated genes (HRGs) (Mustroph et al., 2009) are plotted as orange dots. The HRG, *ALCOHOL*
1499 *DEHYDROGENASE 1* (*ADH1*) is tracked as a red line. RPKM values for cytosolic ribosomal proteins
1500 (RPs) are plotted in blue, with *RIBOSOMAL PROTEIN 37B* tracked between datasets (blue dashed line).
1501 Mean ± SD are depicted within violins as a dark gray dashed line.

1502 **Supplemental Figure 2 (on two pages)**

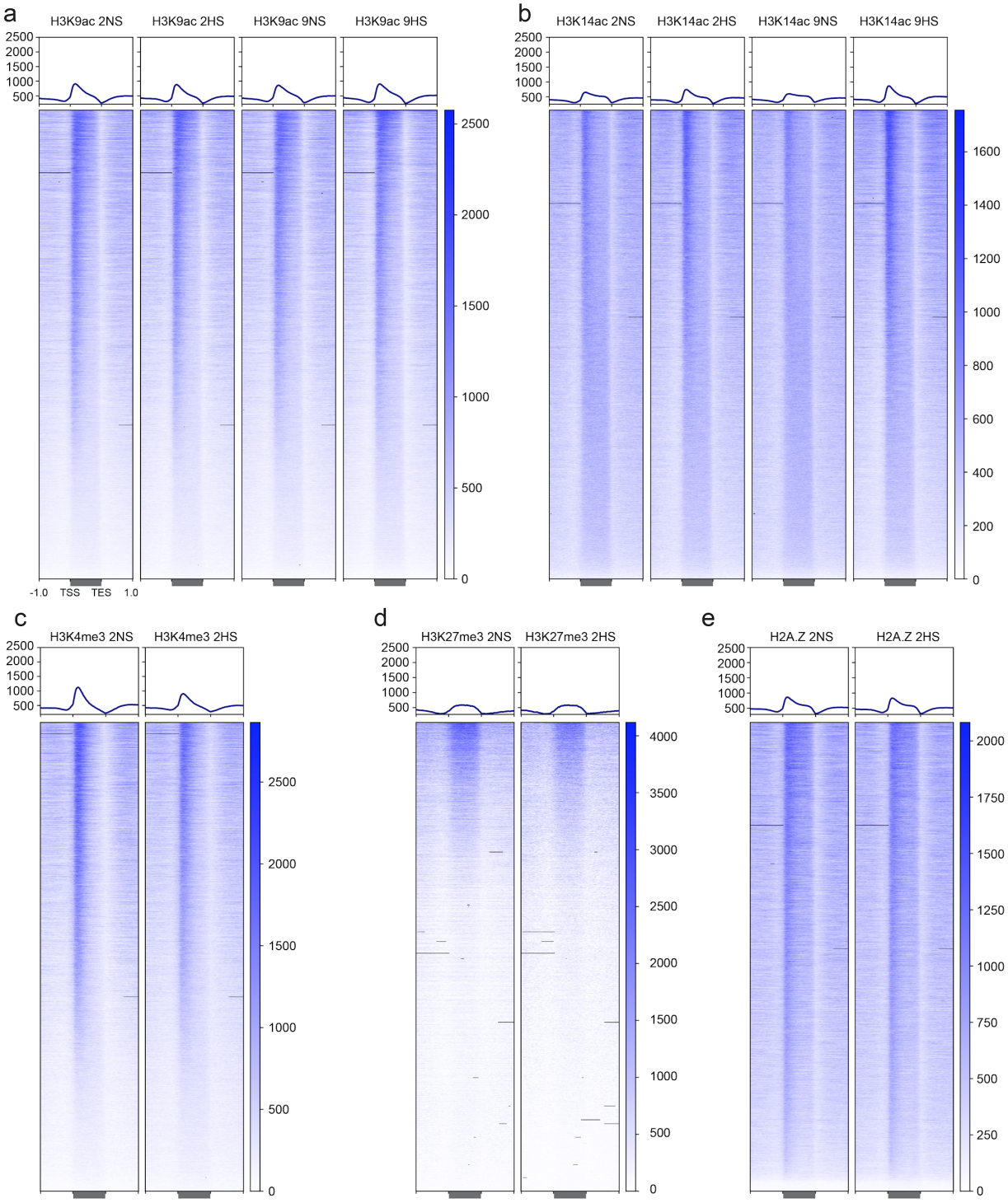

1503

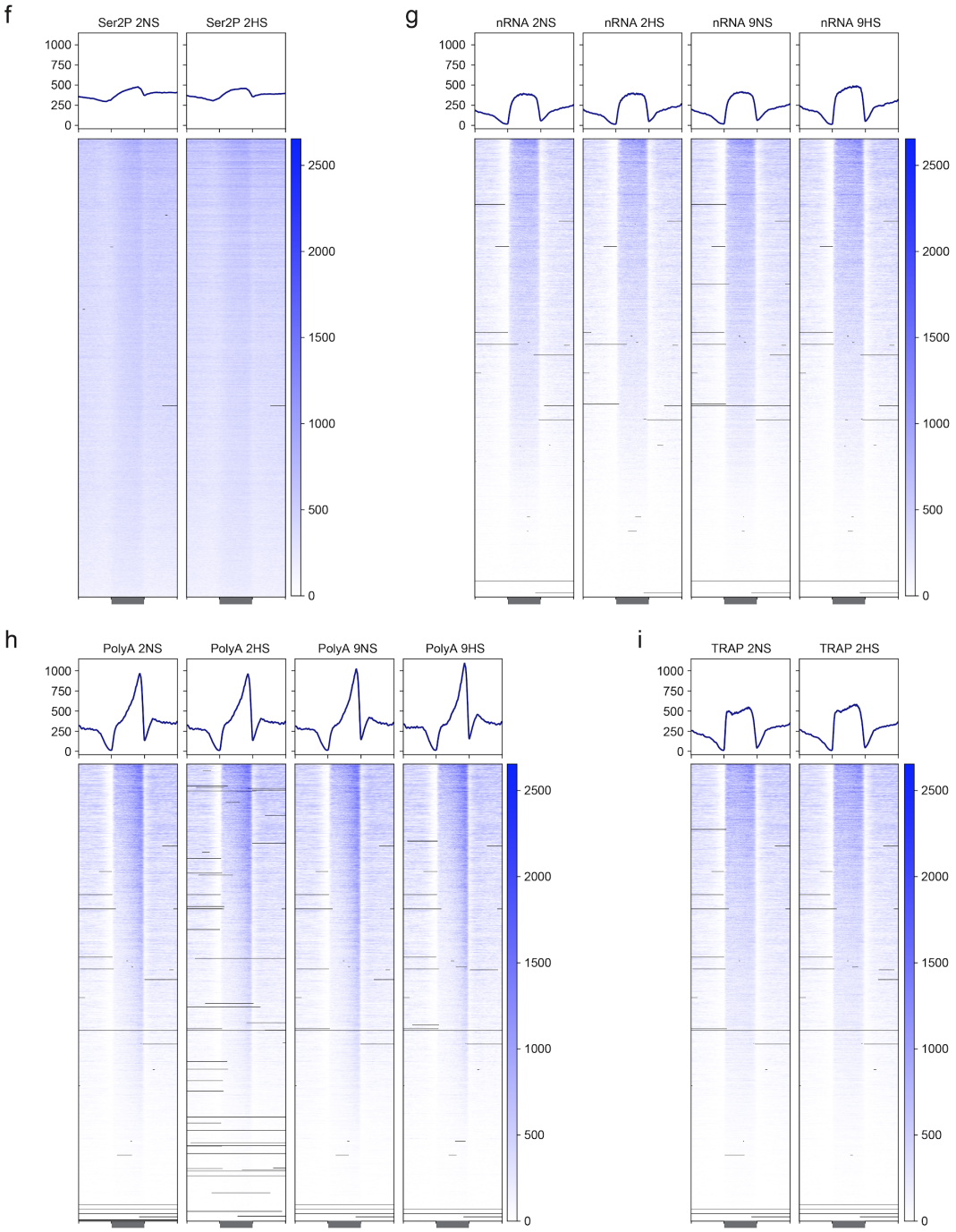

Supplemental Figure 2. Average signal plots and heat maps for the global distribution of reads of chromatin and RNA data. a-h The genomic region from 1 kb upstream of the transcription start site (TSS) to 1 kb downstream of the transcription end site (TES) is depicted for each histone modification and variant, RNAPII-Ser2P (Ser2P), nuclear RNA (nRNA), polyadenylated RNA (polyA RNA) and ribosome- associated RNA (TRAP RNA) for nonstress (2NS, 9NS) and hypoxia (2HS, 9HS) stressed seedlings. Each heat map ranks genes from the highest signal (top) to the lowest (bottom). Heatmap intensity scale values differ between plots of different readouts and are shown. Blacklisted regions of the

1512 genome with disproportionately high reads are tabulated in Supplemental Table 5 and depicted as a black
1513 line.

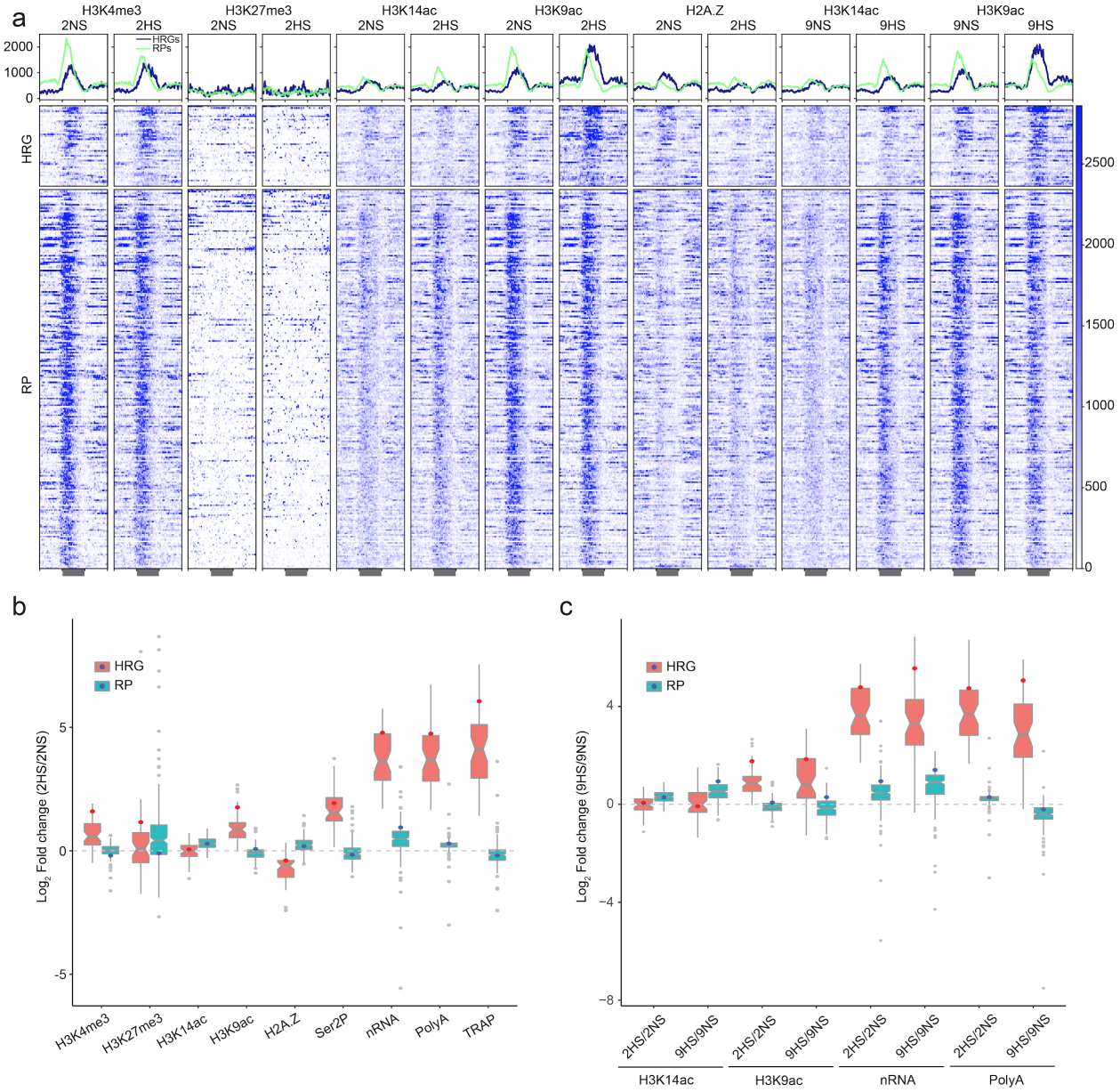

Supplemental Figure 3. Multi-level evaluation of histone and gene regulation activity of the *HRG*s and *RP*s. a The average signal profile and read distribution heatmap for *HRG*s (blue) and *RPs* (green) is depicted for each histone dataset and condition. Analysis of the hypoxia responsive genes (*HRG*s) (n=49) and cytosolic ribosomal protein genes (n=223). Each row in the heat map represents an individual gene; gene order is the same in all plots. **b,c** Box plots of log_2 fold change assayed for (**b**) short (2 h) and (**c**) prolonged (9 h) hypoxic stress compared to control (2HS/2NS, 9HS/9NS). Data for *ADH1* is indicated as a red dot and that of *RPL37B* is indicated as a blue dot. Range of dataset and upper and lower quantiles are depicted within each boxplot.

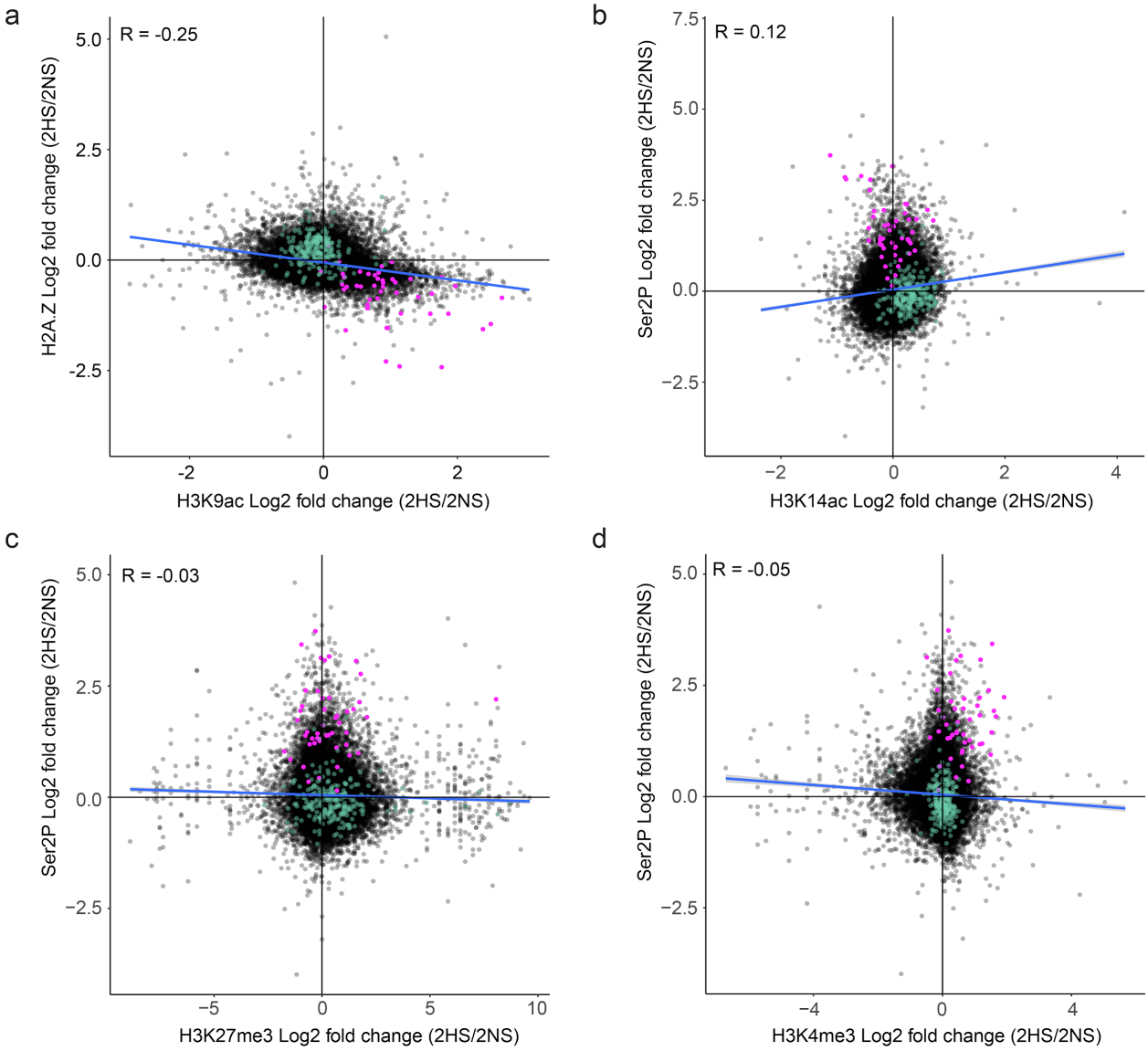

Supplemental Figure 4. Evidence of cooperative association between H2A.Z eviction and H3K9ac and the relation between Histone H3 modification and RNAPII engagement. Plots comparing genome-wide changes in histone modifications and RNAP-Ser2P on individual gene bodies in response to hypoxia. **a** Comparison of $\log_2$ fold change (2HS/2NS) values of H3K9ac and H2A.Z association on gene bodies. **b-d** Comparison of $\log_2$ fold change (2HS/2NS) values of (**b**) H3K14ac, (**c**) H3K27me3, and (**d**) H3K4me3 and Ser2P on gene bodies. In all panels, *HRG*s are plotted in pink and *RP*s in green; the Pearson correlation coefficient for all genes is shown and the slope depicted with a blue line.

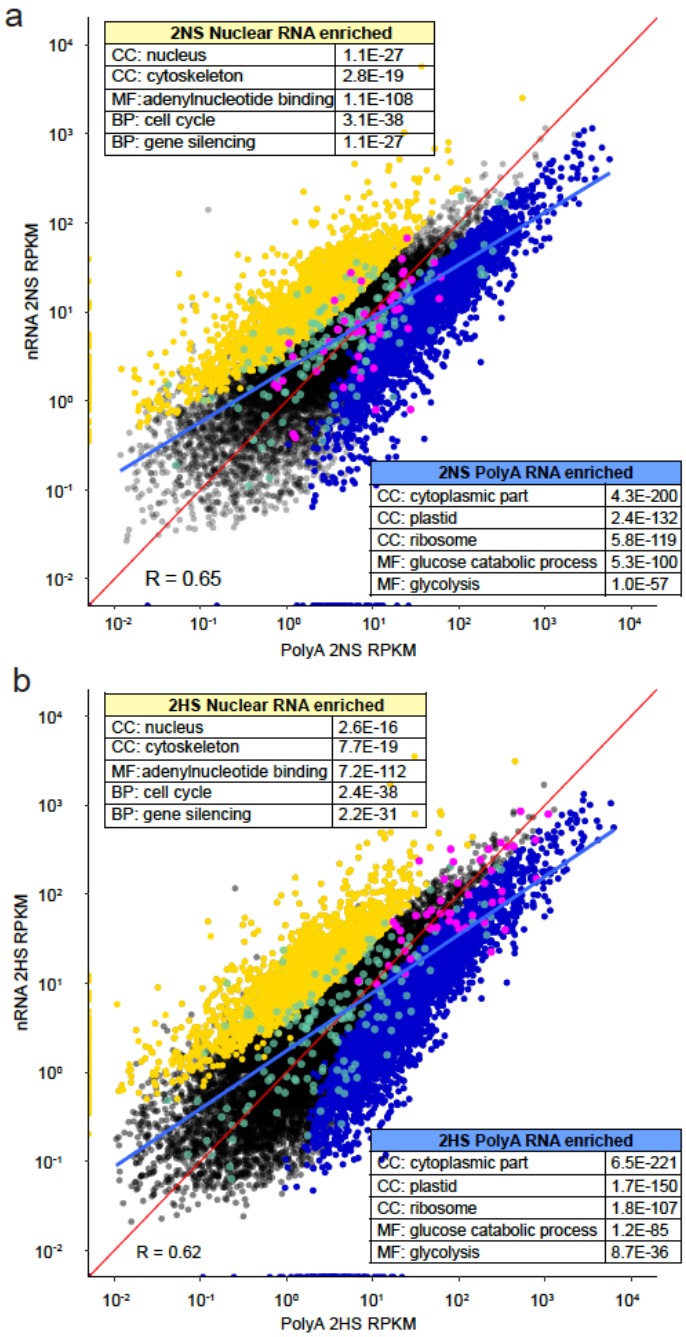

Supplemental Figure 5. Genome-wide comparison of nRNA to polyA RNA demonstrates nuclear and cytoplasmic enrichment of transcripts under two conditions. a, b Scatterplot of normalized read values (per kilobase per million reads; RPKM) on genes in nRNA and polyA RNA populations at (**a**) 2NS and (**b**) 2HS. Transcripts enriched in nRNA (yellow; 2NS: 2,855, 2HS: 2,377) or polyA RNA (blue; 2NS: 3,139, 2HS: 4,029) are depicted ($|\log_2 FC > 1|$, $p < 0.05$). *HRG*s and *RP*s are also indicated in pink and green dots, respectively. The genome-wide Pearson correlation coefficient is shown and the slope depicted with a blue line. The red line is a slope of 1. Inserted tables describe representative Gene

1539 Ontology categories that are over-represented in nuclear RNA and polyA under the two conditions (data
1540 from Supplemental Table 2). Many of the same groups of cell component (CC) and molecular (MF) were
1541 over-represented in the nRNA and polyA RNA populations obtained in the same manner in rice (Reynoso
1542 et al., 2017).

1543 **Supplemental Figure 6 (on two pages)**

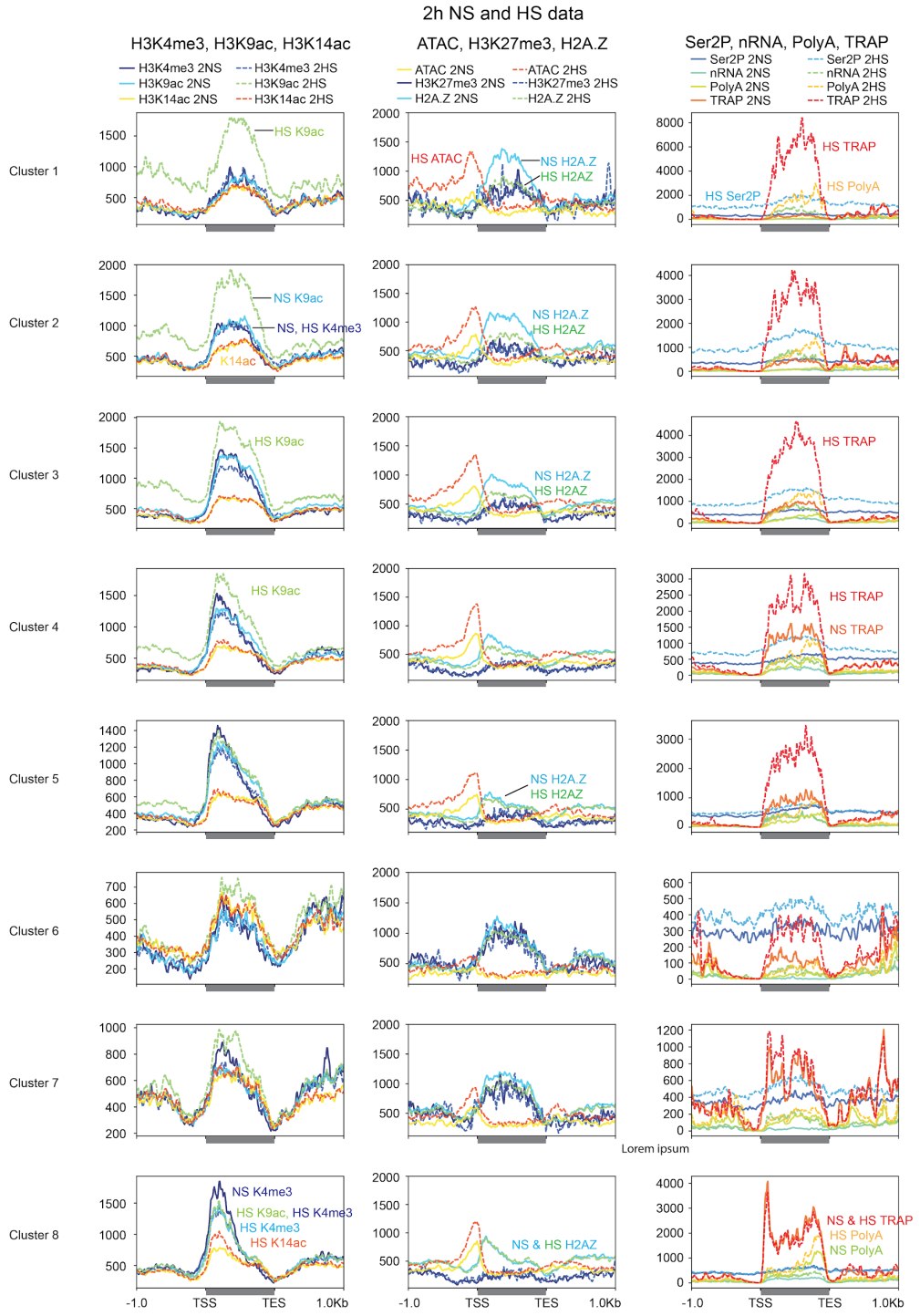

1544

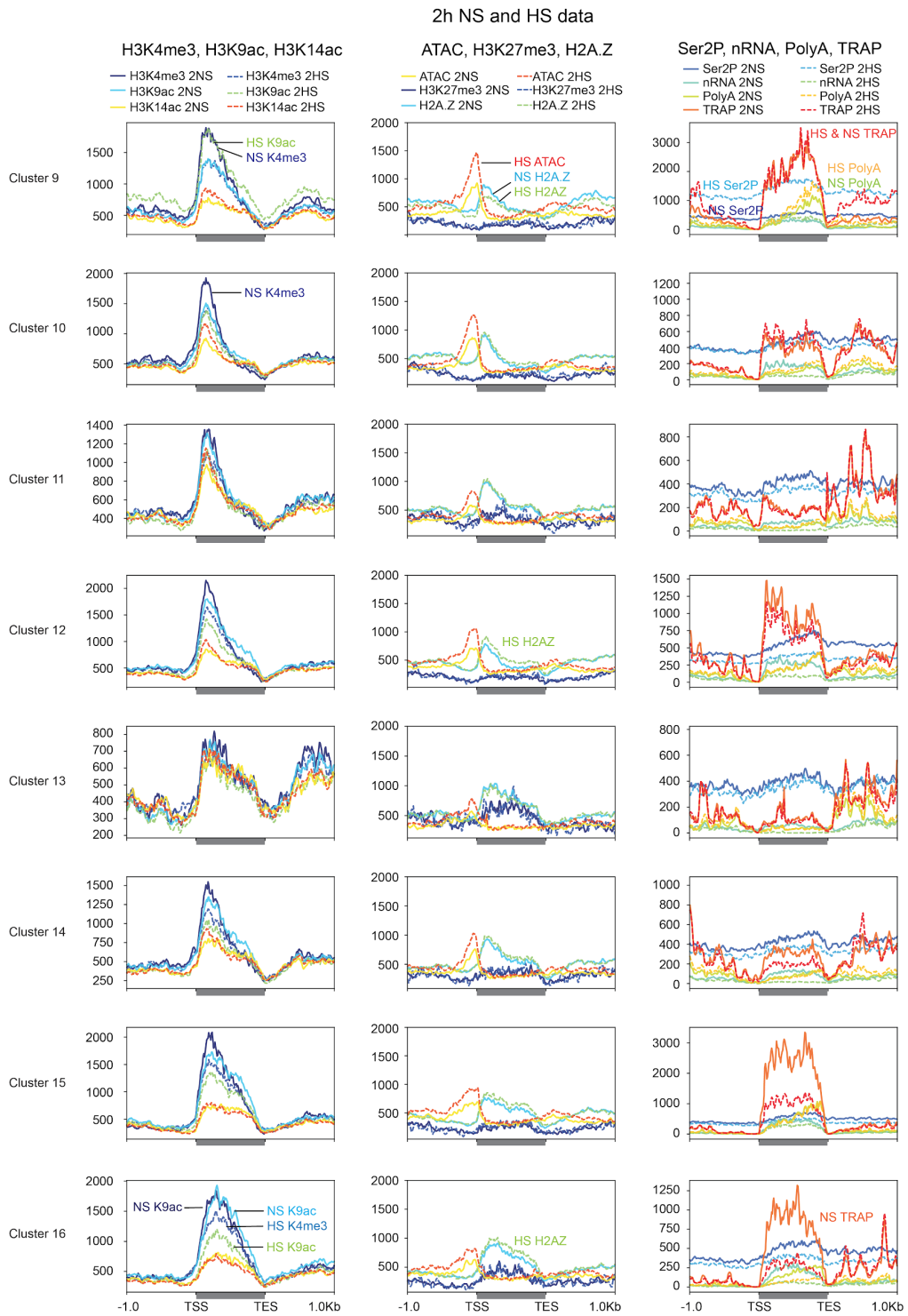

Supplemental Figure 6. Distinctions in histones, RNAPII-Ser2P and RNA levels on genes that are co-regulated in response to hypoxic stress. Average signal of chromatin and RNA outputs for clustered genes identified from the 2HS comparison in Figure 4c. Hypoxic sample data are dashed lines. Signal values are plotted from 1 kb upstream of the TSS to 1 kb downstream of the TES. Signal scale of graphs may differ.

1551 **Supplemental Figure 7 (on two pages)**

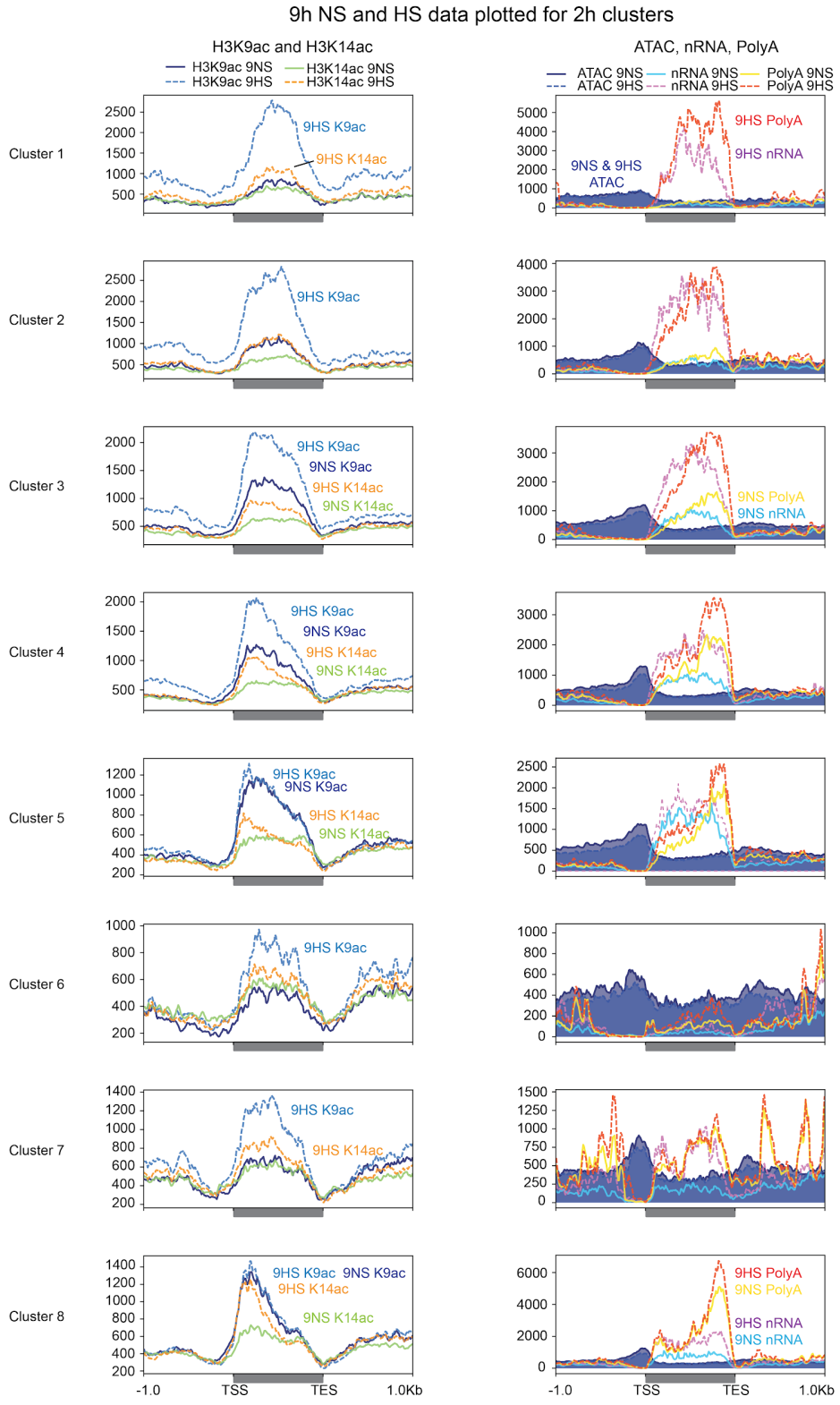

1552

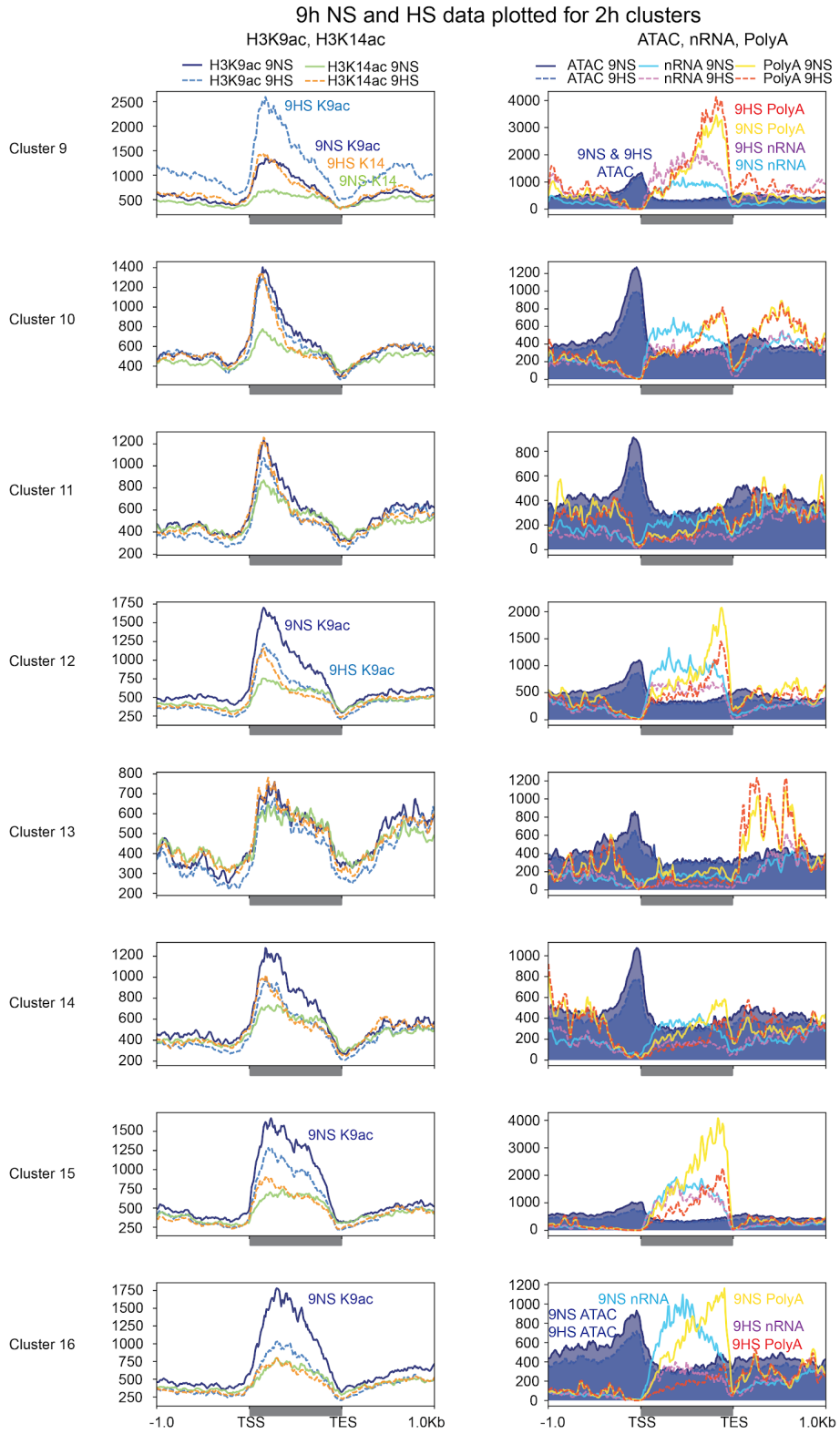

Supplemental Figure 7. Progressive regulation of variations in gene activity in response to hypoxia. Average signal of chromatin and RNA outputs for clustered genes identified from the 9HS (9HS/9NS) comparison in Figure 4c. Plotting is as described for Supplemental Figure 6.

1557 **Supplemental Figure 8 (on two pages)**

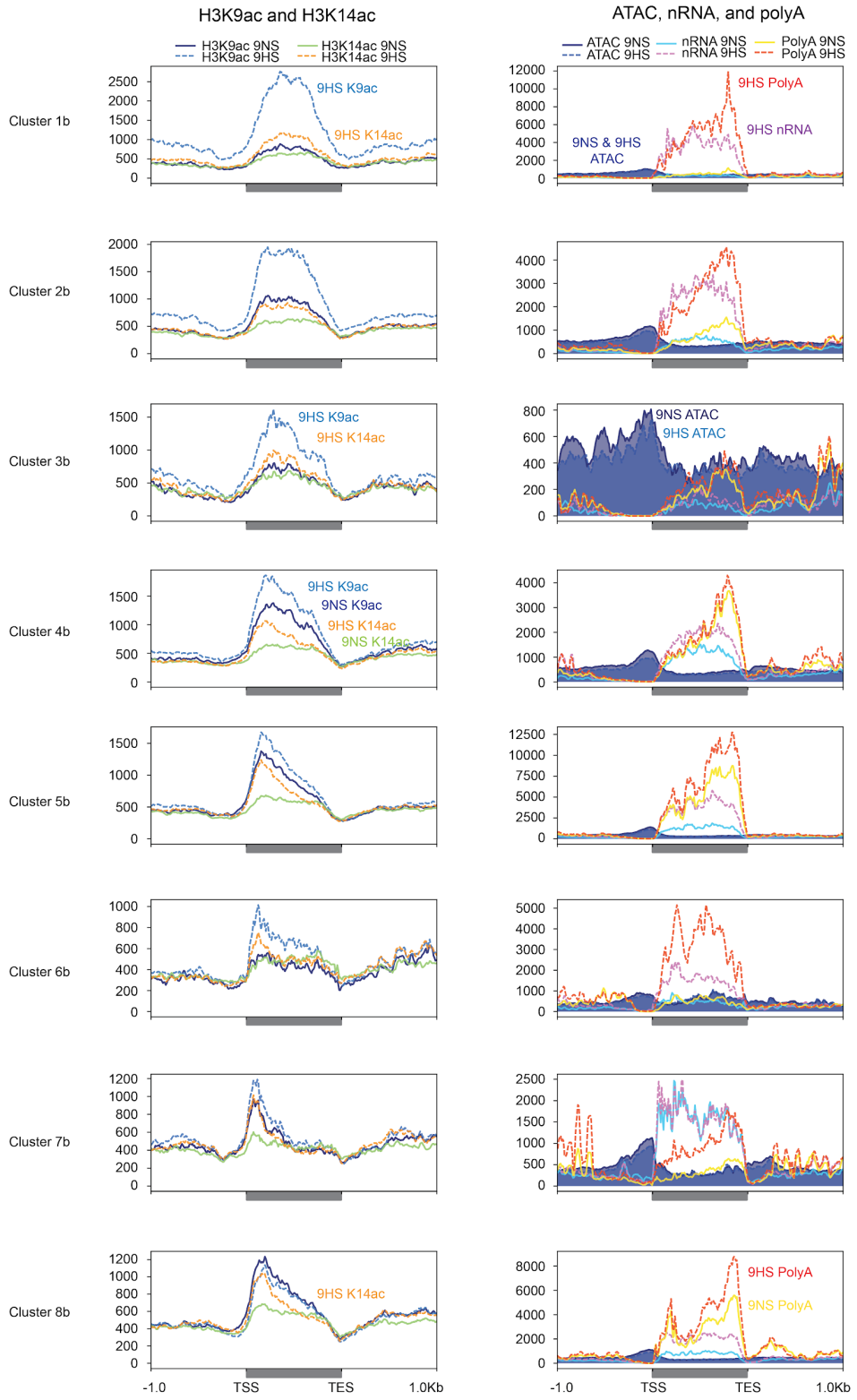

1558

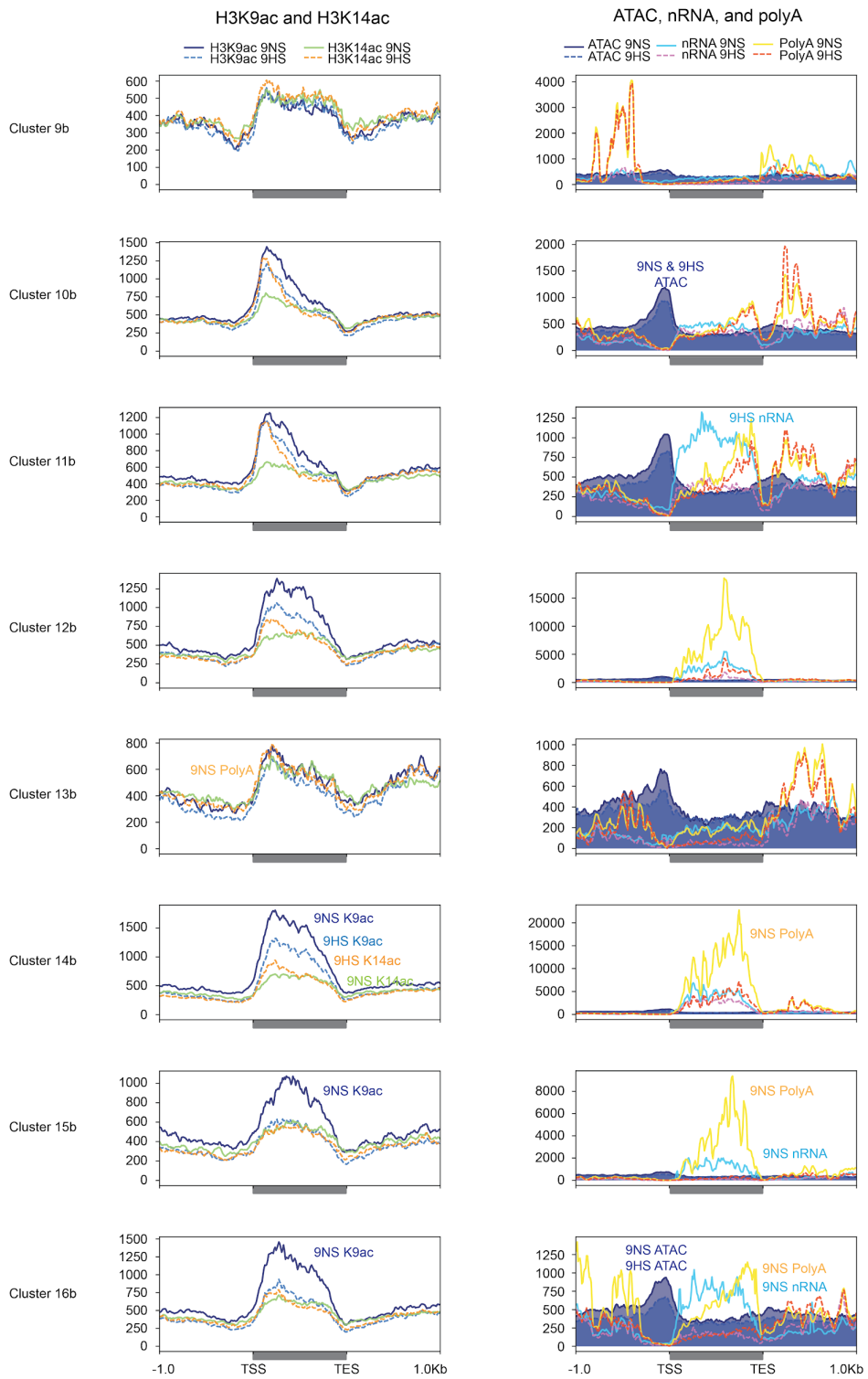

Supplemental Figure 8. Histone and gene activity comparisons of genes co-regulated after 9 h of hypoxic stress. Average signal of chromatin and RNA data for co-regulated gene clusters identified from the 9 h hypoxic stress comparison (9HS/9NS) in Figure 6b. Plotting is as described for Supplemental Figure 6.

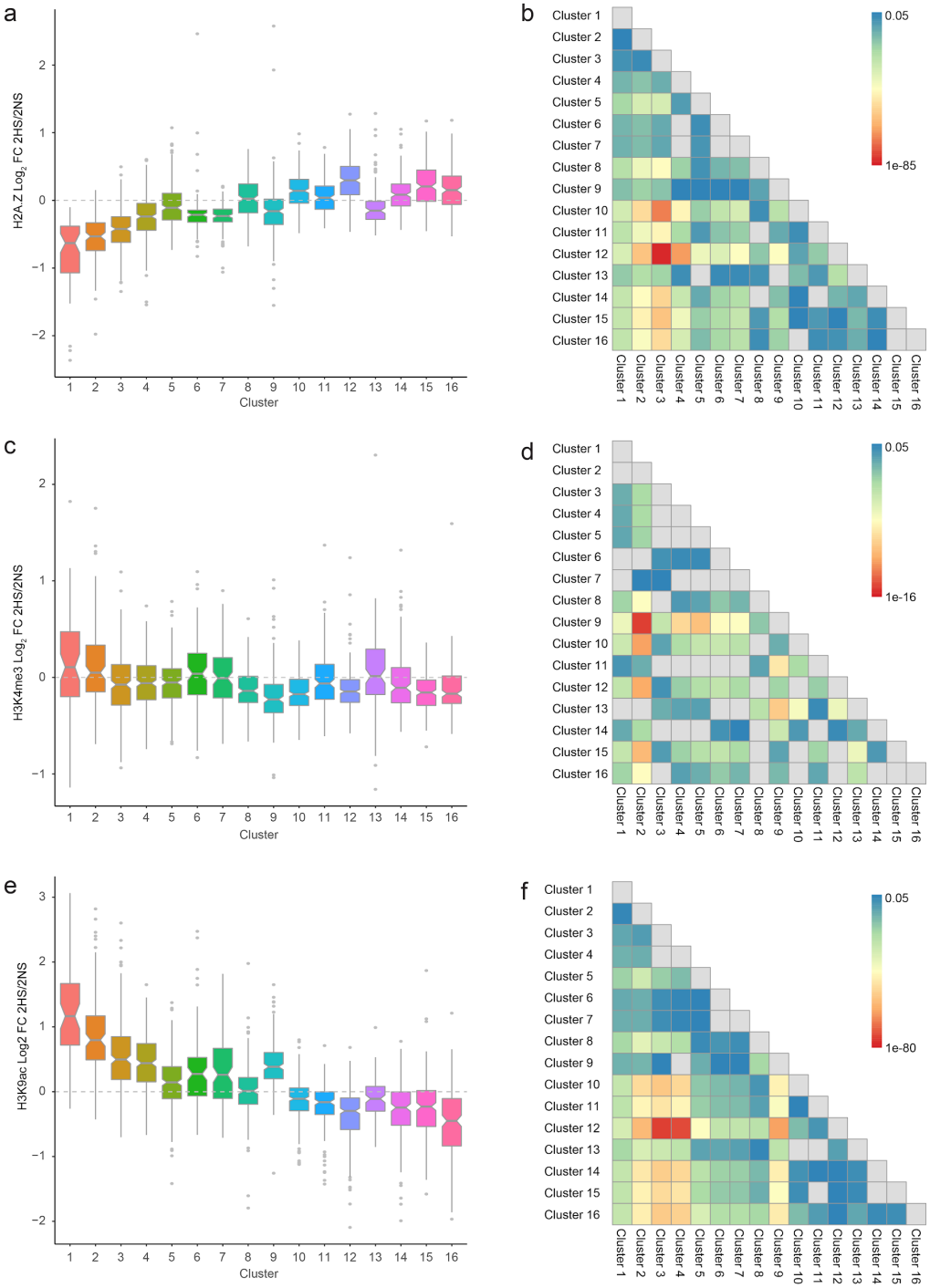

Supplemental Figure 9. Quantitative analysis of dynamics in histone modifications of co-regulated gene clusters after 2 h of hypoxic stress. a, c, e Box plots of $\log_2$ fold change in response to 2 h hypoxic stress of H2A.Z, H3K4me3 and H3K9ac for the 16 clusters shown in Panels **b**, **d**, **f** provide Wilcoxon signed rank test values of gene clusters in an all by all matrix. Grey boxes denote no significant difference between clusters. Heatmap scale depicts significance values of $p < 0.05$.

1570

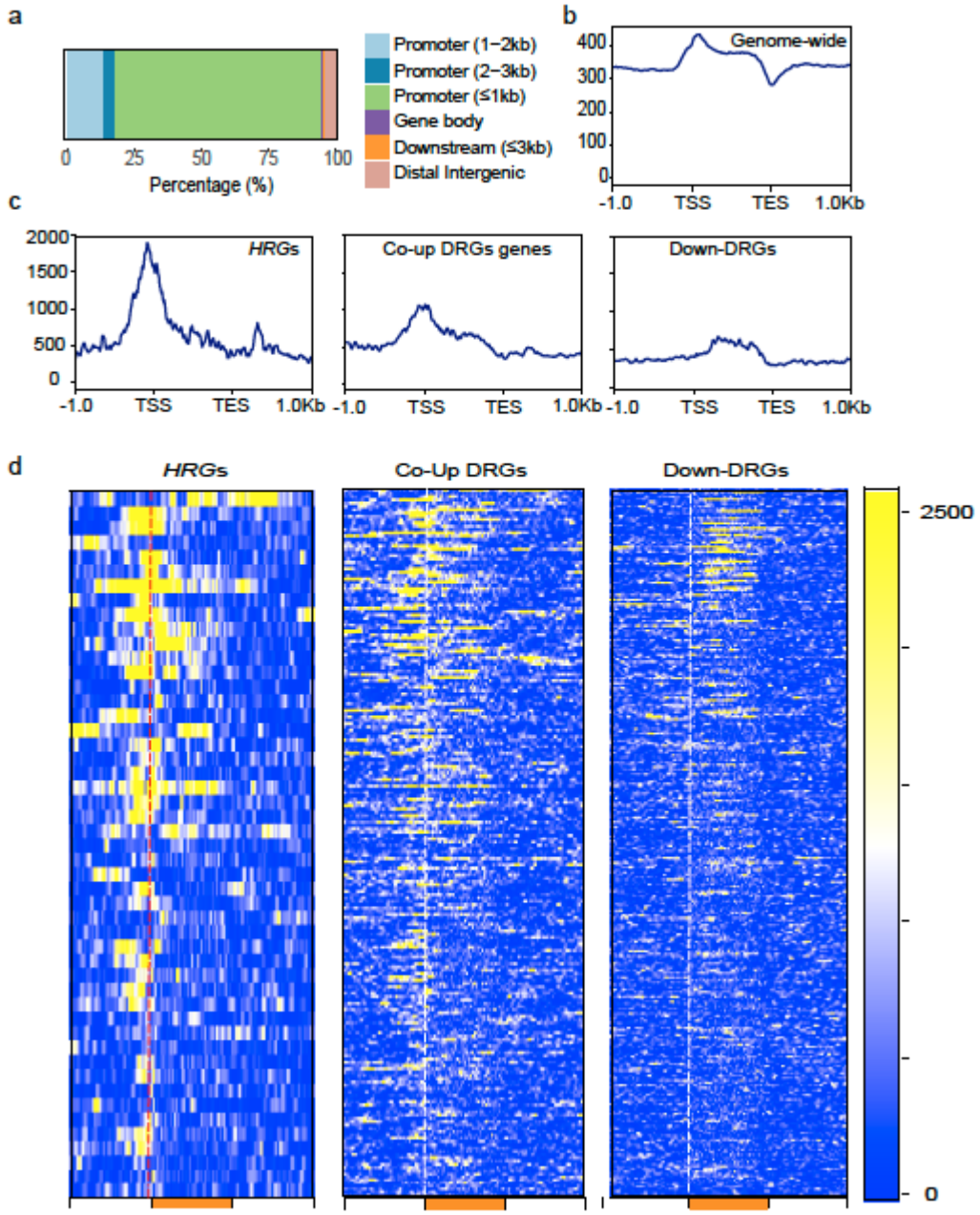

1571

1572 **Supplemental Figure 10. Genome-wide binding dynamics of HRE2 determined by ChIP-seq. a**
1573 Distribution of 1,764 mapped HRE2 peaks on genomic features. **b, c** Average HRE2-ChIP read
1574 distribution in regions spanning 1 kb upstream to 1 kb downstream of gene features: **b** genome wide and
1575 **c** for the *HRG*s, Coordinately upregulated genes (Co-Up), and Down regulated genes (RGs). **d** Heat map
1576 of the HRE2- ChIP reads for genes in each group (*HRG*s) (n=49) and co-UP (n=213, and down-RGs
1577 (n=297). Each row in the heat map represents an individual gene; gene order is the same in all plots.

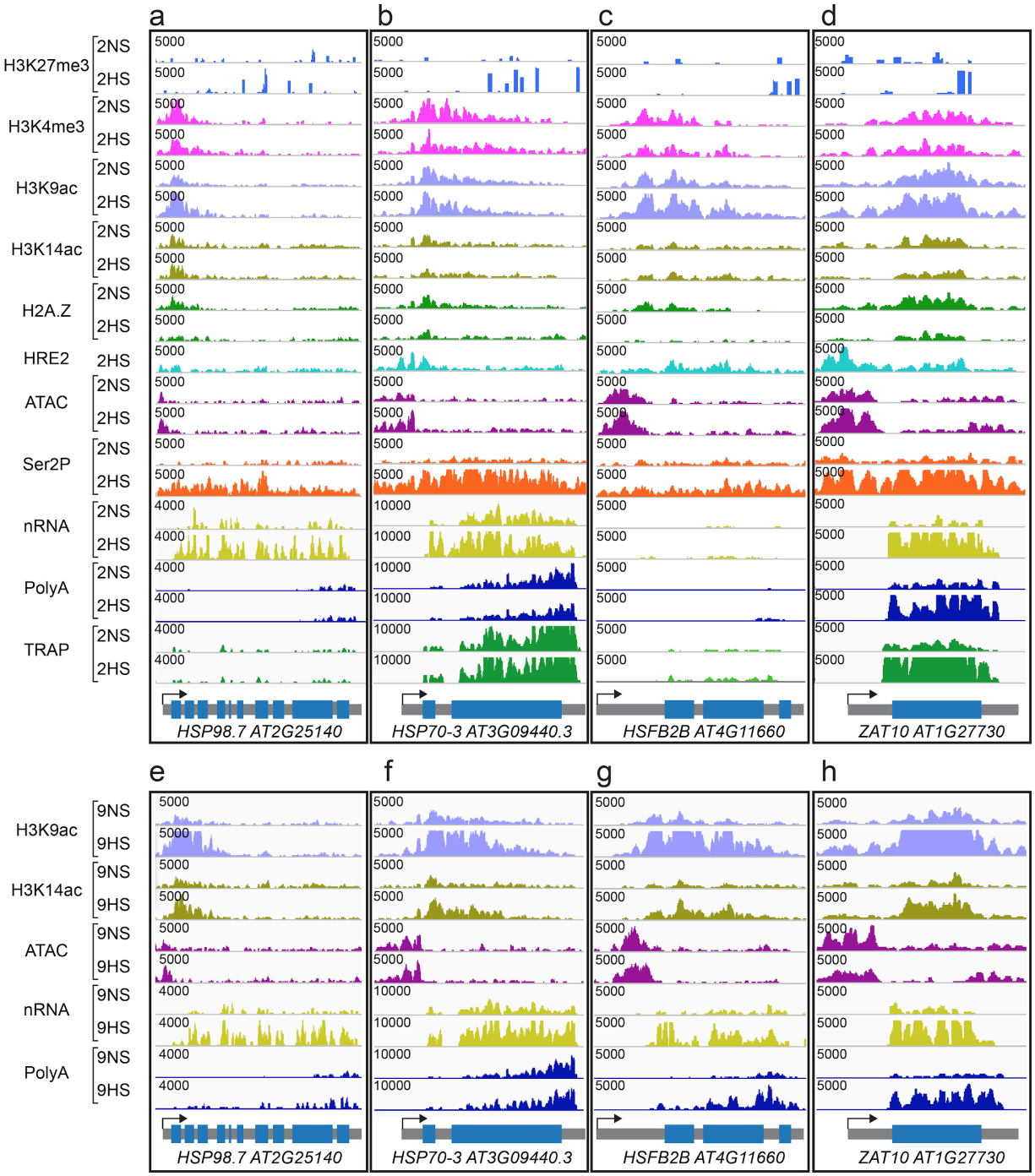

Supplemental Figure 11. Genome browser view of normalized read coverage of histone, ATAC-seq, RNAPII-Ser2P, HRE2-chromatin immunopurification and RNA outputs for representative genes of cluster 9. a-d Normoxia (2NS) and 2 h hypoxic stress (2HS). **e-h** 9NS and 9HS samples. **a,e** *HEAT SHOCK PROTEIN (HSP) 98-7* **b,f** *HSP70-3,* **c,g** *HEAT SHOCK TRANSCRIPTION FACTOR B2B* and **d,h** *ZAT10.* The maximum read scale value used for chromatin based and RNA based outputs is provided. At bottom, the transcription unit is shown in grey with the transcription start site marked with an arrow.

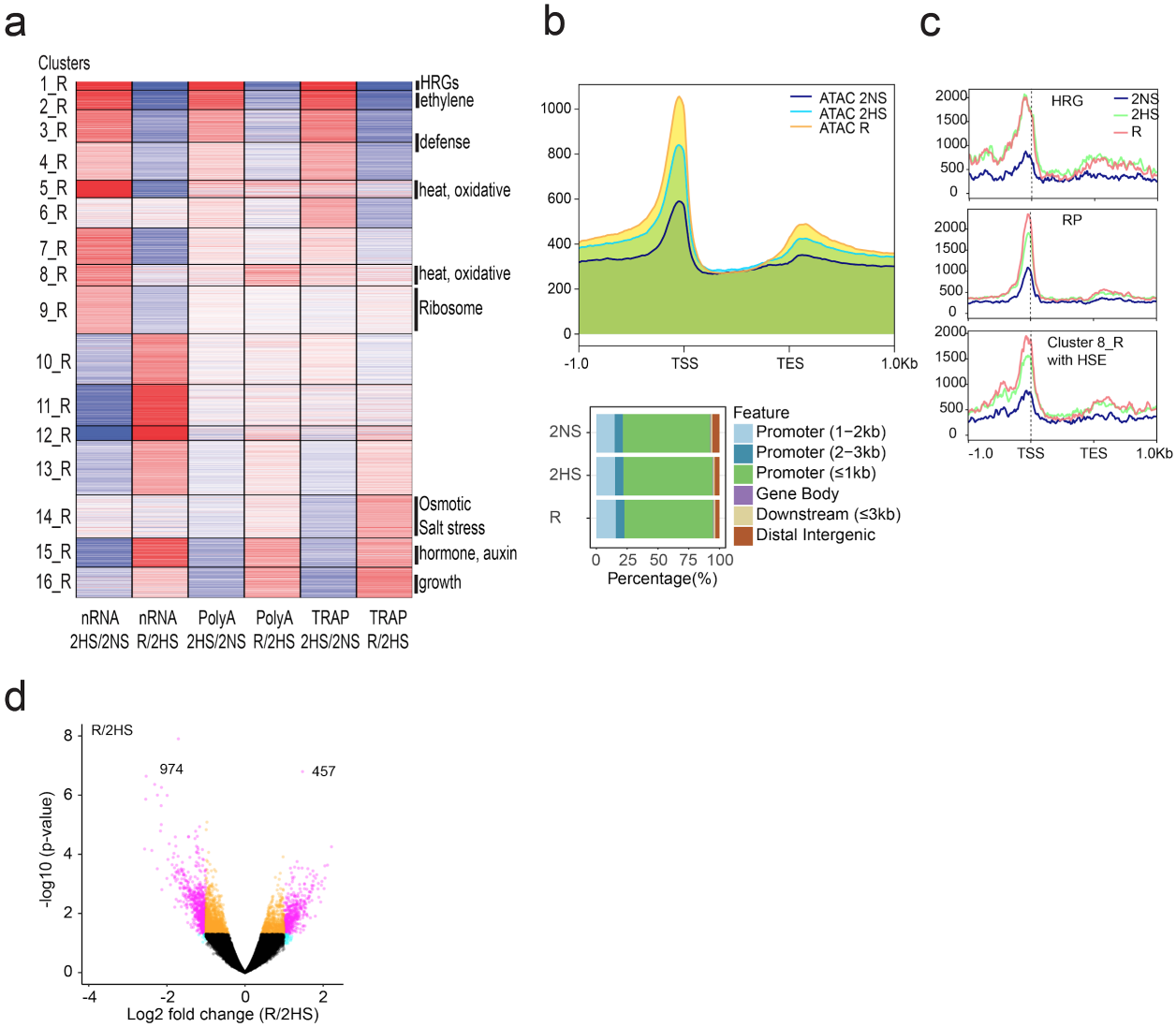

Supplemental Figure 12. Reoxygenation following hypoxia promotes global dynamics in chromatin accessibility and RNA populations. a Heatmap showing similarly regulated genes based on dynamics in nRNA, polyA RNA, and TRAP in response to hypoxia (2HS/2NS) and reoxygenation (R/2HS). Partitioning around medoids (PAM) clustering of 4,784 differentially regulated genes; 16 clusters. Selected enriched Gene Ontology terms are shown at right (p adj. < 1.37E-06), |FC| > 1, FDR < 0.05. **a** number of clusters showed high nRNA at 2 HS that was not accompanied by high polyA or TRAP mRNA at 2HS clusters 5_R, 8_R, 10_R-13_R). Of these, cluster 8_R was the only with elevated polyA mRNA at R, suggesting these mRNAs accumulate to higher levels during reaeration. *HSP70-4* is a member of cluster 5_R. Both cluster 5_R and cluster 8_R genes are enriched for HSE elements within their promoters (cluster 5_R 85 of 123 genes have an HSE; cluster 8_R 81 of 153 genes have an HSE). Cluster 14_R is enriched for GOs associated with osmotic and salt stress. These stress-related mRNAs show preferential TRAP RNA accumulation at R, indicating a preferential translation at at this time point. **b** Average ATAC-seq read distribution of chromatin accessibility for all protein-coding genes at three

1600 timepoints and distribution of transposase hypersensitive sites on genomic features for each condition. **c**
1601 Dynamic chromatin accessibility in response to reaeration. 457 up- and 974 downregulated
1602 THSs. An increase in accessibility near the TSS was observed for the *RP*s but neither the
1603 *HRG*s nor the HSE-containing genes of cluster 8_R showed reduced accessibility within this
1604 time period. **d** Average signal of chromatin and RNA readouts for HRGs, RPs, and HSE
1605 containing cluster 8_R genes. Average signal is plotted from 1 kb upstream of the transcription
1606 start site (TSS) to 1 kb downstream of the transcript end site (TES). **d** Volcano plot of $\log_2$ fold
1607 change in THSs identifiable under 2HS and R conditions and the significance value of their difference.
1608 Genes indicated in pink meet the criteria of $\log_2$ fold change value > |1|, 0.05 < p. value.

1609 **Supplemental Figure 13 (on two pages)**

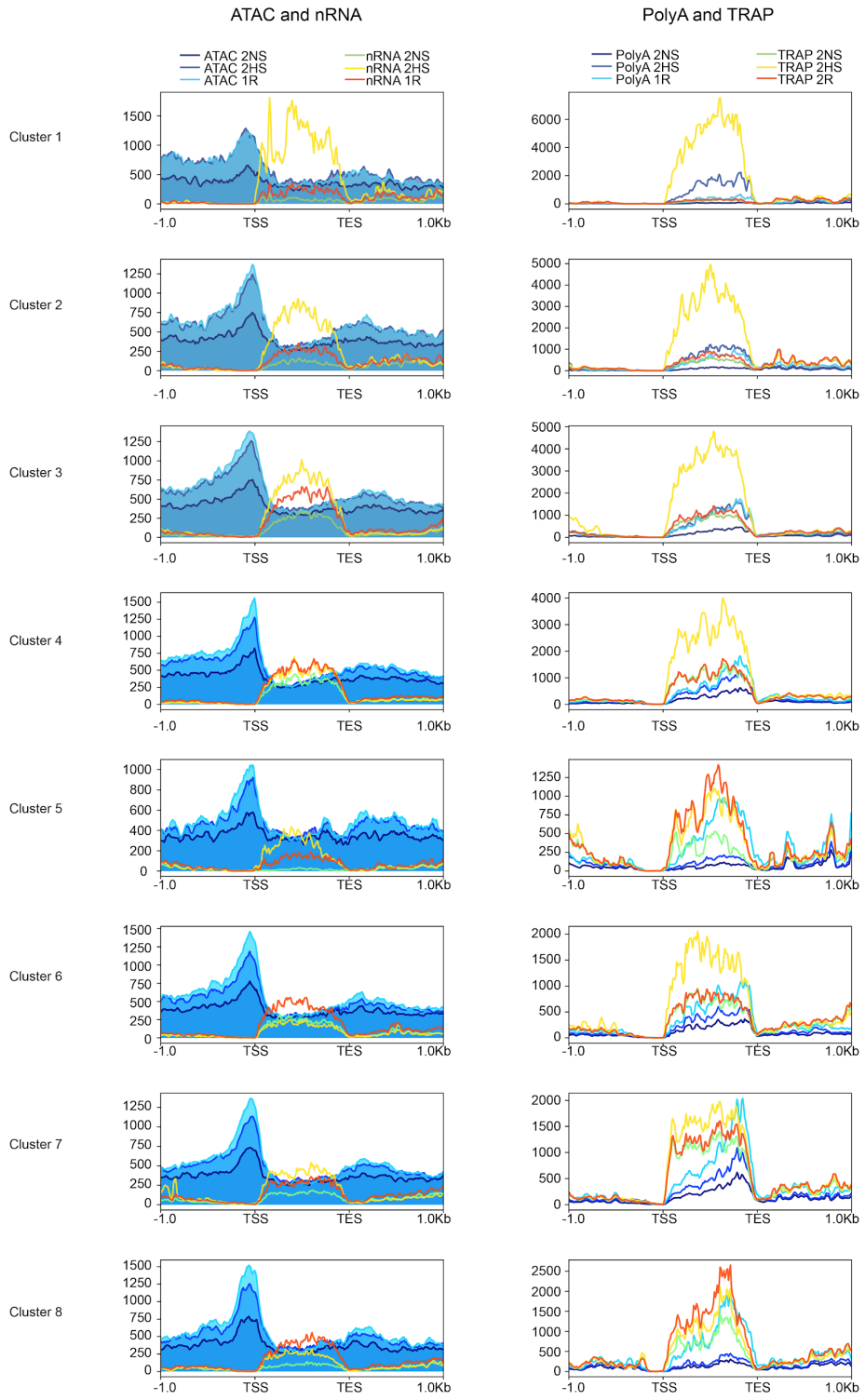

1610

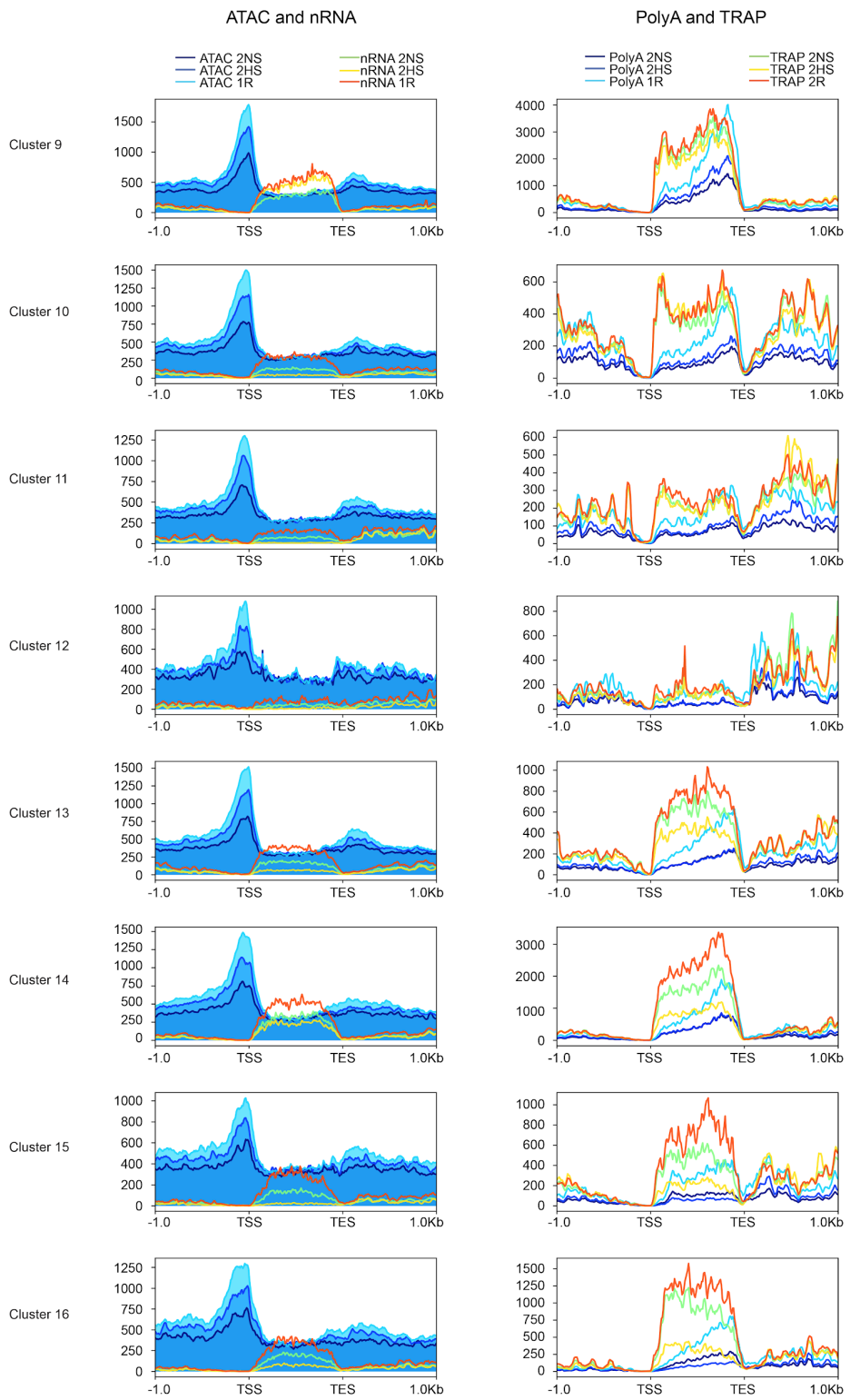

Supplemental Figure 13. Regulation of variations in gene activity in response to hypoxia and reoxygenation. Average signal of chromatin and RNA outputs for clustered genes identified from the reoxygenation (2HS/2NS, R/2HS) comparison in Supplemental Figure 12. Plotting is as described for Supplemental Figure 6.